NAVAL POSTGRADUATE SCHOOL
Monterey, California

THESIS

THE ATTITUDE CONTROL
OF
FLEXIBLE SPACECRAFT

by

R. Joseph Watkins Jr.

June, 1991

Thesis Advisor: Prof. Brij N. Agrawal

Approved for public release; distribution is unlimited.

REPORT DOCUMENTATION PAGE

1a. REPORT SECURITY CLASSIFICATION Unclassified	1b. RESTRICTIVE MARKINGS
2a. SECURITY CLASSIFICATION AUTHORITY	3. DISTRIBUTION/AVAILABILITY OF REPORT Approved for public release; distribution is unlimited
2b. DECLASSIFICATION/DOWNGRADING SCHEDULE	
4. PERFORMING ORGANIZATION REPORT NUMBER(S)	5. MONITORING ORGANIZATION REPORT NUMBER(S)
6a. NAME OF PERFORMING ORGANIZATION Naval Postgraduate School 6b. OFFICE SYMBOL (*If applicable*) 39	7a. NAME OF MONITORING ORGANIZATION Naval Postgraduate School
6c. ADDRESS (*City, State, and ZIP Code*) Monterey, CA 93943-5000	7b. ADDRESS (*City, State, and ZIP Code*) Monterey, CA 93943-5000
8a. NAME OF FUNDING/SPONSORING ORGANIZATION 8b. OFFICE SYMBOL (*If applicable*)	9. PROCUREMENT INSTRUMENT IDENTIFICATION NUMBER
8c. ADDRESS (*City, State, and ZIP Code*)	10. SOURCE OF FUNDING NUMBERS Program Element No / Project No / Task No / Work Unit Accession Number

11. TITLE (*Include Security Classification*)
The Attitude Control of Flexible Spacecraft

12. PERSONAL AUTHOR(S) Watkins, Richard Joseph Jr.

13a. TYPE OF REPORT	13b. TIME COVERED	14. DATE OF REPORT (*year, month, day*)	15. PAGE COUNT
Master's Thesis	From To	June 1991	85

16. SUPPLEMENTARY NOTATION
The views expressed in this thesis are those of the author and do not reflect the official policy or position of the Department of Defense or the U.S. Government

17. COSATI CODES			18. SUBJECT TERMS (*continue on reverse if necessary and identify by block number*)
FIELD	GROUP	SUBGROUP	Flexible Appendage, Finite Element Analysis, Mode Shapes, Equations of Motion

19. ABSTRACT (*continue on reverse if necessary and identify by block number*)

This thesis details the design of the Naval Postgraduate School's Flexible Spacecraft Simulator and the first attempts at simulation and control of the model. The effect of flexible structures on the attitude control of spacecraft has been a topic of research for many years. Only recently has the technology to actually test models and theory on the ground been available. At the Naval Postgraduate School, an experimental testbed for research into this area has been constructed. This facility has a model of a satellite with a flexible arm floating on air pads to eliminate the effects of friction. A mathematical model of the system has been constructed and simulations of various maneuvers have been run, utilizing proportional-derivative (PD) control as well as a Linear-Quadratic-Gaussian (LQG) compensator. Results show that both PD and LQG work well for station keeping, but that the LQG compensator is better for slewing the arm.

20. DISTRIBUTION/AVAILABILITY OF ABSTRACT	21. ABSTRACT SECURITY CLASSIFICATION	
☒ UNCLASSIFIED/UNLIMITED ☐ SAME AS REPORT ☐ DTIC USERS	Unclassified	
22a. NAME OF RESPONSIBLE INDIVIDUAL Brij N. Agrawal	22b. TELEPHONE (*Include Area code*) 408-646-3338	22c. OFFICE SYMBOL AA/Ag

DD FORM 1473, 84 MAR 83 APR edition may be used until exhausted
All other editions are obsolete

Approved for public release; distribution is unlimited.

The Attitude Control of Flexible Spacecraft

by

R. Joseph Watkins Jr.
Lieutenant, United States Navy
B.S.ChE., Auburn University, 1983

Submitted in partial fulfillment
of the requirements for the degree of

MASTER OF SCIENCE IN ASTRONAUTICAL ENGINEERING

from the

NAVAL POSTGRADUATE SCHOOL
June, 1991

ABSTRACT

This thesis details the design of the Naval Postgraduate School's Flexible Spacecraft Simulator and the first attempts at simulation and control of the model. The effect of flexible structures on the attitude control of spacecraft has been a topic of research for many years. Only recently has the technology to actually test models and theory on the ground been available. At the Naval Postgraduate School, an experimental testbed for research into this area has been constructed. This facility consists of a satellite model with a flexible arm floating on air pads to eliminate the effects of friction. The Flexible Spacecraft Simulator will become fully operational in July, 1991. A mathematical model of the system has been constructed and simulations of various maneuvers have been run, utilizing proportional-derivative (PD) control as well as a Linear-Quadratic-Gaussian (LQG) compensator. Results show that both PD and LQG work well for station keeping, but that the LQG compensator is better for slewing the arm.

TABLE OF CONTENTS

I. INTRODUCTION

A. REASON FOR ANALYSIS

The control of flexible spacecraft structures has been a topic for research for several years. Every since Explorer I began it's now famous tumble, dynamicists have been concerned with the effect flexible structures have on spacecraft attitude and control. In the early days of the space program, most satellites and vehicles consisted of rigid bodies with very small, flexible appendages. The effects of these appendages were considered mostly in terms of energy dissipation and in turn the effect on attitude stability. Current spacecraft have much higher power requirements than in the past, thus requiring larger solar arrays. Dish antennas with substantial support structures are being utilized. Lighter structural materials are being employed to save launch costs. Higher pointing accuracies are now required. All of these factors contribute to a wider control bandwidth and a lower structural frequency resulting in the possibility of control/structure interactions. These interactions must be known and controlled in order to meet the demands of the next generation of spacecraft.

In order to determine the effect of flexibility on the control of spacecraft, experiments in the design and location of sensors and actuators as well as the control laws should be conducted. Conducting experiments in space is prohibitively expensive. Simulations on computers are very important and useful, but nonetheless cannot be proven accurate until actually implemented. Conducting experiments on the ground in

a gravity-free environment is impossible. However, by proper design, two-dimensional experiments may be conducted in a frictionless environment.

B. SCOPE OF THESIS

This thesis covers the design of the Naval Postgraduate School's Flexible Spacecraft Simulator or FSS. This experimental testbed was designed for the analysis, simulation and implementation of different control systems for flexible spacecraft. The FSS is a two-dimensional model of a spacecraft with a deployed, flexible, support structure for an antenna. The initial basic design and choice of actuator/sensors was presented in Ward [Ref. 1]. This thesis details the integration of the actuator and sensors as well as the construction of the model. The equations of motion for the model are derived, as well as the state-space form for digital implementation. Finally, the first attempts at simulating the motion and control of the model are presented.

II. EXPERIMENTAL SETUP

The configuration of the experimental setup for the Flexible Spacecraft Simulator, (FSS), is shown in Figure 1.

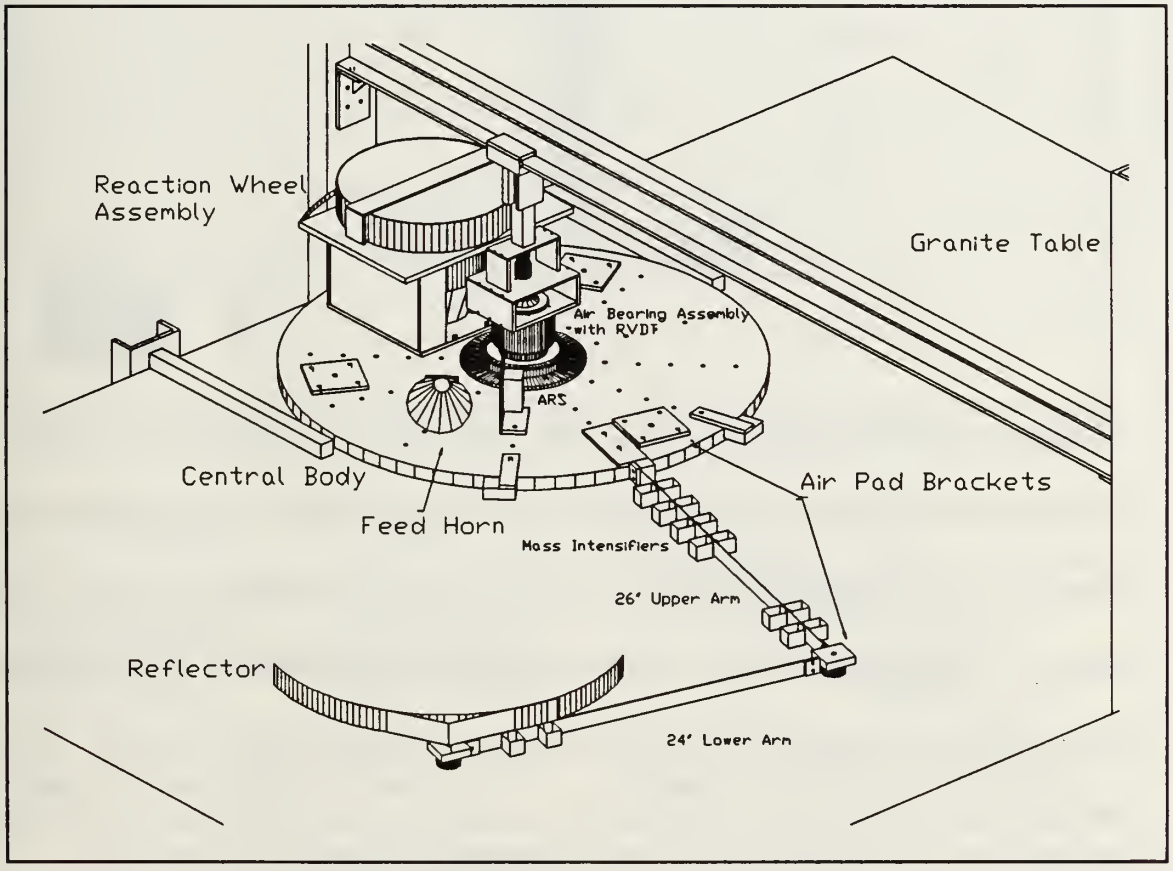

Figure 1 Flexible Spacecraft Simulator

A. SATELLITE MODEL

The satellite model consists of an 'L' shaped flexible appendage attached to a circular rigid body as shown in Figure 2. For this phase of the experiment, the reflector and feed horn are not used. The rigid body, denoted the "central body", is a 2.22 cm

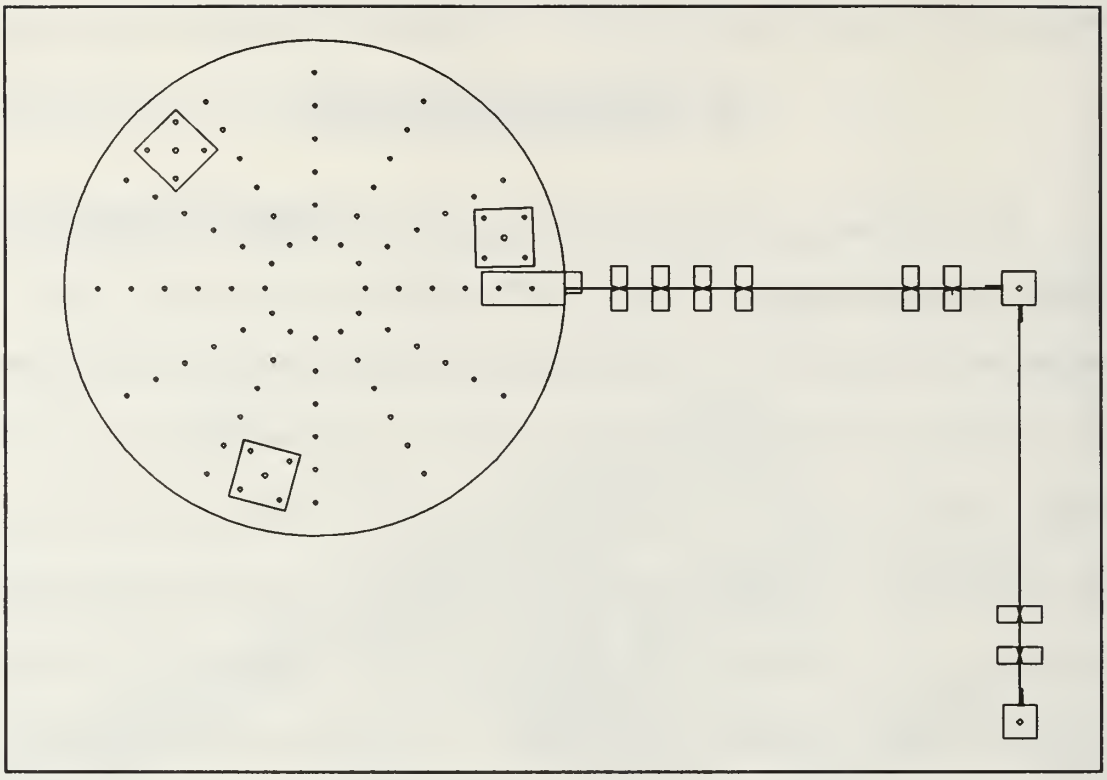

Figure 2: Satellite Model

(7/8 inch) thick aluminum disk of 0.381 m (15 inch) radius. The central body is supported by three aluminum air pads and restricted from translational motion by an air bearing. The air pads are spaced equally about the circumference of the disk and are inset into the central body to minimize the height of the system above the table. The air bearing is connected to the central body by means of a thin, 0.127 mm (0.005 inch), flexible sheet of metal. This reduces the effect of any torque about the X or Y axis upon the air bearing, which has very little tilt stiffness. The top of the air bearing is connected to an I-beam with an adjustable bracket. The bracket and associated movable supports allow positioning of the model anywhere on the table's surface. A cross sectional view of the air support system is shown in the following figures.

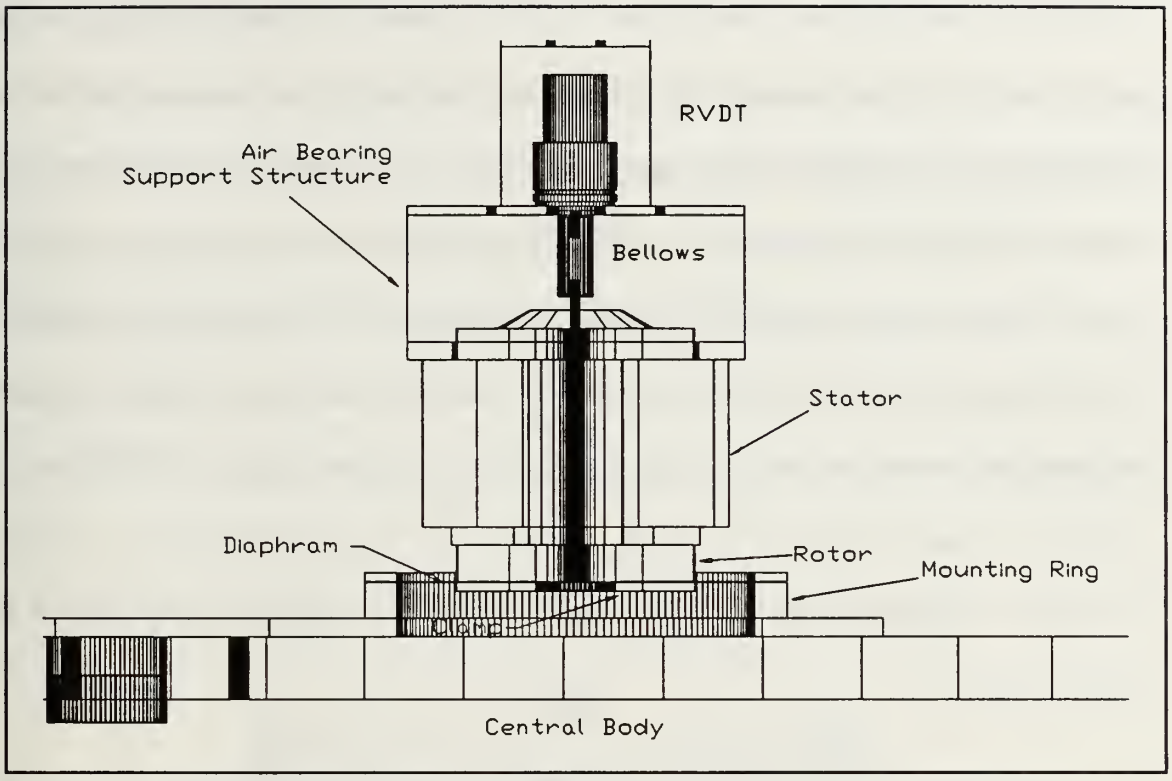

Figure 3 Cross Section of Air Bearing Mounting System

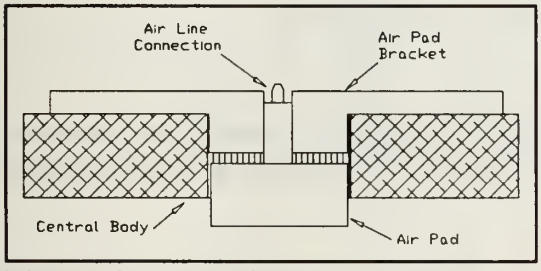

Figure 4 Body Air Pad Mounting

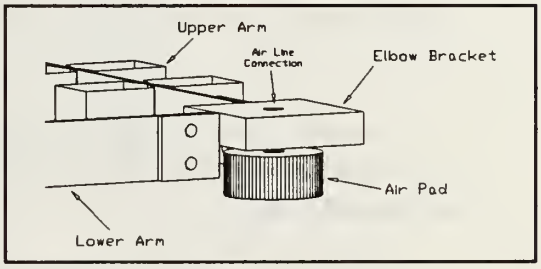

Figure 5 Arm Air Pad Mounting

The flexible appendage, denoted the "arm", is two 2.54 cm (1.0 inch) wide strips of aluminum, 1.58 mm (1/16 inch) thick, joined at the elbow by a bracket, which also supports an air pad. The end point is also a bracket for an air pad. The "upper arm" is connected to the central body by means of a clamped bracket. "Mass intensifiers", [Ref. 2], each with 0.467 kg (1.03 lb) of mass, are utilized to lower the fundamental structural frequency of the arm to about 0.13 Hz. The mass intensifiers are connected

to the arm at a single point, (see Figure 2). This increases the mass of the arm without significantly stiffening the arm. With this setup, large structures with low fundamental frequencies can be simulated using assemblies of much smaller physical dimensions. The upper arm has six mass intensifiers, and the "lower arm" has two at the end. One 0.467 kg (1.03 lb) weight was added to the "elbow" bracket and two weights to the end bracket in order to prevent chatter in the air pads. This combination of weights yields the desired fundamental frequency. 6.35 mm (1/4 inch) air line tubing, 130 PSIG test, is connected to each air pad and to the air bearing from the air supply system. Appendix A contains information concerning the mass, dimensions and inertia properties of the satellite model.

B. SENSORS

Four types of sensors are employed on the satellite model:

1. A rotary variable differential transformer, (RVDT), is connected to the rotor of the air bearing by a bellows-type device. The RVDT senses the angular position of the central body.

2. An angular rate sensor, (ARS), is mounted on the central body and is used to determine the angular speed of the central body.

3. An integral analog tachometer is used by the DC servo motor to report momentum wheel speed.

4. Two accelerometers are connected to the endpoint of the lower arm and sense accelerations at the endpoint.

The manufacturers specifications are given in Appendix B.

C. ACTUATOR

The actuator for the FSS, in this phase of the experiment, is a DC servo motor with a 10.7 kg (23.5 lb) steel disc connected to the shaft. The motor and disc assembly act as a momentum wheel for the satellite model. The entire assembly is housed in a separate aluminum structure which is then attached to the central body. Figure 6 shows the momentum wheel assembly with some of the panels removed for clarity. The DC servo motor is manufactured by PMI and the specifications are given in Appendix B.

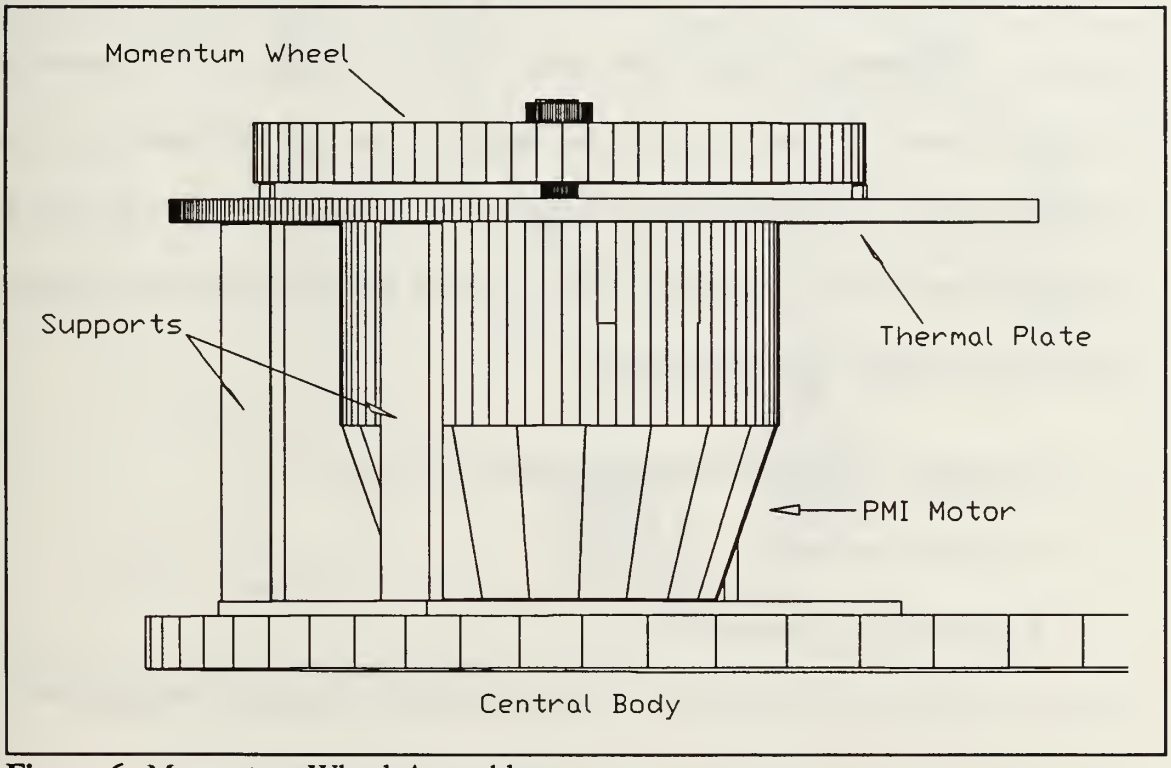

Figure 6: Momentum Wheel Assembly

The motor housing includes a bottom plate which is connected to the central body, a thermal plate to which the motor is mounted, and side panels which support the thermal plate. The size of the thermal plate is dictated by the heat output of the motor during

worst case conditions. The steel wheel is covered by an aluminum safety housing to prevent injury during operation.

D. CONTROLLER

The control system consists of a VAXStation 3100 model 30, (networked to a mainframe VAX), the AC-100 controller, and the associated software for the AC-100. The VAXStation is a 2.8 MIPS (million instructions per second) workstation configured with eight Mbytes of main memory, a 19 inch color monitor, two 104 Mbyte winchester hard disks, and a mouse. The development software, which includes $MATRIX_X$, AutoCode, Interactive Animation, RTMONIT Real-Time Monitor, a 'C' Compiler and the Linker/Loader, is used to create the model of the FSS and executes on the VAXStation under the VMS operating system. The AC-100 Controller provides the real-time testbed execution environment. It consists of the following standard hardware components and their associated drivers:

1. An 80386 based MULTIBUS II Application Processor.
2. An 80387 Coprocessor.
3. A Weitek 3167 Coprocessor.
4. An 80186 based MULTIBUS II Input/Output Communications Processor.
5. A/D, D/A and Digital Data Translation DT2402 I/O Board.
6. Two INX-04 Encoder and D/A Servo Boards.
7. An External Trigger Board for the first application processor.

For details of the operating system see the ***AC-100 Users Guide***, [Ref. 3]. The simplified electrical schematic for the sensors, actuator and controller is shown in Figure 7. The controller, servo-amplifier, power supply and transformer are housed in a 19 inch rack.

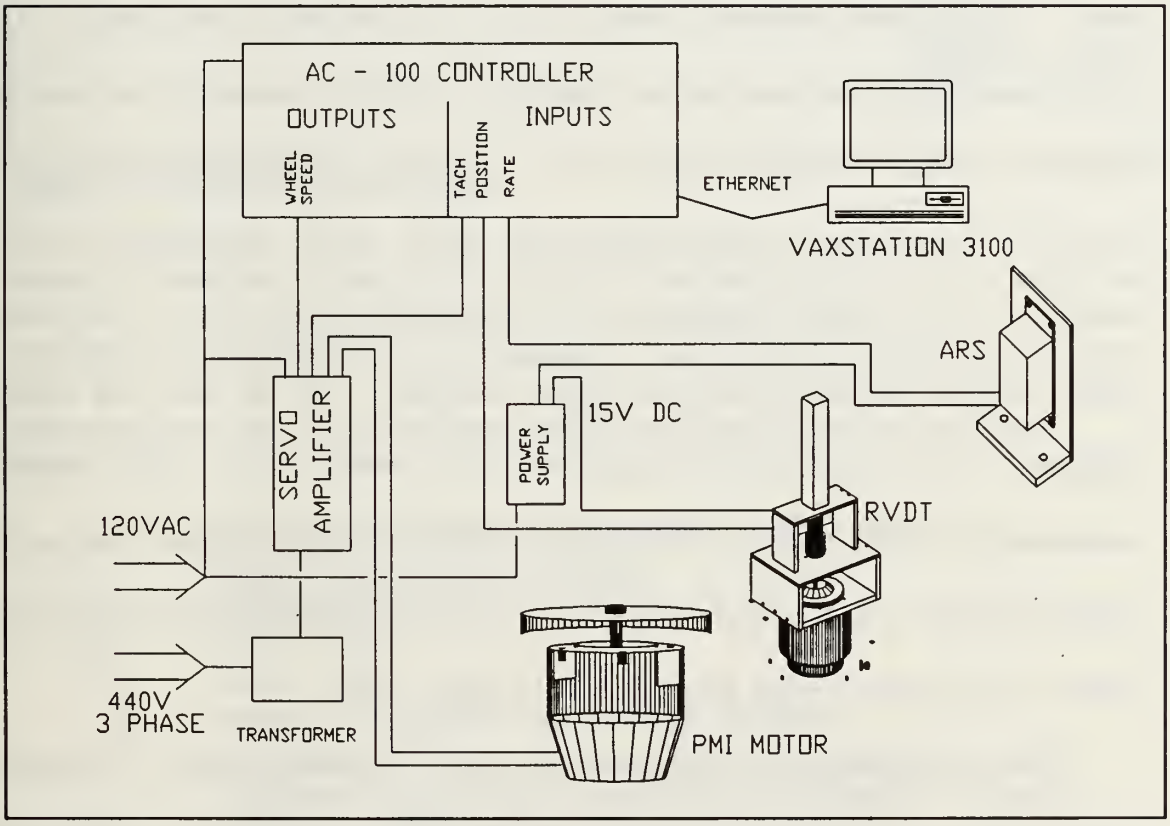

Figure 7 Simplified Electrical Schematic

III. THEORETICAL ANALYSIS

A. EQUATIONS OF MOTION

In order to control the satellite model efficiently, the dynamics of the system must be thoroughly understood. The first step is to determine the equations of motion of the model. The hybrid-coordinate system of Ref. 4 is utilized in this study. The hybrid-coordinate system separates the model into two distinct subsystems which may be classified as either a flexible appendage or a rigid body. The flexible appendage is assumed to be a linearly elastic structure for which "small" deformations may be anticipated such that elastic stresses remain proportional to deformations. The flexible body is further broken up into small rigid "subbodies". In this case, the flexible appendage is the "arm" and the rigid body is the "central body". Each subbody corresponds to a mass intensifier or an air pad bracket on the flexible arm. Lagrange's equation together with the hybrid-coordinate system are used to derive the equations of motion of the model. Figure 8 depicts the coordinate system.

Three coordinate axis are used in the derivation. A fixed, ("inertial"), coordinate system is located at the center of rotation of the system, (constrained by the airbearing to be the center of the rigid body). The origin of the second coordinate system is also located at the center of rotation, rotates with the body, and is the body coordinate system. The third coordinate system is located at the center of mass, (CM) of the system and is the CM coordinate system. The CM and body coordinate axis are parallel to one

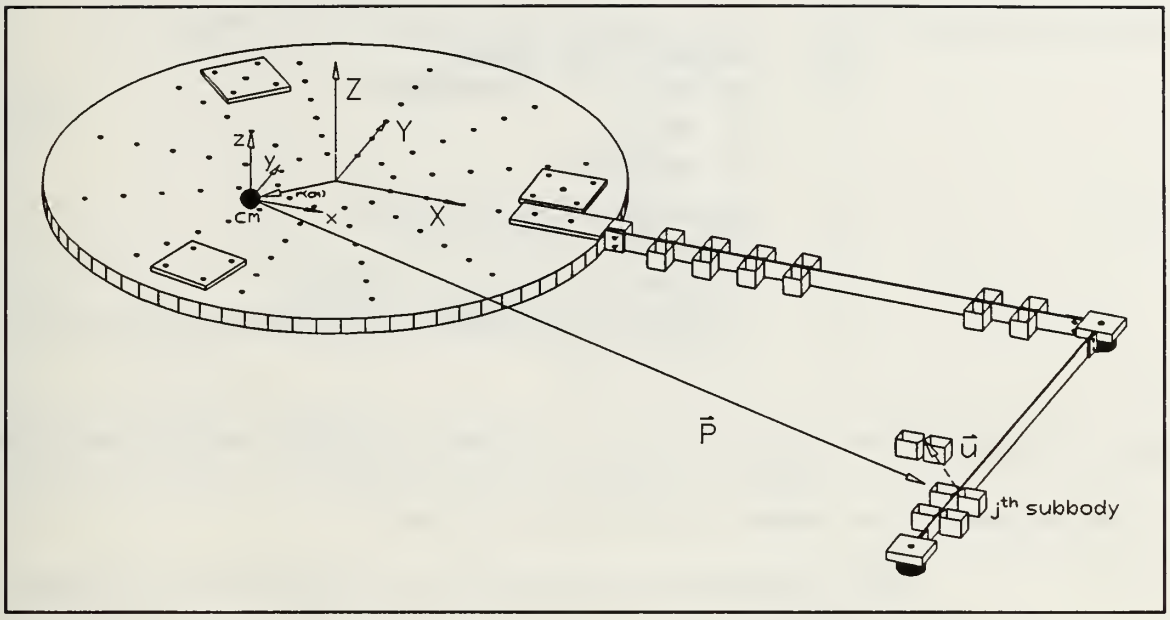

Figure 8 Hybrid-Coordinate System

another. Subscript A corresponds to the flexible appendage, C to the rigid body. Subscript W corresponds to the momentum wheel system and subscript S denotes a subbody on the arm. The other symbols used in the derivation are as follows:

$\vec{V}$ - *VELOCITY VECTOR OF AN INFINITISIMAL MASS*
$\bar{\vec{V}}$ - *VELOCITY OF CM OF SYSTEM*
$\vec{r}$ - *POSITION VECTOR*
M_T - *TOTAL MASS*
M - *MASS*
$\vec{\omega}$ - *ANGULAR VELOCITY VECTOR OF SYSTEM*
$\vec{P}$ - *POSITION VECTOR OF UNDEFORMED SUBBODY*
$\vec{u}$ - *POSITION FROM UNDEFORMED TO DEFORMED SUBBODY*
θ_W - *ANGULAR POSITION OF MOMENTUM WHEEL*
ψ - *ROTATION ABOUT Z (FIXED COORDINATE SYSTEM)*
I - *INERTIA*
ϕ - *MODAL COORDINATE*
q - *MODAL AMPLITUDE*

m - *NUMBER OF MODES*
n - *NUMBER OF SUBBODIES*
i - *i^{th} MODE*
j - *j^{th} SUBBODY*
ω_i - *FREQUENCY OF i^{th} MODE*
ζ - *DAMPING*
T - *KINETIC ENERGY OF SYSTEM*
V - *POTENTIAL ENERGY OF SYSTEM*
L - *LAGRANGIAN*

In order to form the Lagrangian, the potential and kinetic energy of the system must be known. The kinetic energy is found as follows:

$$\begin{aligned} T &= \frac{1}{2}\int_{M_T}(\vec{V}\cdot\vec{V})\,dM + T_W \\ &= \frac{1}{2}M_T\bar{V}^2 + \frac{1}{2}\int_{M_T}\vec{V}\,|^2_{cm}dM + T_W \\ &= \frac{1}{2}M_T[\vec{\omega}\times\vec{r}\,(cm)]^2 + \frac{1}{2}\int_C(\vec{V}_C\cdot\vec{V}_C)\,dM + \frac{1}{2}\int_A(\vec{V}_A\cdot\vec{V}_A)\,dM + T_W \end{aligned} \tag{1}$$

where V_C is the velocity of a particle on body **C** with respect to the CM coordinates and V_A is the velocity of a particle on body **A** with respect to the CM coordinates. The position of the center of mass from the fixed coordinate system is denoted ***r(cm)***, and T_W is the kinetic energy of the system due to the momentum wheel. V_C will be due only to the rotation of the central body:

$$V_C = \dot{\vec{r}} = \vec{\omega}\times\vec{r}_C \tag{2}$$

The over-dot denotes differentiation of the vector with respect to time.

V_A will have both rotational and translational terms. If the assumption is made that:

$$\int_A \vec{V}_A \cdot \vec{V}_A dM \approx \sum_{j=1}^{n} [\vec{V}_j \cdot \vec{V}_j] M_j \tag{3}$$

V_j may be expanded as follows:

$$V_j = \dot{\vec{P}}_j + \dot{\vec{u}}_j = \vec{\omega} \times \vec{P}_j + \dot{\vec{u}}_j + \vec{\omega} \times \vec{u}_j \tag{4}$$

Expanding the dot product of V_j with itself for each subbody, yields:

$$\vec{V}_j \cdot \vec{V}_j = \vec{V}_j \cdot (\vec{\omega} \times \vec{P}_j) + \vec{V}_j \cdot \dot{\vec{u}}_j + \vec{V}_j \cdot (\vec{\omega} \times \vec{u}_j) \tag{5}$$

$$\begin{aligned} \vec{V}_j \cdot \vec{V}_j &= (\vec{\omega} \times \vec{P}_j) \cdot (\vec{\omega} \times \vec{P}_j) + (\vec{\omega} \times \vec{P}_j) \cdot \dot{\vec{u}} + (\vec{\omega} \times \vec{P}_j) \cdot (\vec{\omega} \times \dot{\vec{u}}) \\ &+ \dot{\vec{u}} \cdot (\vec{\omega} \times \vec{P}_j) + \dot{\vec{u}} \cdot \dot{\vec{u}} + \dot{\vec{u}} \cdot (\vec{\omega} \times \vec{u}_j) + (\vec{\omega} \times \vec{u}_j) \cdot (\vec{\omega} \times \vec{P}_j) \\ &+ (\vec{\omega} \times \vec{u}_j) \cdot \dot{\vec{u}} + (\vec{\omega} \times \vec{u}_j) \cdot (\vec{\omega} \times \vec{u}_j) \\ &= |\vec{\omega} \times \vec{P}_j|^2 + 2[(\dot{\vec{u}} \cdot (\vec{\omega} \times \vec{P}_j)) + (\vec{\omega} \times \vec{P}_j) \cdot (\vec{\omega} \times \vec{u}_j) + \dot{\vec{u}} \cdot (\vec{\omega} \times \vec{u}_j)] \\ &+ |\dot{\vec{u}}|^2 + |\vec{\omega} \times \vec{u}_j|^2 \end{aligned} \tag{6}$$

Finally, expanding the kinetic energy term due to the momentum wheel:

$$T_W = \frac{1}{2}M_W[(\vec{\omega}\times\vec{r}(W))\cdot(\vec{\omega}\times\vec{r}(W))] + \frac{1}{2}I_W\dot{\theta}_W^2 \tag{7}$$

where ***r(W)*** is the vector from the origin of the fixed coordinate system to the center of the momentum wheel.

Utilizing the constraints of the experimental setup and the superscripts x, y and z to denote components of a vector along the CM coordinate axis, the vector equations are replaced by the following:

$$\begin{aligned}
\vec{\omega} &= \dot{\Psi}\hat{k} \\
\vec{\omega}\times\vec{P}_j &= (-\dot{\Psi}P_j^y)\hat{i} + (\dot{\Psi}P_j^x)\hat{j} \\
\vec{\omega}\times\vec{u}_j &= (-\dot{\Psi}u_j^y)\hat{i} + (\dot{\Psi}u_j^x)\hat{j} \\
\therefore \vec{V}_j\cdot\vec{V}_j &= \dot{\Psi}^2\left[(P_j^x)^2 + (P_j^y)^2\right] + \dot{u}_j^x(\dot{u}_j^x - 2\dot{\Psi}P_j^y - 2\dot{\Psi}u_j^y) \\
&\quad + \dot{u}_j^y(\dot{u}_j^y + 2\dot{\Psi}P_j^x + 2\dot{\Psi}u_j^x) \\
&\quad + u_j^x[\dot{\Psi}^2(2P_j^x + u_j^x)] \\
&\quad + u_j^y[\dot{\Psi}^2(2P_j^y + u_j^y)]
\end{aligned} \tag{8}$$

Noting that the components of the deflection vector, $\vec{u}$, may be written as below:

$$u_j^x = \sum_{i=1}^{m}\phi_{ij}^x q_i(t), \qquad u_j^y = \sum_{i=1}^{m}\phi_{ij}^y q_i(t), \tag{9}$$

the kinetic energy of the system may now be written in terms of the modal coordinates and amplitudes, and the systems angular velocity:

$$
\begin{aligned}
T = {} & \frac{1}{2}\dot{\Psi}^2[M_T|r(cm)|^2 + \int_C |\vec{r}_C|^2 dM + \sum_{j=1}^{n} M_j|\vec{P}_j|^2] \\
& + \frac{1}{2}M_W\dot{\Psi}^2|\vec{r}_W|^2 + \frac{1}{2}I_W\dot{\theta}_W^2 \\
& + \frac{1}{2}\sum_{j=1}^{m}\sum_{i=1}^{n}\{M_j[(\phi_{ij}^x)^2\dot{q}_i^2 + 2\dot{\Psi}(\phi_{ij}^y\dot{q}_i P_j^x - \phi_{ij}^x\dot{q}_i P_j^y) + (\phi_{ij}^y)^2\dot{q}_i^2 \\
& + 2\dot{\Psi}^2(\phi_{ij}^x q_i P_j^x + \phi_{ij}^y q_i P_j^y) + \dot{\Psi}^2[(\phi_{ij}^x)^2 q_i^2 + (\phi_{ij}^y)^2 q_i^2]\}
\end{aligned}
\tag{10}
$$

The first term in the brackets is the inertia of the system about the **Z** axis (fixed coordinate system), minus the terms due to the momentum wheel itself, or:

$$
I_{ZZ}^o = M_T|\vec{r}(cm)|^2 + \int_C |\vec{r}_C|^2 dM + \sum_{j=1}^{n} M_j|\vec{P}_j|^2 \tag{11}
$$

The potential energy is now calculated using standard matrix notation:

$$
\begin{aligned}
V &= \frac{1}{2}[u]^T[k][u] \qquad [u] = [\phi][q] \\
&= \frac{1}{2}[q]^T[\phi]^T[k][\phi][q]
\end{aligned}
\tag{12}
$$

where ***[k]*** is the stiffness matrix. If ***[ϕ]*** is normalized such that the mass matrix is unity, then

$$
[\phi]^T[k][\phi] = \begin{bmatrix} \ddots & & \\ & \omega_i^2 & \\ & & \ddots \end{bmatrix} \tag{13}
$$

where the term on the right is the diagonal matrix of natural frequencies for each mode. This results in:

$$V = \frac{1}{2}[q]^T \begin{bmatrix} \ddots & & \\ & \omega_i^2 & \\ & & \ddots \end{bmatrix} [q] \qquad (14)$$
$$= \frac{1}{2}\sum_{i=1}^{m} q_i^2 \, \omega_i^2$$

Now that the potential and kinetic energy of the system have been determined, the Lagrangian, $L = T - V$, may be formed. Lagrange's equation is written:

$$\frac{d}{dt}\left(\frac{\partial L}{\partial \dot{\mu}_i}\right) - \frac{\partial L}{\partial \mu_i} = Q_i \qquad (15)$$

with each generalized coordinate represented by μ_i and the generalized forces by Q_i. The generalized coordinates for this system are Ψ, θ_W, and each of the q_i's. The virtual work principle may be utilized to determine the Q_i's. Taking N to be the total number of generalized coordinates:

$$\delta w = \sum_{i=1}^{N} Q_i \cdot \delta \mu_i = T\delta\Psi - T\delta\theta_W \qquad (16)$$
$$\therefore \quad Q_{\theta_W} = -T \qquad Q_\Psi = T$$

where T is the torque applied by the motor. Lagrange's equation for each of the generalized coordinates can now be written as follows:

$$I_W\ddot{\theta}_W = -T \qquad (17)$$

$$I_{ZZ}^{o}\ddot{\Psi} + \sum_{j=1}^{n}\sum_{i=1}^{m}\Big\{\Big[M_j\Big(2\phi_{ij}^{x}P_j^{x}q_i + (\phi_{ij}^{x})^2q_i^2 + 2\phi_{ij}^{y}P_j^{y}q_i + (\phi_{ij}^{y})^2q_i^2\Big) + M_W|\vec{r}(W)|^2\Big]\ddot{\Psi}$$
$$+ M_j\Big[\phi_{ij}^{y}P_j^{x} - \phi_{ij}^{x}P_j^{y}\Big]\ddot{q}_i$$
$$+ M_j\Big[2\phi_{ij}^{x}P_j^{x} + 2(\phi_{ij}^{x})^2q_i + 2\phi_{ij}^{y}P_j^{y} + 2(\phi_{ij}^{y})^2q_i\Big]\dot{\Psi}\dot{q}_i\Big\} = T$$

(18)

$$\sum_{j=1}^{n}\Big\{M_j\Big[(\phi_{ij}^{x})^2 + (\phi_{ij}^{y})^2\Big]\ddot{q}_i - \Big[M_j\Big((\phi_{ij}^{x})^2 + (\phi_{ij}^{y})^2\Big) - \omega_i^2\Big]q_i$$
$$- M_j\Big[\phi_{ij}^{x}P_j^{x} + \phi_{ij}^{y}P_j^{y}\Big]\dot{\Psi}^2 + M_j\Big[\phi_{ij}^{y}P_j^{x} - \phi_{ij}^{x}P_j^{y}\Big]\ddot{\Psi}\Big\} = 0 \qquad \textbf{(19)}$$

Equation (19) above is repeated for each of the m modes. Assuming that the body slew rate is small, the nonlinear terms will tend toward zero. Dropping the nonlinear terms and introducing a damping term for each mode yields the following linearized equations of motion:

$$I_{ZZ}^{ol}\ddot{\Psi} + \sum_{i=1}^{m}D_i\ddot{q}_i = T = -I_W\ddot{\theta}_W$$
$$E_i\ddot{q}_i + 2\zeta\omega_i\dot{q}_i + (\omega_i)^2q_i + D_i\ddot{\Psi} = 0$$

$$\text{where: } I_{ZZ}^{ol} = I_{ZZ}^{o} + M_W|\vec{r}(W)|^2 \qquad \textbf{(20)}$$
$$D_i = \sum_{j=1}^{n}\Big[\phi_{ij}^{y}P_j^{x} - \phi_{ij}^{x}P_j^{y}\Big]M_j$$
$$E_i = \sum_{j=1}^{n}\Big[(\phi_{ij}^{x})^2 + (\phi_{ij}^{y})^2\Big]M_j$$

Again, the last equation is repeated for each of the m modes, resulting in $m + 1$ equations to be solved in order to determine the motion of the model. The D_i term is designated the flexible coupling term and E_i is the modal mass term. If the modal

coordinates, ϕ_{ij}, are normalized such that the mass matrix is unity, then E_i will also be unity. This fact is used to check the results of the finite element analysis of the arm. The damping term ζ must be assumed or experimentally determined.

In order to implement the equations on a digital computer, a state-space representation of the system of equations is constructed. The state-space format is:

$$\begin{aligned} \dot{X} &= [A]X + [B]U \\ Y &= [C]X + [D]U \end{aligned} \tag{21}$$

where X is the vector of state variables, Y is the output vector, and U is the vector of inputs. The matrices A, B, C and D complete the description of the system of equations in state-space form. For the FSS, the state variables are chosen to be:

$$X = \left[\Psi,\ q_1,\ q_2,\ \ldots,\ q_m,\ \dot{\Psi},\ \dot{q}_1,\ \dot{q}_2,\ \ldots,\ \dot{q}_m\right]^T \tag{22}$$

The output vector Y, is defined by the sensors installed on the model:

$$Y = \left[\Psi,\ \dot{\Psi}\right]^T \tag{23}$$

The input vector U is the torque applied by the motor:

$$U = \mathrm{T} \tag{24}$$

Rearranging the equations of motion to explicitly solve for the second derivative with respect to time of the state variables, in terms of the state variables and the input torque T:

$$\ddot{\Psi} = \frac{T + \sum_{i=1}^{m}\left[2\zeta\omega_i\dot{q}_i + D_i(\omega_i)^2 q_i\right]}{I_{ZZ}^{ol} - \sum_{i=1}^{m}(D_i)^2}$$

$$\ddot{q}_i = -(\omega_i)^2 q_i - 2\zeta\omega_i\dot{q}_i - D_i\left[\frac{\sum_{i=1}^{m}\left[D_i\left(2\zeta\omega_i\dot{q}_i + (\omega_i)^2 q_i\right)\right] - T}{I_{ZZ}^{ol} - \sum_{i=1}^{m}(D_i)^2}\right] \tag{25}$$

Note that if a rigid body were assumed, all of the $\mathbf{q_i}$'s and $\dot{\mathbf{q}}_\mathbf{i}$'s would be zero and Euler's equation would result:

$$\ddot{\Psi} = \frac{T}{I_{ZZ}} \tag{26}$$

The state-space representation can now be written as follows:

$$\begin{bmatrix} \dot{\Psi} \\ \dot{q}_1 \\ \dot{q}_2 \\ \vdots \\ \dot{q}_m \\ \ddot{\Psi} \\ \ddot{q}_1 \\ \ddot{q}_2 \\ \vdots \\ \ddot{q}_m \end{bmatrix} = \left(\frac{1}{I_{ZZ}^{o2}}\right) \begin{bmatrix} 0 & 0 & 0 & 0 & \dots & 0 & I_{ZZ}^{o2} & 0 & 0 & \dots & 0 \\ 0 & 0 & 0 & 0 & \dots & 0 & 0 & I_{ZZ}^{o2} & 0 & \dots & 0 \\ 0 & 0 & 0 & 0 & \dots & 0 & 0 & 0 & I_{ZZ}^{o2} & \dots & 0 \\ \vdots & & & \vdots & & \vdots & & & \vdots & & \vdots \\ 0 & 0 & 0 & 0 & \dots & 0 & 0 & 0 & 0 & \dots & I_{ZZ}^{o2} \\ 0 & F_1 & F_2 & F_3 & \dots & F_m & H_1 & H_2 & H_3 & \dots & H_m \\ 0 & -G_1 & -D_1F_2 & -D_1F_3 & \dots & -D_1F_m & -J_1 & -D_1H_2 & -D_1H_3 & \dots & -D_1H_m \\ 0 & -D_2F_1 & -G_2 & -D_2F_3 & \dots & -D_2F_m & -D_2H_1 & -J_2 & -D_2H_3 & \dots & -D_2H_m \\ \vdots & & & \vdots & & \vdots & & & \vdots & & \vdots \\ 0 & -D_mF_1 & -D_mF_2 & -D_mF_3 & \dots & -G_m & -D_mH_1 & -D_mH_2 & -D_mH_3 & \dots & -J_m \end{bmatrix} \begin{bmatrix} \Psi \\ q_1 \\ q_2 \\ q_3 \\ \vdots \\ q_m \\ \dot{\Psi} \\ \dot{q}_1 \\ \dot{q}_2 \\ \vdots \\ \dot{q}_m \end{bmatrix} \quad (27)$$

$$+ \left(\frac{1}{I_{ZZ}^{o2}}\right) \begin{bmatrix} 0 \\ 0 \\ 0 \\ 0 \\ \vdots \\ 0 \\ 1 \\ -D_1 \\ -D_2 \\ \vdots \\ -D_m \end{bmatrix} (T)$$

$$\text{where: } I_{ZZ}^{o2} = I_{ZZ}^{o1} - \sum_{i=1}^{m} (D_i)^2, \; F_i = D_i\omega_i^2$$

$$G_i = \omega_i^2 I_{ZZ}^{o2} + D_i F_i, \qquad H_i = 2\zeta\,\omega_i D_i \qquad (28)$$

$$J_i = 2\zeta\,\omega_i I_{ZZ}^{o2} + D_i H_i$$

The observation equation is written below:

$$\begin{bmatrix} \Psi \\ \dot{\Psi} \end{bmatrix} = \begin{bmatrix} 1 & 0 & 0 & \dots & 0 & 0 & 0 & 0 & \dots & 0 \\ 0 & 0 & 0 & \dots & 0 & 1 & 0 & 0 & \dots & 0 \end{bmatrix} \begin{bmatrix} \Psi \\ q_1 \\ q_2 \\ \vdots \\ q_m \\ \dot{\Psi} \\ \dot{q}_1 \\ \dot{q}_2 \\ \vdots \\ \dot{q}_m \end{bmatrix} + [0]\,(T) \qquad (29)$$

B. FINITE ELEMENT MODEL OF APPENDAGE

In order to utilize the state-space equations written above, the mode shapes and associated frequencies must be determined. For simple geometries, the required modal coordinates and natural frequencies may be solved for by analytical means. However, for complex geometries such as the FSS, a finite element analysis is required. The interactive finite element program GIFTS was utilized to model the arm.

The appendage was modeled using beam elements with the same cross-section as the model's arm, and point masses at the location of the mass intensifiers. Point masses were also placed at the elbow and tip to simulate the air pad brackets, air pads and associated masses. The appendage was divided into 20 nodes, each corresponding to a subbody in the hybrid-coordinate system. All degrees of freedom were suppressed at

node one, (the central body attachment point), resulting in a fixed-free analysis. The rotations about the **X** and **Y** axis were also suppressed for all the nodes, in order to more closely approximate the constraints imposed by the two dimensional model. The modal analysis program was run resulting in the desired modal coordinates, normalized for a unity mass matrix, and the associated natural frequencies. The first six mode shapes are shown below.

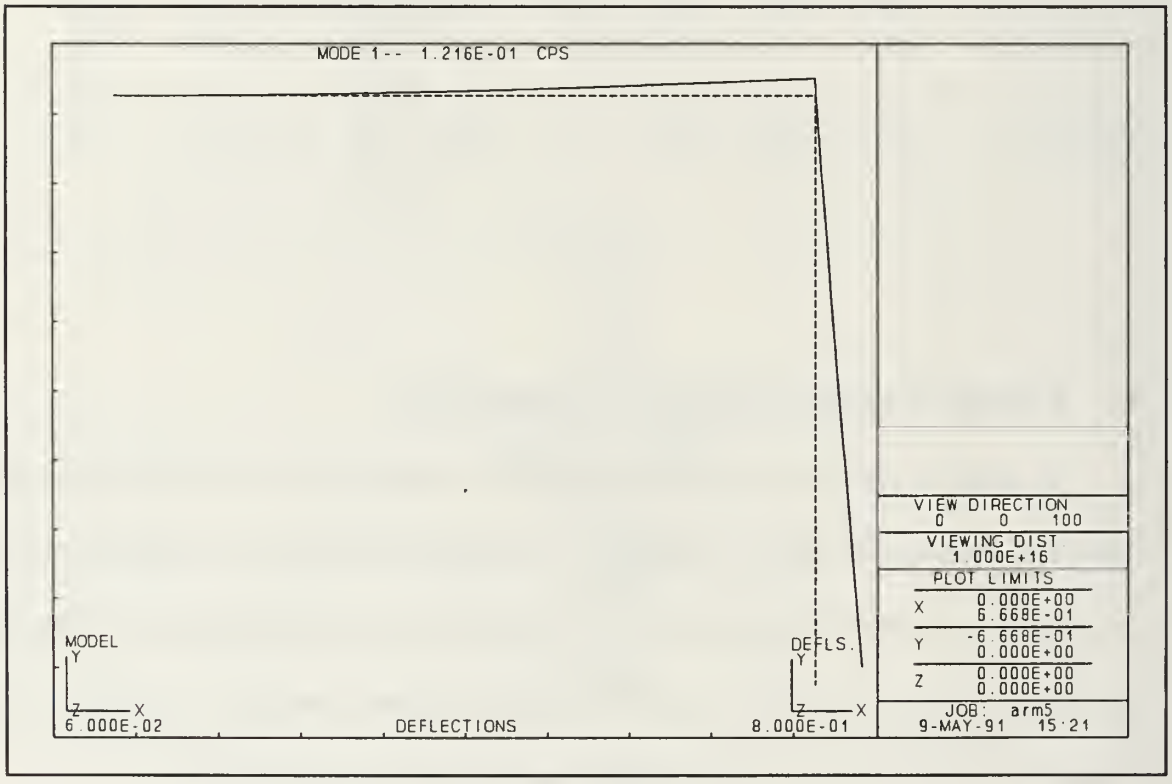

Figure 9 Mode Shape One

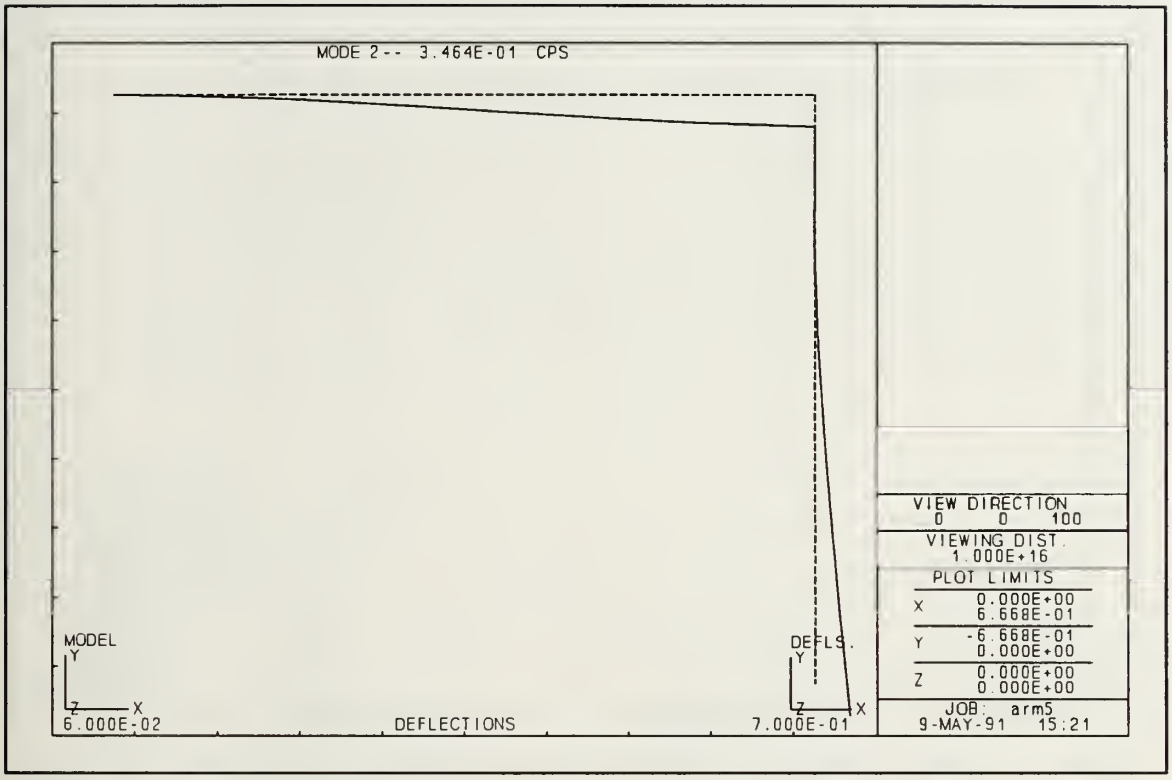

Figure 10 Mode Shape Two

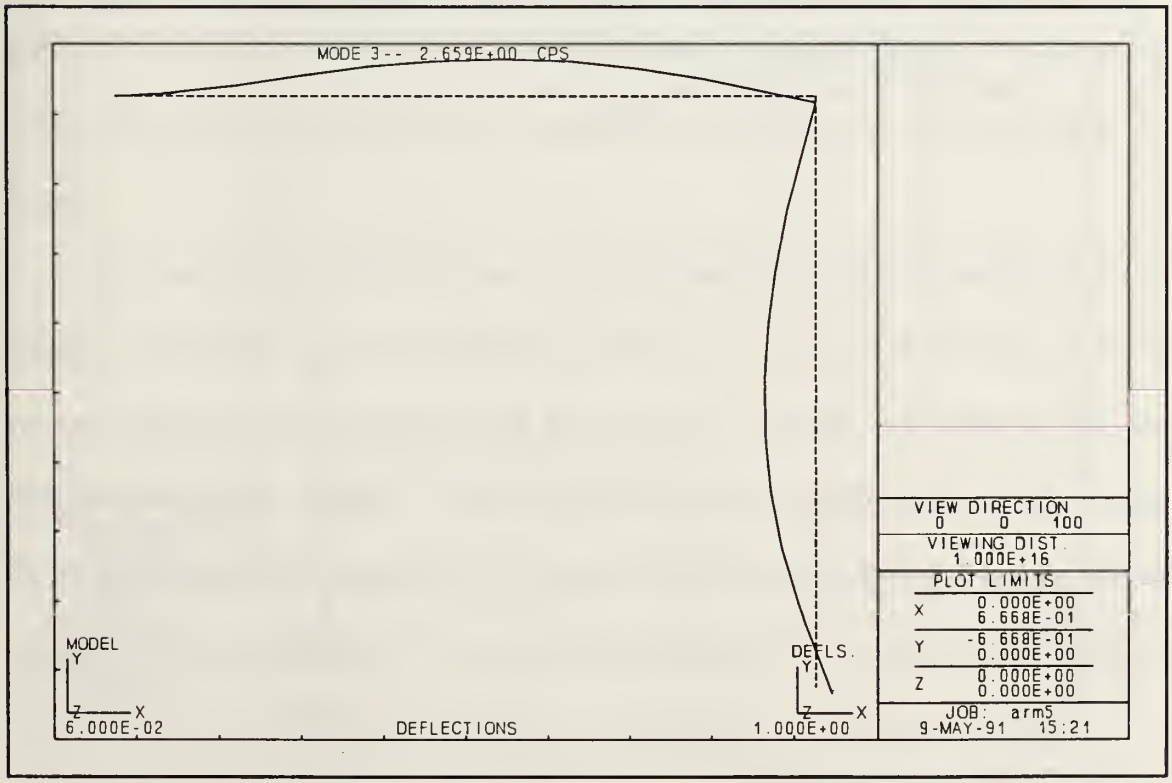

Figure 11 Mode Shape Three

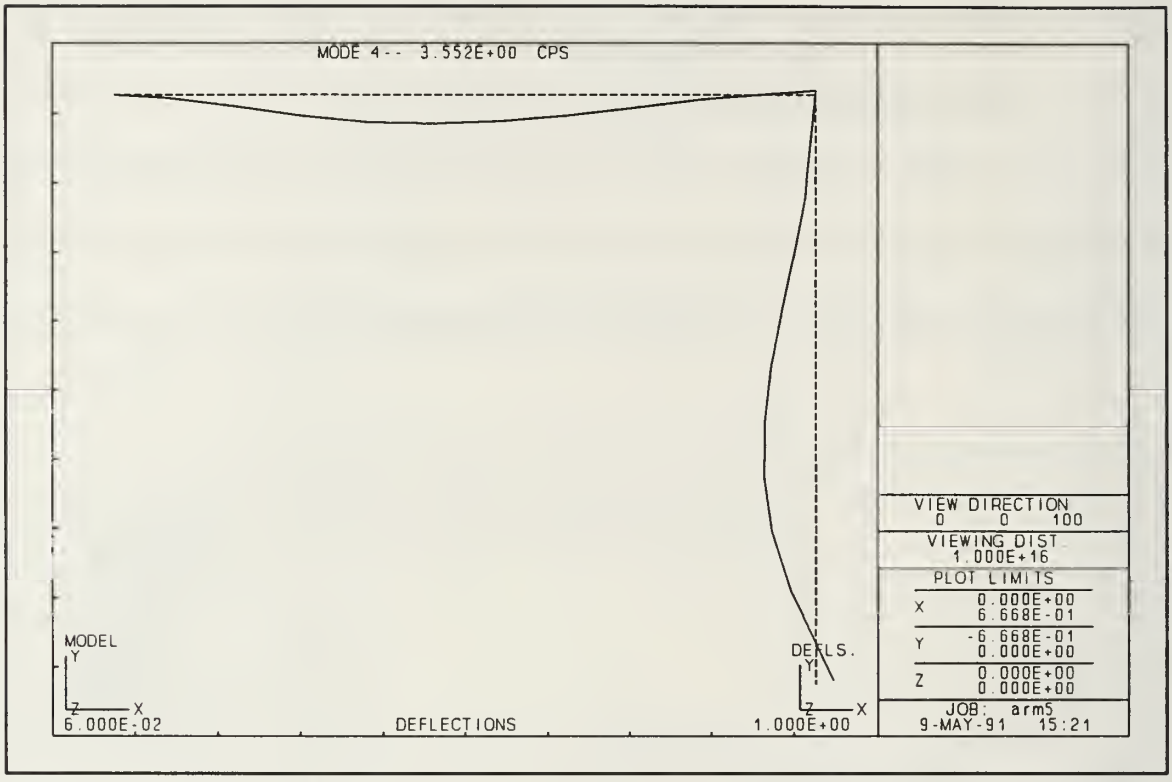

Figure 12 Mode Shape Four

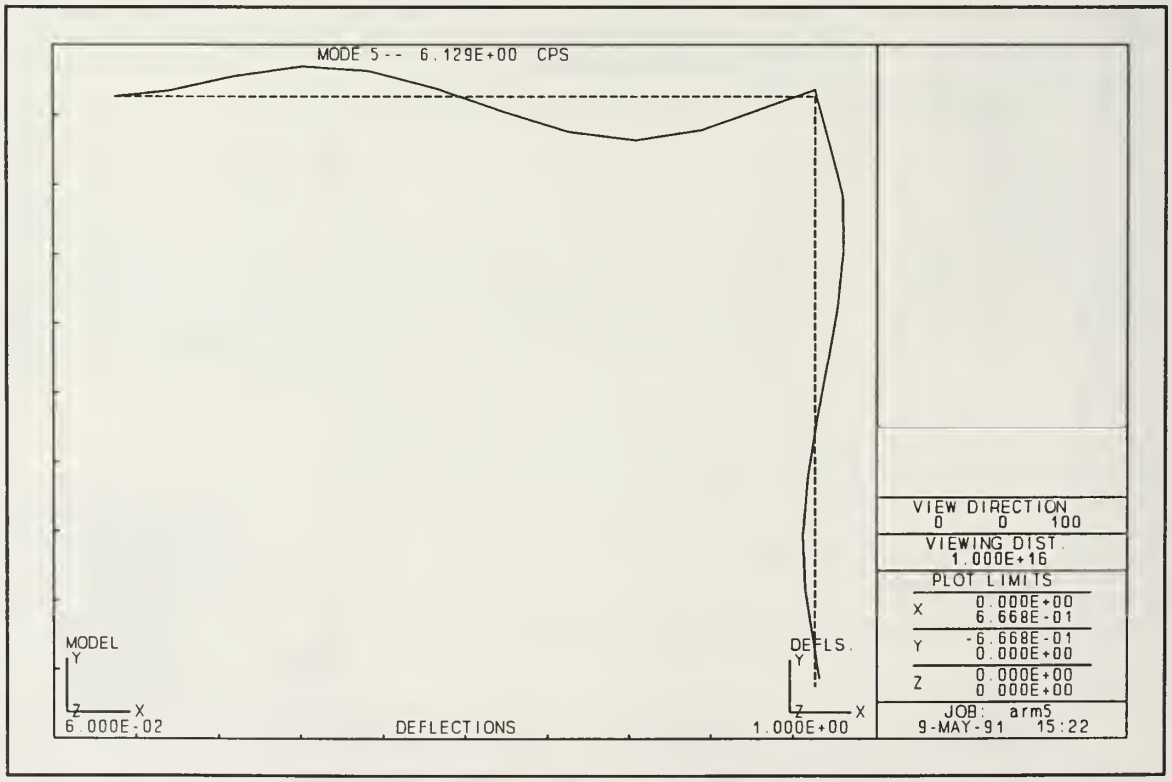

Figure 13 Mode Shape Five

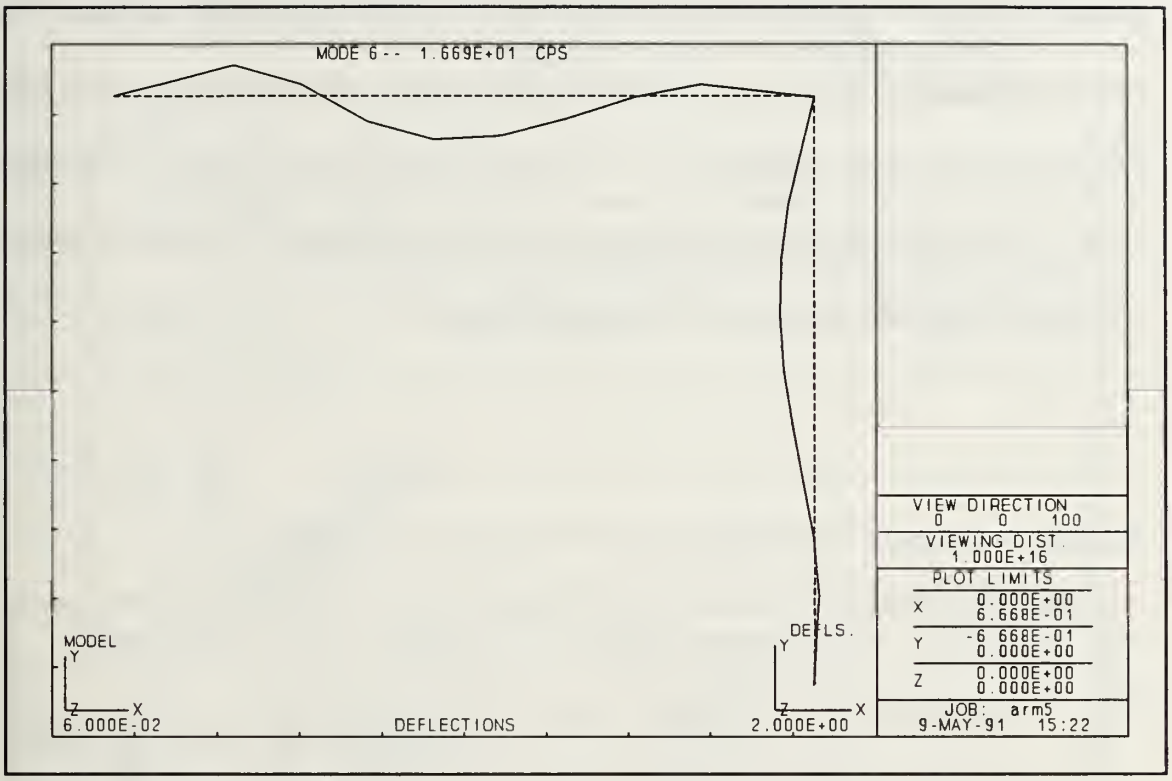

Figure 14 Mode Shape Six

The output of the GIFTS program is given in Appendix C. Also given is a Fortran program that inputs the GIFTS result and outputs the ***A*** and ***B*** matrices of the state-space system described previously, in a form required by $MATRIX_X$ for use in modeling the system.

As a check on the GIFTS output, an experiment was conducted on the model to determine the fixed-free natural frequencies of the arm. The model was floated on the air pads and the central body restrained from rotation. The arm was deflected into the first mode shape and released. The accelerations at the endpoint were measured using the PCB accelerometer, (described in Appendix B), and a HP-3561A Dynamic Signal Analyzer. The accelerometer was mounted perpendicular to the lower arm. Table I

shows the results. Figure 15 and Figure 16 show the actual output of the analyzer. The first two frequencies agree very well with the GIFTS data. Any frequencies above mode two had too low of an amplitude to be measured accurately and could not be verified. Even initially deflecting the arm into these mode shapes resulted in very low amplitude oscillations, not measurable by the installed equipment.

TABLE I Comparison of GIFTS Data with Experimental Results

Mode	Experimental	GIFTS	Difference
one	0.13 Hz	0.122 Hz	-6%
two	0.39 Hz	0.346 Hz	-11.3%

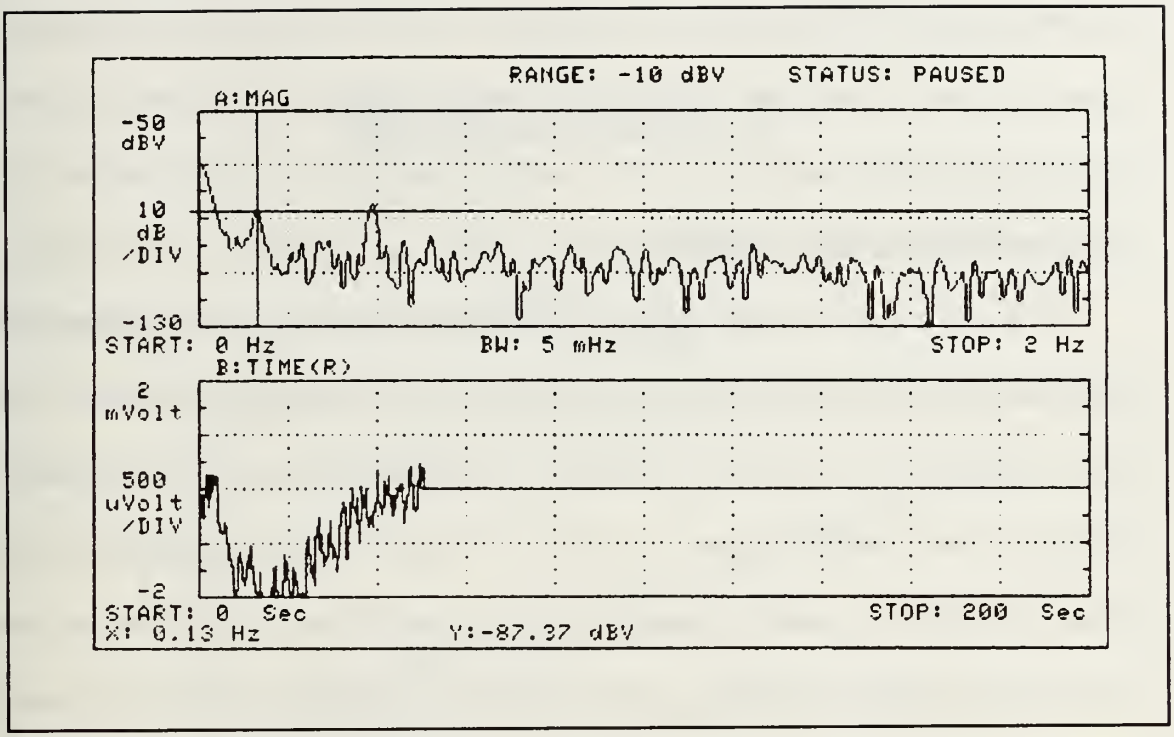

Figure 15 First Modal Frequency

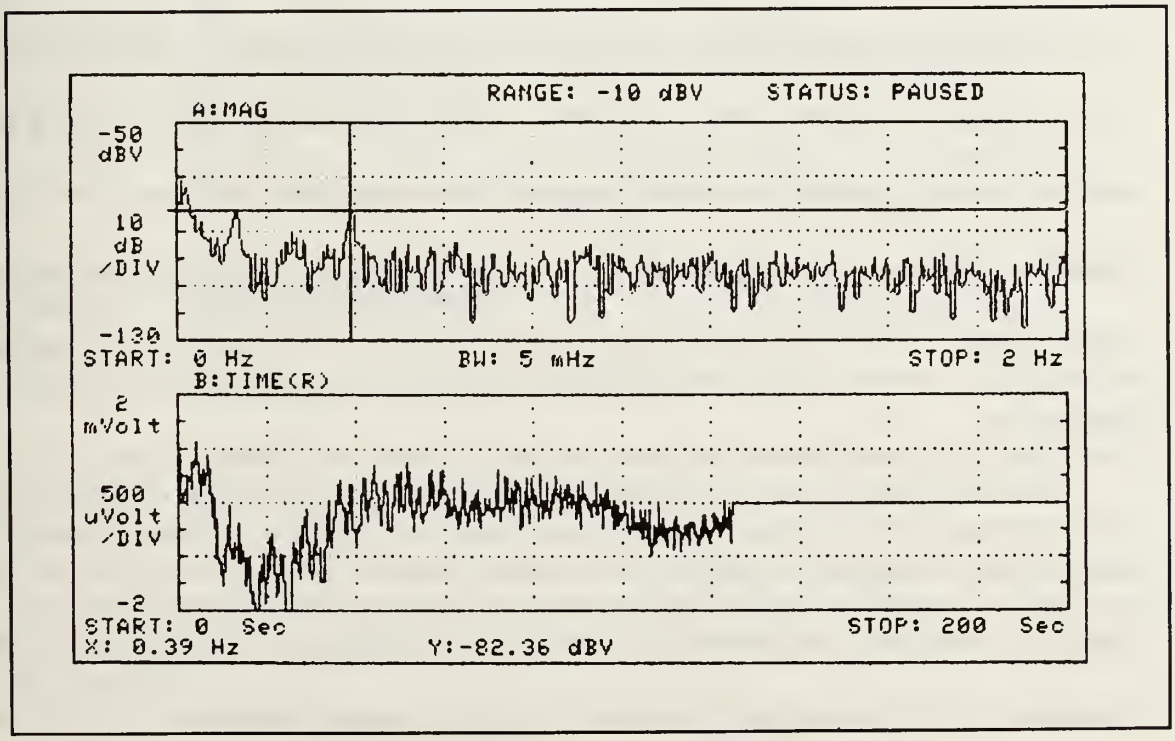

Figure 16 Second Modal Frequency

IV. DYNAMIC SIMULATION

A. MATHEMATICAL MODEL

As a step in understanding the FSS and in attempting to control it, a mathematical model was constructed. The mathematical model can also be used as an observer in the control system, since only two of the state variables may be fed back. In constructing this model, the number of modes, m, must be truncated to some reasonable number. Modal truncation is a matter of importance and demands some study. However, since there are no sensors or actuators on the arm that are to be used in the present control system, a simple algorithm was used. As a minimum, include those modes that are observed in the motion of the arm, but do not include so many modes that the resulting matrices will be computationally difficult and time consuming to solve. As a result, the first six modes were used in the simulation. In deflecting the arm and observing the resulting motion, the first two modes appeared to be prevalent, with very little high frequency motion. Six modes result in a 14 by 14 dynamics matrix which may be readily solved. The first six modes also cover a factor of 100 increase in the natural frequencies.

The state-space system is generated by the Fortran program Form ,(Appendix C), assuming that structural damping of the aluminum beam is two per cent of critical. The system of matrices is implemented on the VAX workstation. In order to use the simulation to run the real time controller, the 'plant' must be discretized. A 0.01 sec

sampling interval was chosen for the discretization, giving approximately ten samples per period of mode six, the highest frequency mode shape simulated. A one N-m torque of 0.1 second duration was simulated to observe the effects of the flexible appendage. This impulse was also simulated on a rigid body with the same mass and inertia properties. The resulting position and rates are plotted in Figure 17.

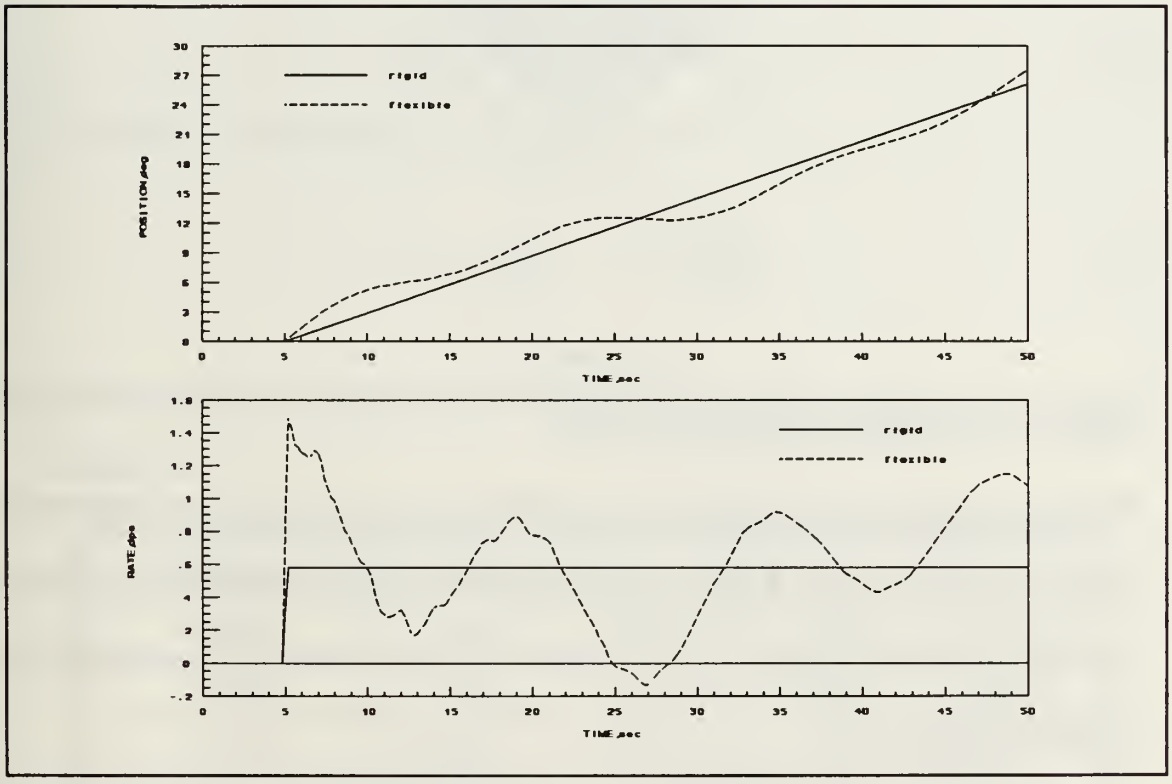

Figure 17 Rigid vs. Flexible Model

These results clearly show the impact of flexibility on attitude control. The rigid body has a smooth transition to rotation about its center of mass whereas the flexible model begins to oscillate, damping out after several hundred seconds. The large variation in body rates for the flexible model is due to the springing action of the arm, as can be seen in Figure 18.

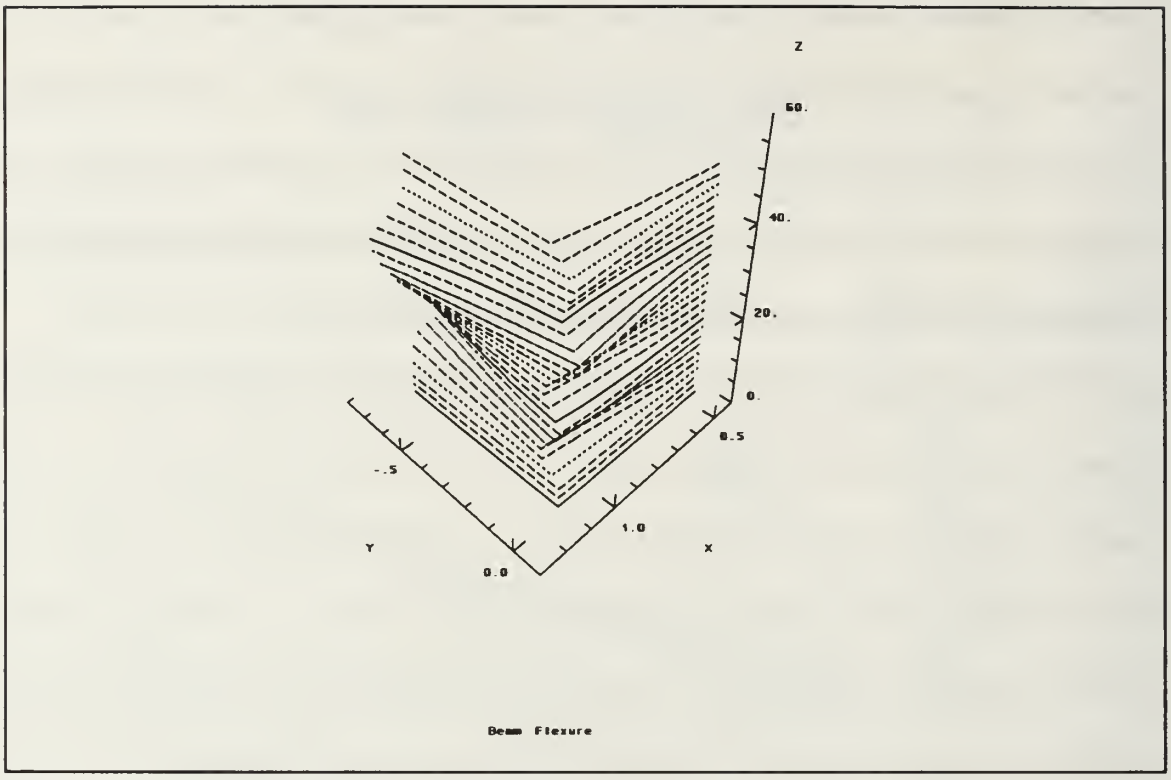

Figure 18 Arm Motion Following Impulse

In the figure above, the position of the arm with respect to the main body is plotted on the **X** and **Y** axis. The **Z** axis represents time in seconds. The arm's position is presented every two seconds. This format will be used to show the motion of the arm during a maneuver.

The next step is to determine the control laws for the flexible model. Each type of control will be subjected to a one N-m impulse, a five degree bias maneuver, and a 30 degree counter-clockwise slew maneuver to determine viability.

B. PROPORTIONAL-DERIVATIVE CONTROL

Proportional-derivative (PD) control is obtained by simply feeding back the body position, Ψ, and the body rate, $\dot{\Psi}$, through a gain block. Three control system

frequencies were chosen: ω_c = 0.05, 0.1 and 0.38 Hz. The first frequency was chosen to minimize control-structural interactions. The second and third were chosen to analyze the effect of a control system operating at the first and second mode's frequencies. Damping, ζ, was chosen as 0.707 of critical. One simulation was run with ζ at critical damping. The gains, K and τ in the control law

$$T_W = -K(\tau\dot{\theta} + \theta) \tag{30}$$

are calculated by the equations, (see Ref. 5):

$$K = \frac{\omega_c^2}{I_{zz}}, \quad \tau = \frac{2\zeta I_{zz}}{K} \tag{31}$$

The values for K and τ are given in the table below.

TABLE II

Designation	ω_c,Hz	ζ	K	τ
PD1A	0.05	0.707	0.98	4.48
PD1B	0.05	1.00	0.98	6.35
PD2	0.10	0.707	3.91	2.25
PD3	0.38	0.707	56.44	0.59

The impulse response, bias and slew maneuvers for PD1A are shown in the following graphs, (Figure 19, Figure 20 and Figure 21). In the graphs, the momentum wheel speed in RPM, wheel torque in N-m, body position in degrees, and body rate in degrees per second, (dps), are plotted versus time in seconds. PD1B shows little

difference from PD1A except in the slew maneuver. PD1B takes about twice as long to reach 30 degrees as PD1A, with very little overshoot, as can be seen in Figure 22. Figure 23 shows the modal amplitudes for modes one and two, (**q1** and **q2**), for the 0.05 Hz system. Modes three through six can just be seen between zero and ten seconds into the slew maneuver. Figure 24 shows the motion of the arm during the first 25 seconds of the slew, while Figure 25 is a "top" view of the motion which shows the extent of movement of the arm. Figure 24 and Figure 25 is obtained by multiplying the modal amplitudes as a function of time by the modal coordinates for each node, summing over all the modes and adding this value to the position of the undeformed node with respect to the center of rotation.

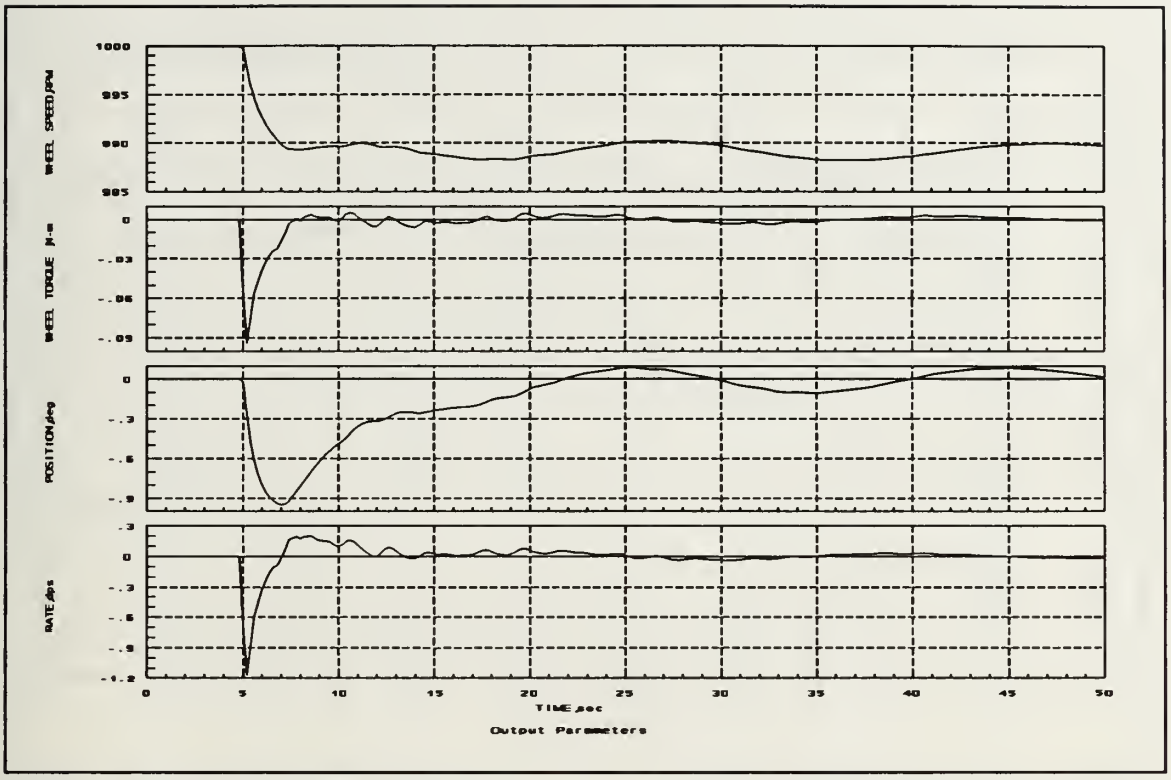

Figure 19 Impulse Response, PD1A

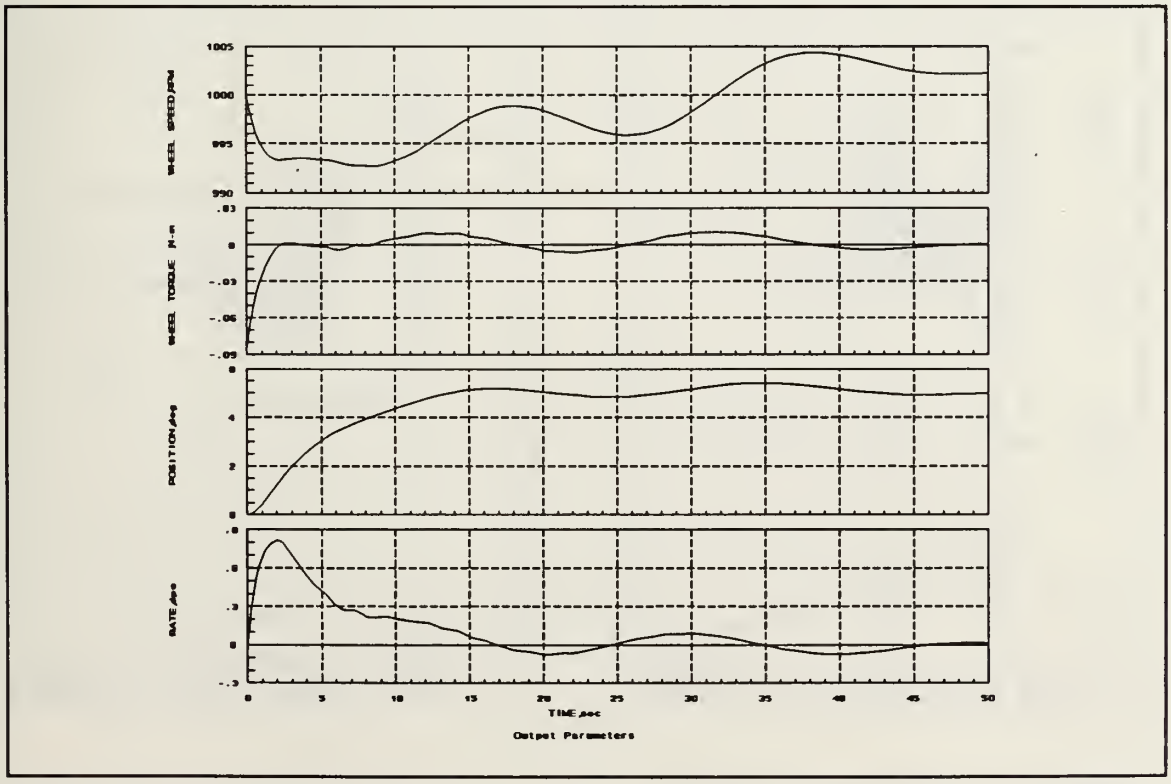

Figure 20 Bias Maneuver, PD1A

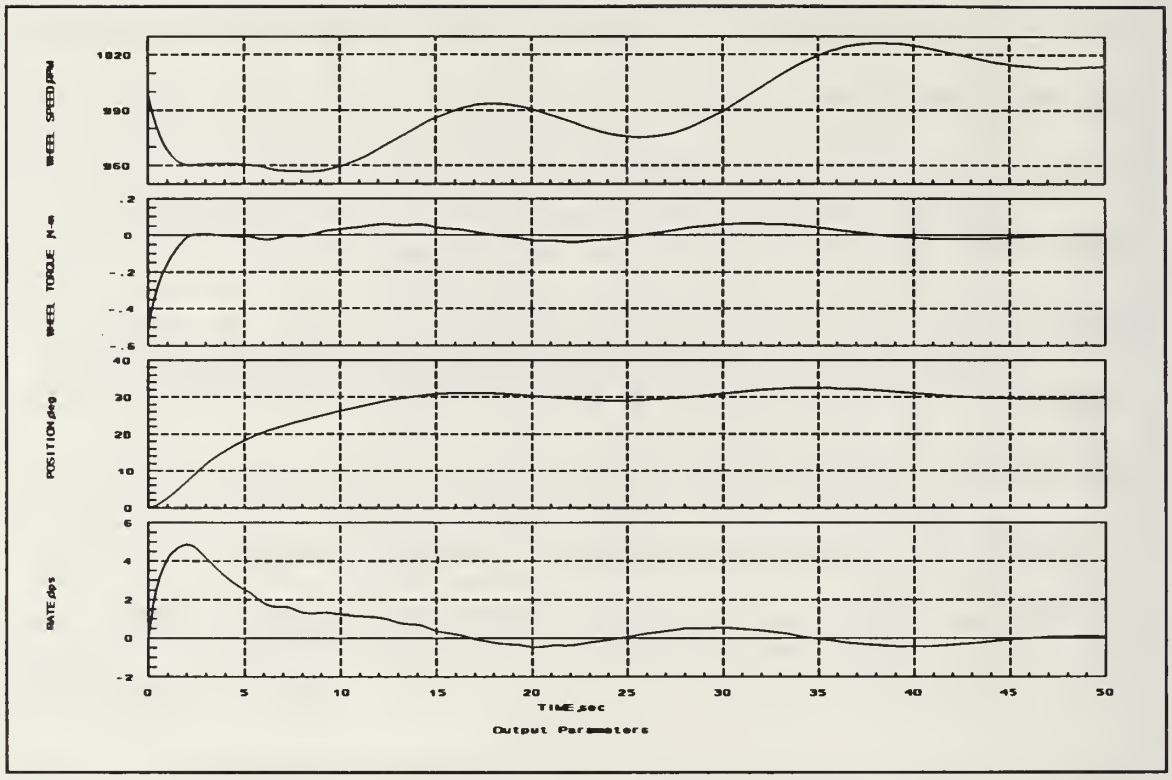

Figure 21 Slew Maneuver, PD1A

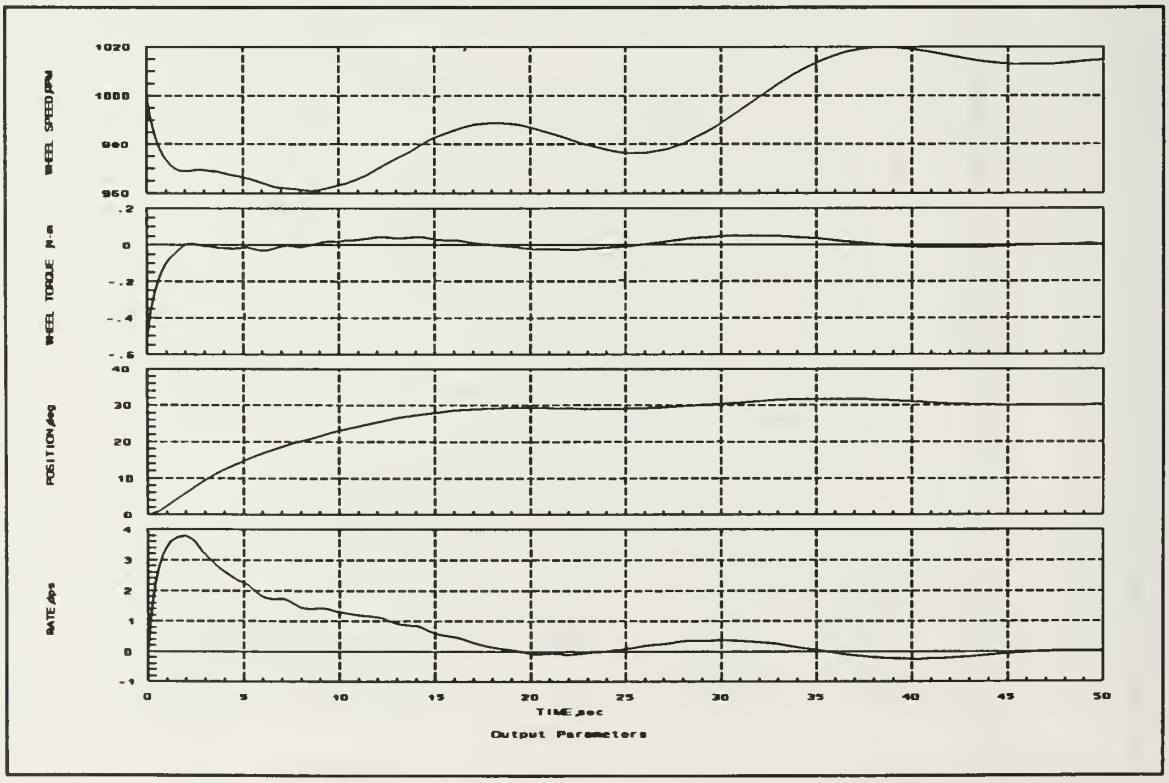

Figure 22 Slew Maneuver, PD1B

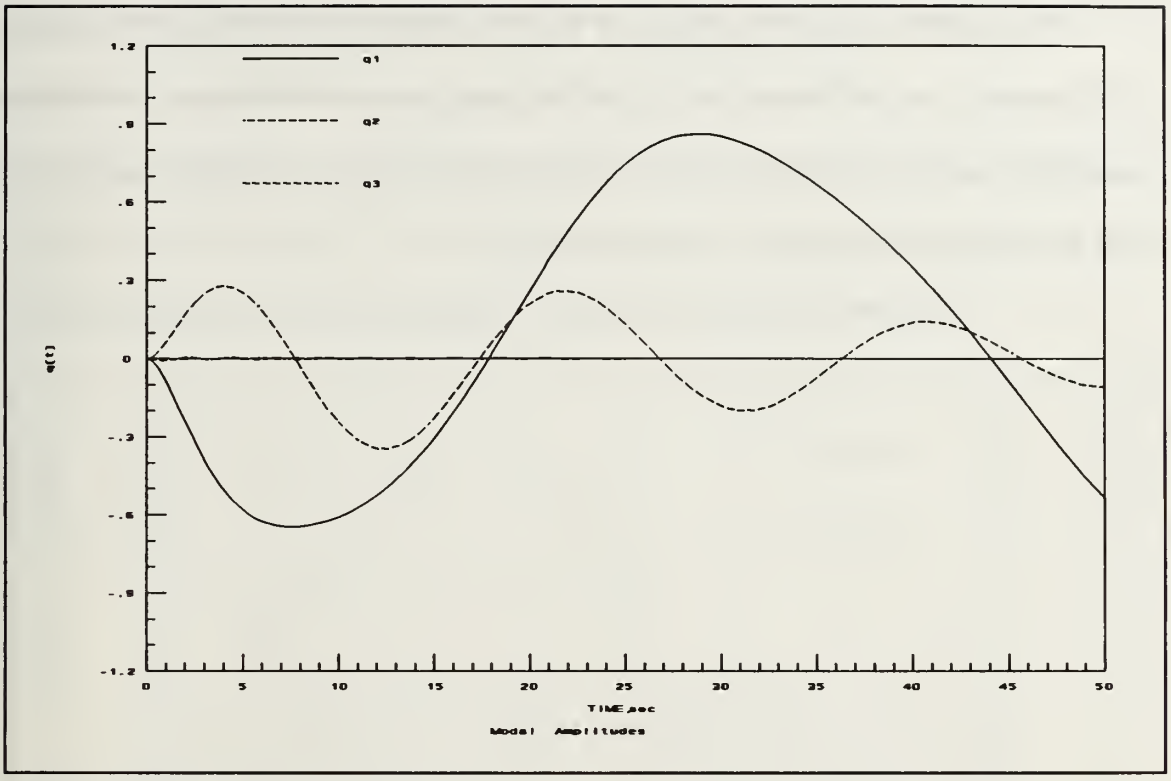

Figure 23 Slew Maneuver, PD1A

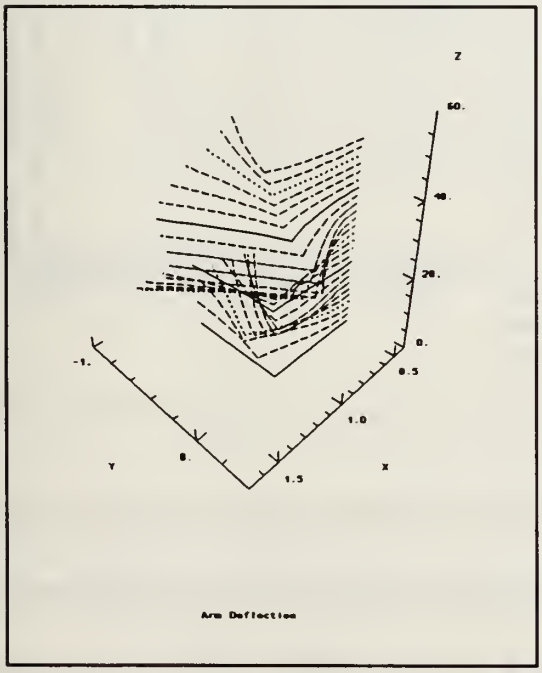

Figure 24 Slew Maneuver, PD1A

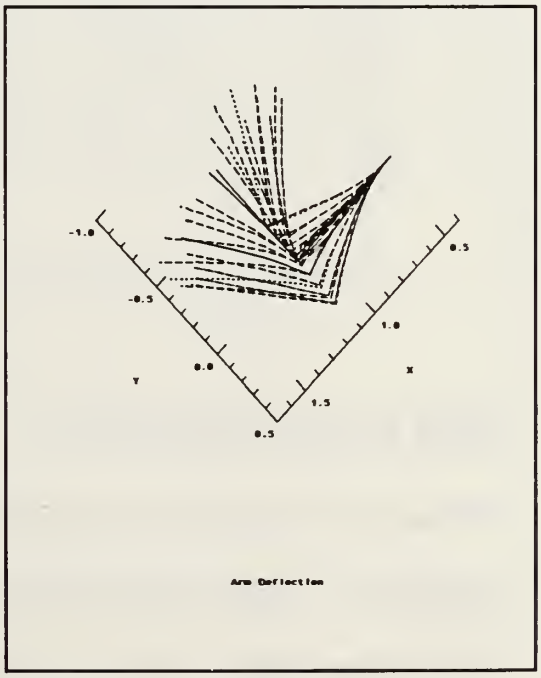

Figure 25 Slew Maneuver, PD1A

PD2 show a quicker time response to the maneuvers as expected, (see Appendix E). However, as can be seen in Figure 26, the amplitude of mode one has increased about 50% and mode two has increased 100% during the slew maneuver. Modes three and four are also beginning to show in this figure.

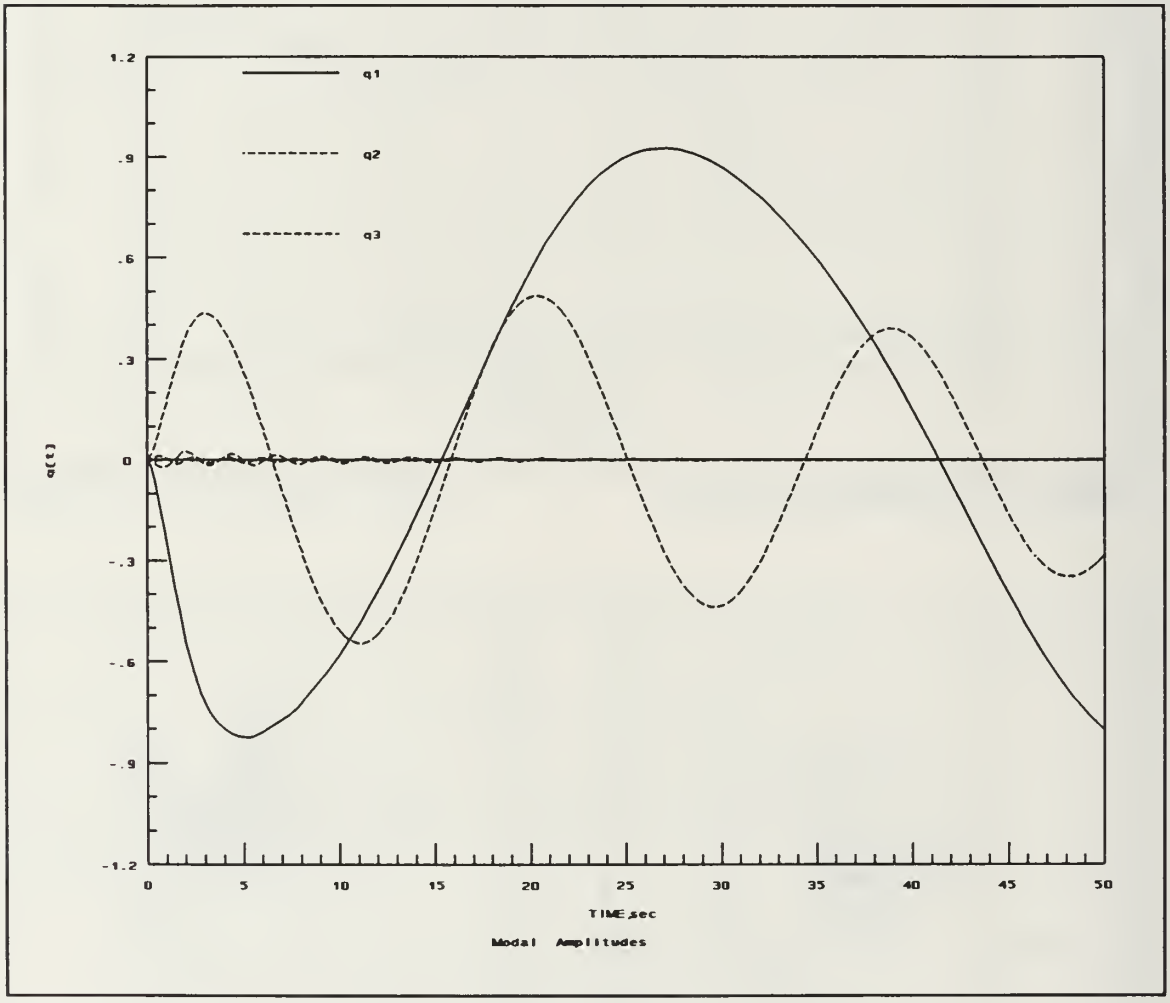

Figure 26 Slew Maneuver, PD2

PD3 has an even quicker time response and very acceptable control of the main body, (Appendix E). Figure 27 presents the 30 degree slew for PD3. The main body reaches the 30 degree position with no overshoot in about two seconds. The 20 N-m wheel

torque required is within the capabilities of the motor. Figure 28 shows that the modal amplitudes, (modes one and two), have increased by a factor of three over the amplitudes in PD1, resulting in the highly undesirable whip-like motion of the arm shown in Figure 29 and Figure 30. Note that the torque on the body from the oscillations of the arm is controllable by the momentum wheel, even at these amplitudes.

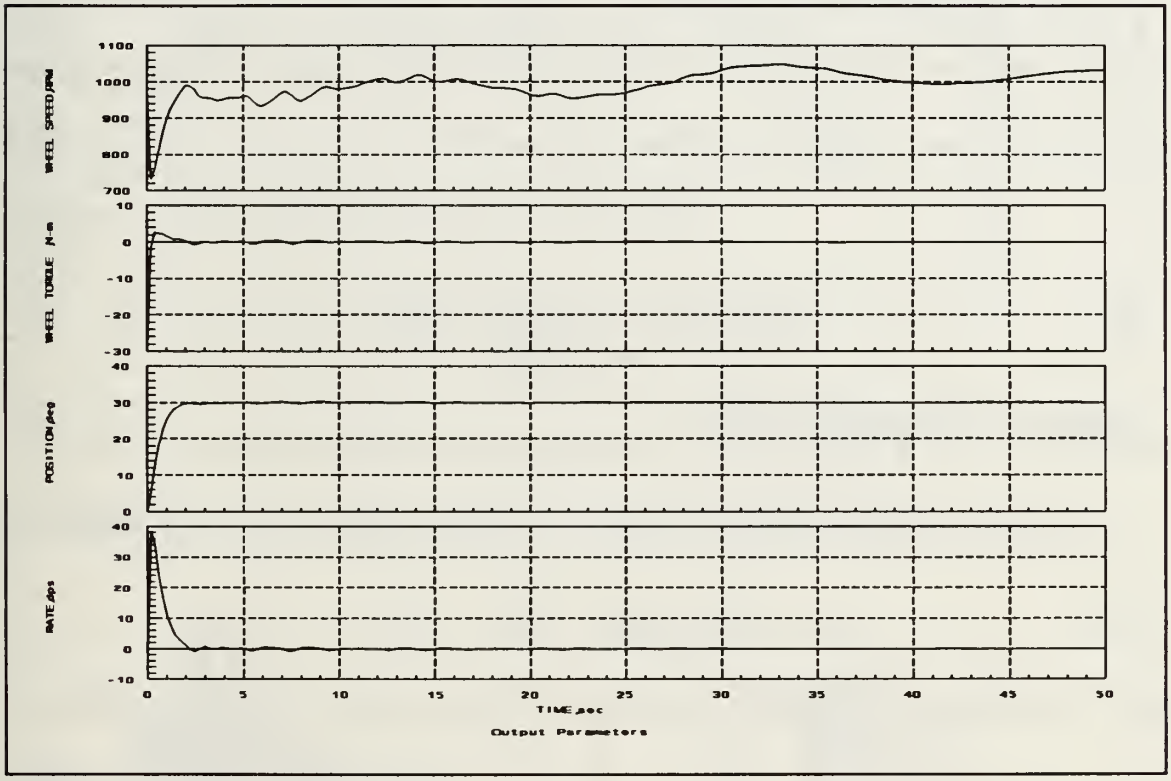

Figure 27 Slew Maneuver, PD3

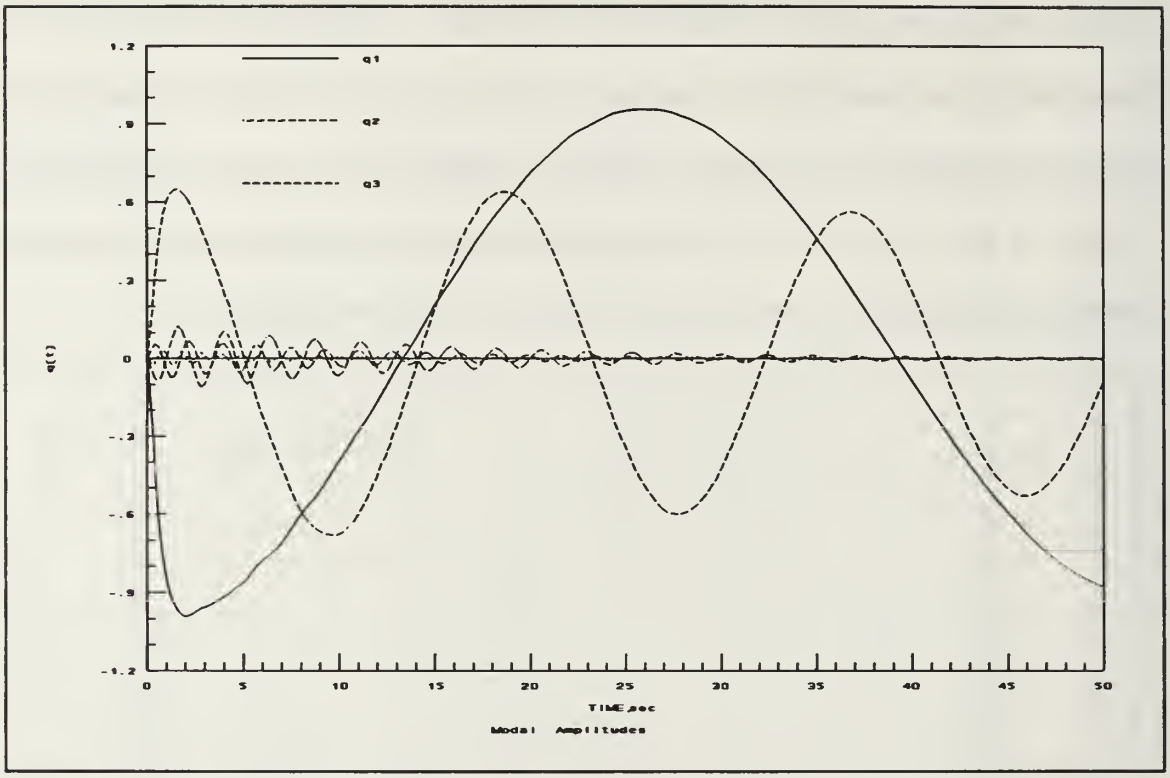

Figure 28 Slew Maneuver, PD3

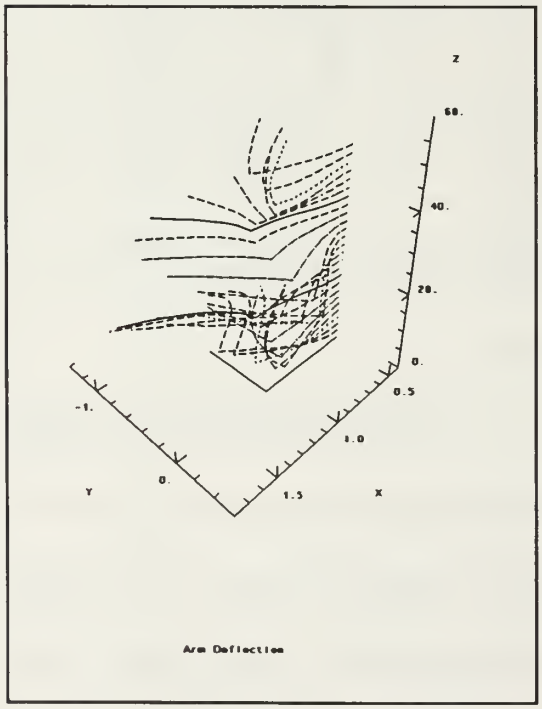

Figure 29 Slew Maneuver, PD3

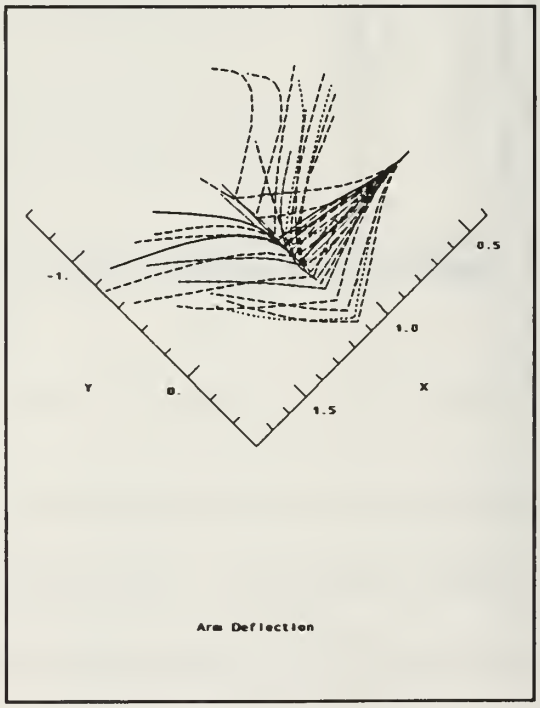

Figure 30 Slew Maneuver, PD3

C. LINEAR-QUADRATIC-GAUSSIAN COMPENSATOR

The second type of control system studied was the *linear-quadratic-gaussian* or LQG compensator. The LQG compensator is formed from a linear regulator and a Kalman filter estimator. The regulator design assumes full-state feedback, and a controllable system. The *controllability grammian*, [Ref. 6], for the system of matrices is computed using MATRIX_X and is found to be of full rank, ensuring controllability, assuming the system to be dynamically stable and time-invariant. The optimal gains are calculated by minimizing the cost function:

$$cost = \int_0^\infty \left(x' R_{xx} x + u' R_{uu} u \right) dt \tag{32}$$

where $\mathbf{R}_{xx}$ is the state weighting matrix and $\mathbf{R}_{uu}$ is the input weighting matrix. The gains are determined by first solving for $\bar{\mathbf{M}}$ in the *algebraic Ricatti equation*, [Ref. 6]:

$$0 = \bar{M}A + A'\bar{M} - \bar{M}BR_{uu}^{-1}B'\bar{M} + R_{xx} \tag{33}$$

where **A** and **B** are the system dynamic and control input matrices respectively. The optimum gain is now given by:

$$G = R_{uu}^{-1}B'\bar{M} \tag{34}$$

These functions are computed by the command ***REGULATOR***, in the MATRIX_X Control Design Module, [Ref. 7].

The Kalman filter design is performed in much the same way, utilizing the duality theorem for estimators and regulators. However, instead of state and input weighting

matrices, $\mathbf{R}_{xx}$ and $\mathbf{R}_{yy}$, the state and observation noise intensities, $\mathbf{Q}_{xx}$ and $\mathbf{Q}_{yy}$, must be determined. For a linear time-invariant system,

$$\begin{aligned} \dot{x} &= Ax + Bu + Fw \\ y &= Cx + Du + v \end{aligned} \tag{35}$$

where w is the input disturbance, F is the input disturbance matrix, and v is the measurement noise, the noise intensity matrices are defined, [Ref.7]:

$$\begin{aligned} E(v(t)v'(\tau)) &= Q_{yy}\delta(t-\tau) \\ E(Fw(t)v'(\tau)) &= Q_{xx}\delta(t-\tau) \end{aligned} \tag{36}$$

where E is the expectation operator and δ is the delta function. The noises, w and v, are assumed to be white with zero mean. For the FSS, the assumption is made that the only disturbance is a random torque of 0.01 N-m amplitude and thus:

$$Q_{xx} = B(0.01)B' \tag{37}$$

$\mathbf{Q}_{yy}$ is assumed to be a two by two diagonal matrix with the first term on the diagonal corresponding to the noise from the RVDT and the second term corresponding to the noise from the angular rate sensor. The best available estimate of noise is used until such time that the experimental value can be used. Thus:

$$Q_{yy} = \begin{bmatrix} 2E\text{-}6 & 0 \\ 0 & 6E\text{-}6 \end{bmatrix} \tag{38}$$

The Ricatti equation is solved again and the gains computed as before, however the gain matrix will now be a 14 by two since there will be two inputs into the estimator, (the two

outputs of the system). The estimator gains are computed in $MATRIX_X$ with the command ***ESTIMATOR*** in the Control Design Module.

The compensator is now synthesized using the **A**, **B**, **C** and **D** matrices of the system and the regulator and estimator gains, ***Kr*** and ***Ke*** respectively. The form of the compensator is as follows:

$$SC = \begin{bmatrix} A - Ke*C - (B - Ke*D) & | Ke \\ Kr & | 0 \end{bmatrix} \qquad (39)$$

where ***SC*** is the compensator system matrix. The ***LQGCOMP*** command in the Control Design Module of $MATRIX_X$ accomplishes this formation. The block diagram for the control system, as well as the points at which inputs and outputs are taken, is given in Figure 31.

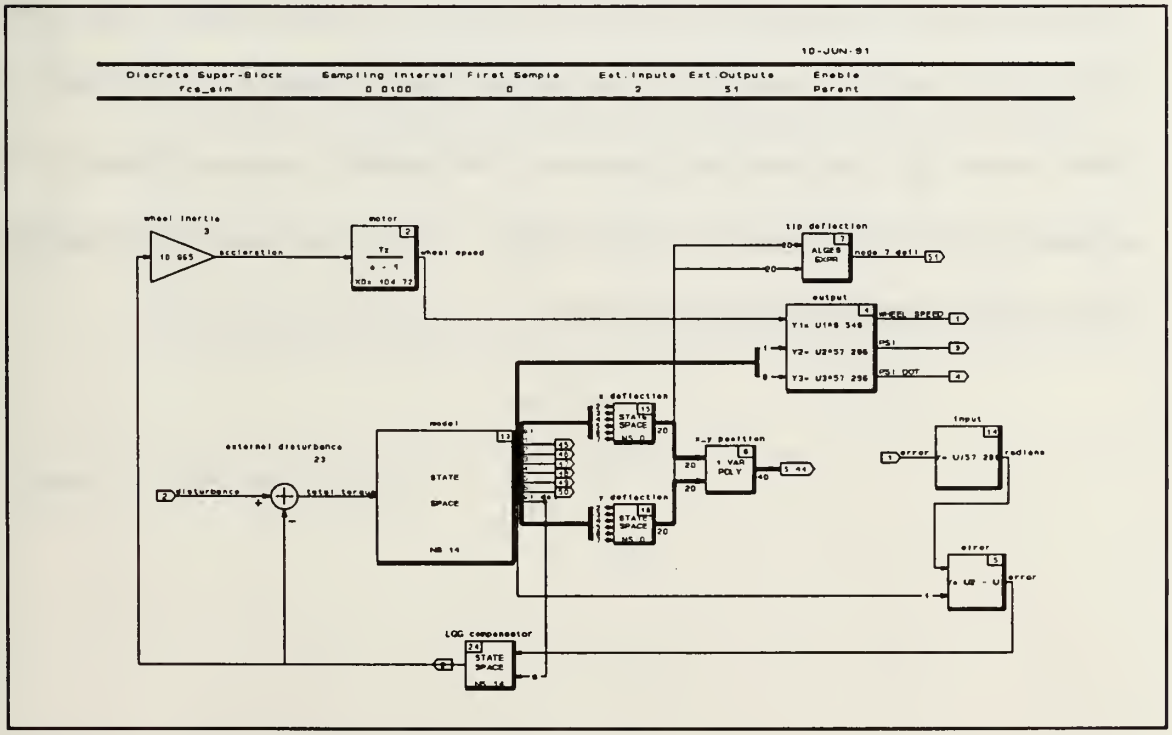

Figure 31 Block Diagram of Control System

All that remains is to determine $\mathbf{R}_{xx}$ and $\mathbf{R}_{uu}$. $\mathbf{R}_{xx}$ is a 14 by 14 matrix and is assumed to be diagonal, with each term on the diagonal corresponding to a state. $\mathbf{R}_{uu}$ is simply a scaler, since there is only one input. Positioning the main body is the primary concern of this thesis and therefore the first term on the diagonal, which corresponds to body position Ψ, is set to one, and all others are set to zero. $\mathbf{R}_{uu}$ is assigned 0.001 in order to prevent exceeding the design limits of the motor. The systems response to the impulse disturbance and bias maneuvers are given in Appendix E. These figures show an acceptable response for the body with a 0.23 degree error during the impulse and three seconds required for the bias maneuver. The arm shows little deflection during the impulse and acceptable oscillations during the bias maneuver. Figure 32 shows the response to a 30 degree slew. The body reaches the desired position in about three seconds and the motor torque is well within limits. Examination of Figure 33 reveals that modes one and two are highly excited during the slew, and modes three and four moderately excited. The resulting extreme motion of the appendage is shown in Figure 34 and Figure 35 . This motion would more than likely result in permanent deformation of the beam.

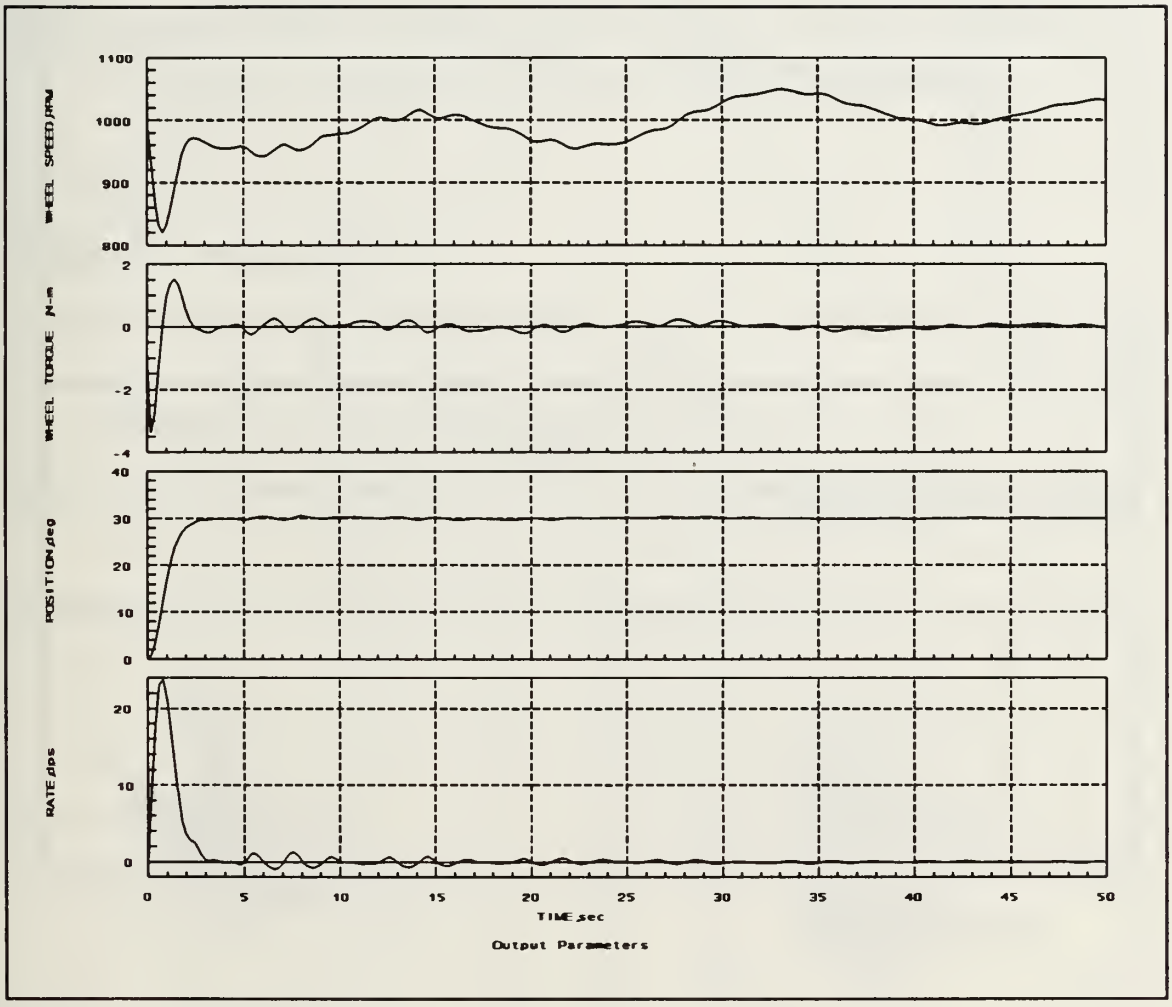

Figure 32 Slew Maneuver, C1

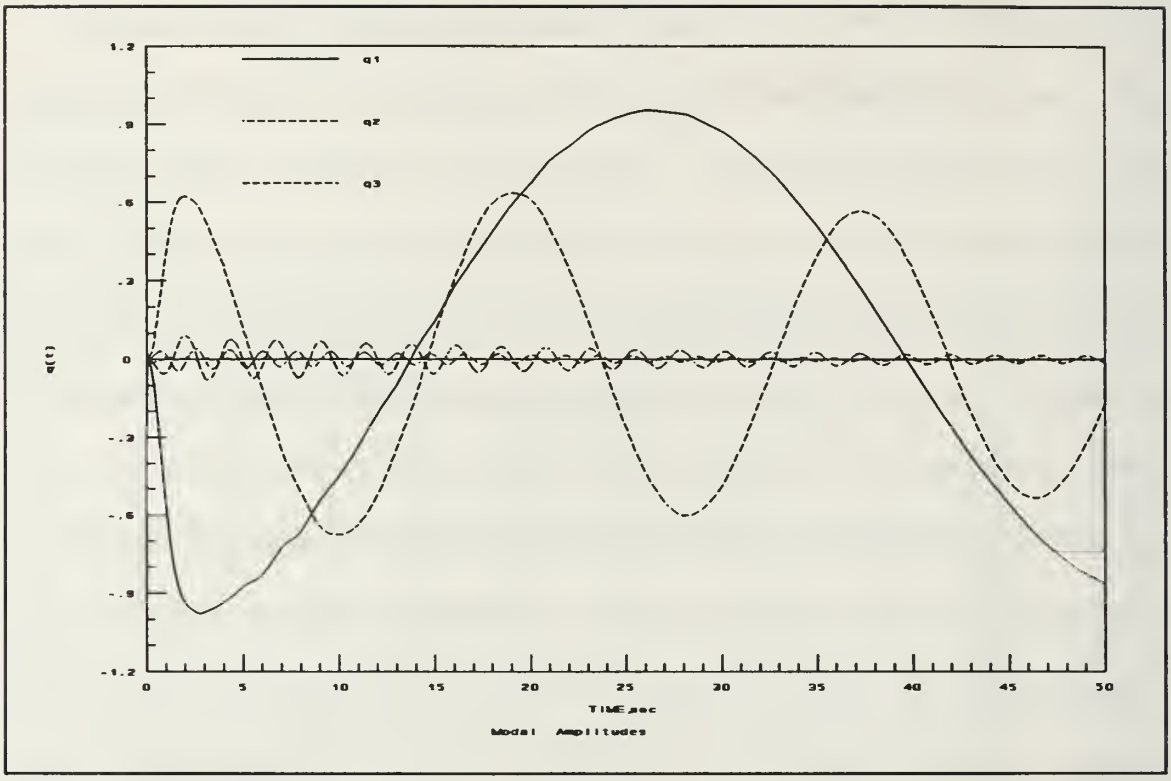

Figure 33 Slew Maneuver, C1

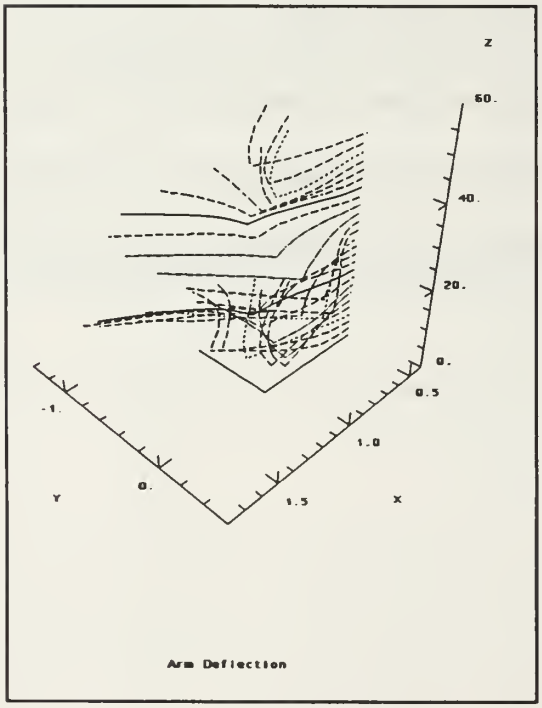

Figure 34 Slew Maneuver, C1

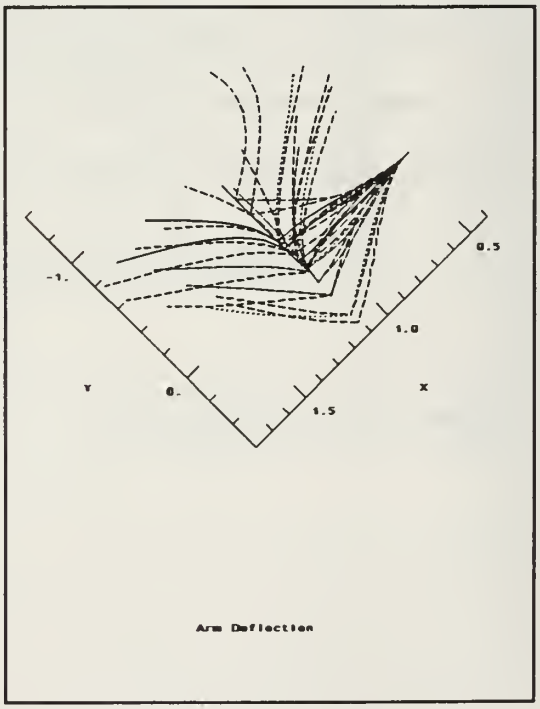

Figure 35 Slew Maneuver, C1

A second means of control is required for large angle maneuvers. The modal amplitude graph indicates that by controlling **q1** and **q2**, acceptable results could be achieved. An attempt to do this is made by varying the weights on the **Ψ**, **$\dot{\Psi}$**, **q1**, **$\dot{q}$1**, **q2**, and **$\dot{q}$2**, as well as the weight on the torque input. TABLE III indicates values used for the significant results. The figures for **C2** through **C7** are given in Appendix E.

TABLE III Weighting Factors

	R_{xx}						R_{uu}
Designation	1	q1	q2	$\dot{\Psi}$	$\dot{q}$1	$\dot{q}$2	T
C1	1	0	0	0	0	0	.001
C2	1	10	10	0	0	0	0.1
C3	1	10^4	10^4	0	0	0	0.1
C3	1	0	0	0	●	●	0.1
C5	1	0	0	0	10^4	10^4	0.1
C6	1	0	0	1	0	0	0.1
C7	1	0	0	1	0.2	0.2	100
C8	1	0	0	1	0.7	0.5	1000

C8 shows the best results for the optimum controller for the slew maneuver. The following four figures show the response of the central body and the flexible arm. The slew rate is slow, but this is required in order to prevent exciting the first and second modes of the arm.

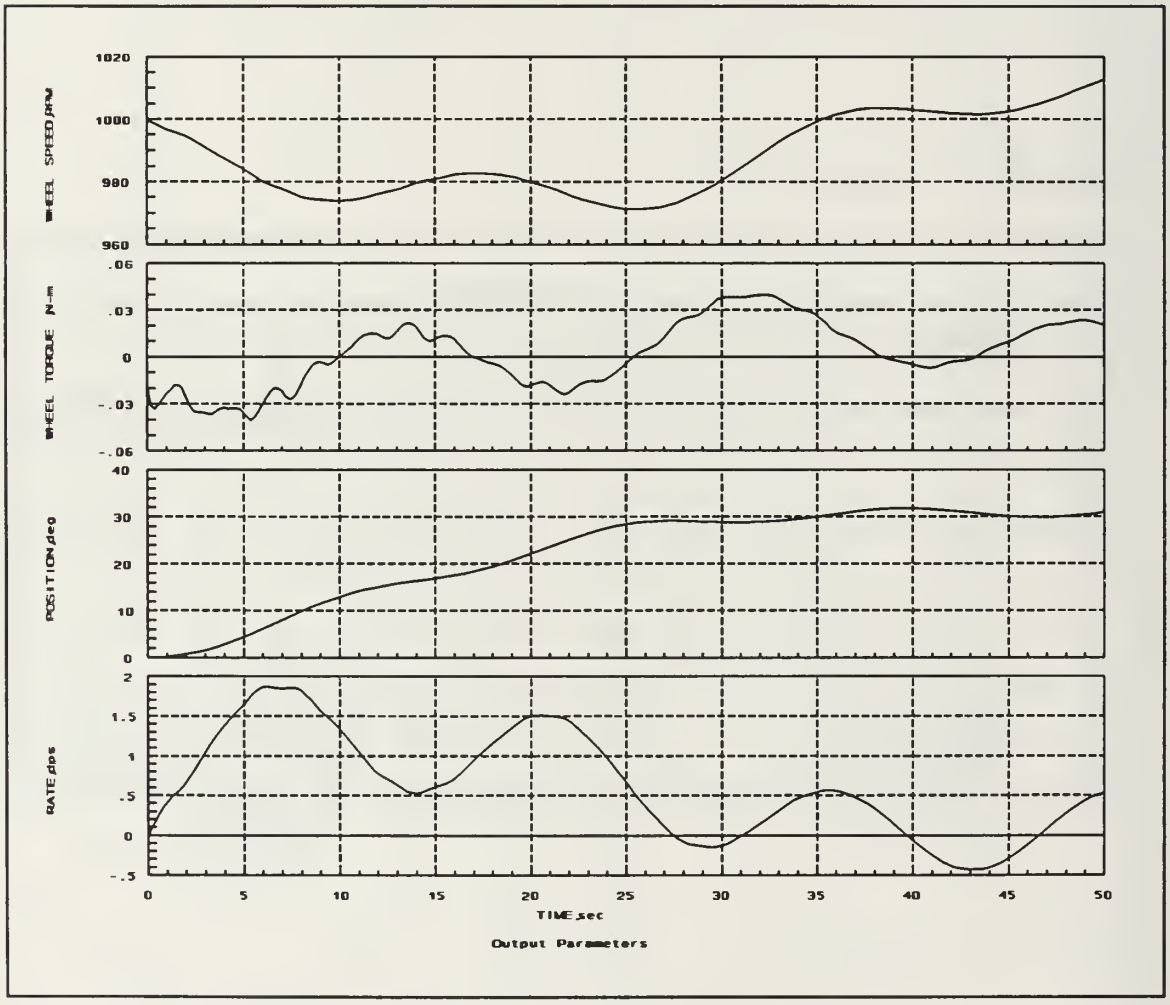

Figure 36 Slew Maneuver, C8

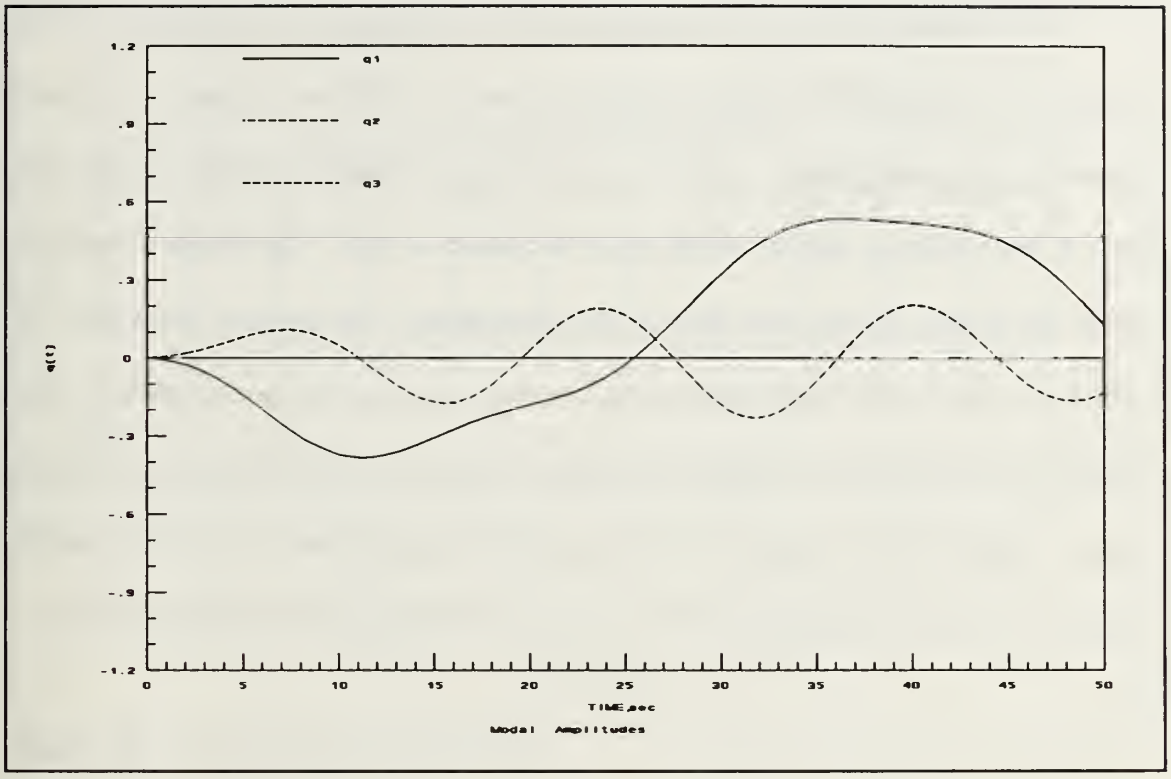

Figure 37 Slew Maneuver, C8

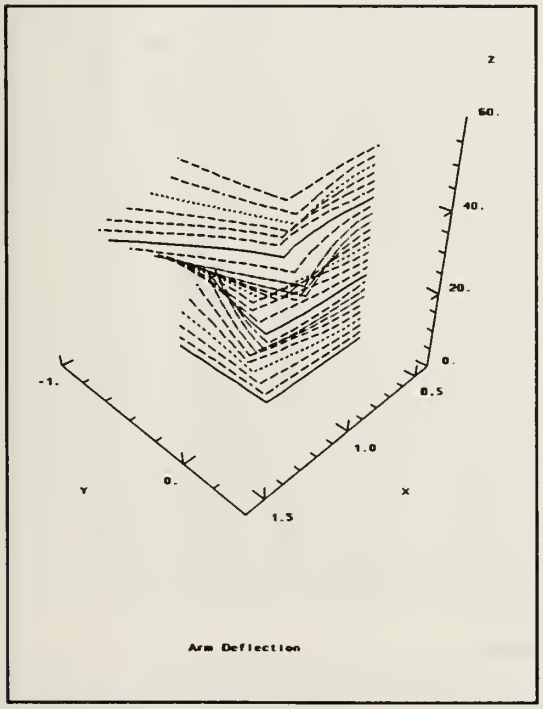

Figure 38 Slew Maneuver, C8

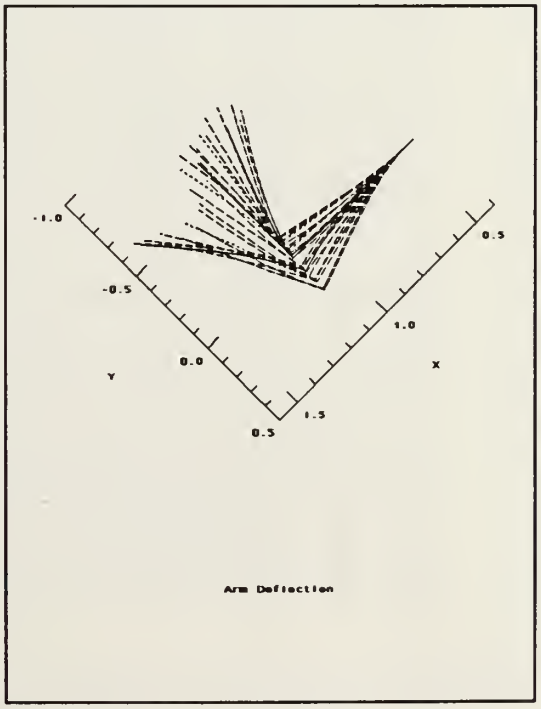

Figure 39 Slew Maneuver, C8

As a comparison of the PD controller and LQG compensator, an on-orbit mode was designed to maintain 0.05 degree pointing accuracy of the central body. For the PD controller, the gains, $\mathbf{K}$ and τ were computed using the equations found on page 139 of Ref. 5, and assuming that the model could be treated as rigid. The inertia of the system about the Z axis, (fixed), was used in the calculations. The required gains are: $\mathbf{K} = 179.3$, $\tau = 84.3$. For the LQG compensator, $\mathbf{R}_{xx}$ was the same as used for C1, but $\mathbf{R}_{uu}$ was set at 10^{-6} in order to maintain 0.05 degree accuracy. $\mathbf{R}_{uu}$ was arrived at by trial and error. The results are presented in Figure 40 through Figure 43. Both controllers control well in the on-orbit mode with only a millimeter movement in the endpoint.

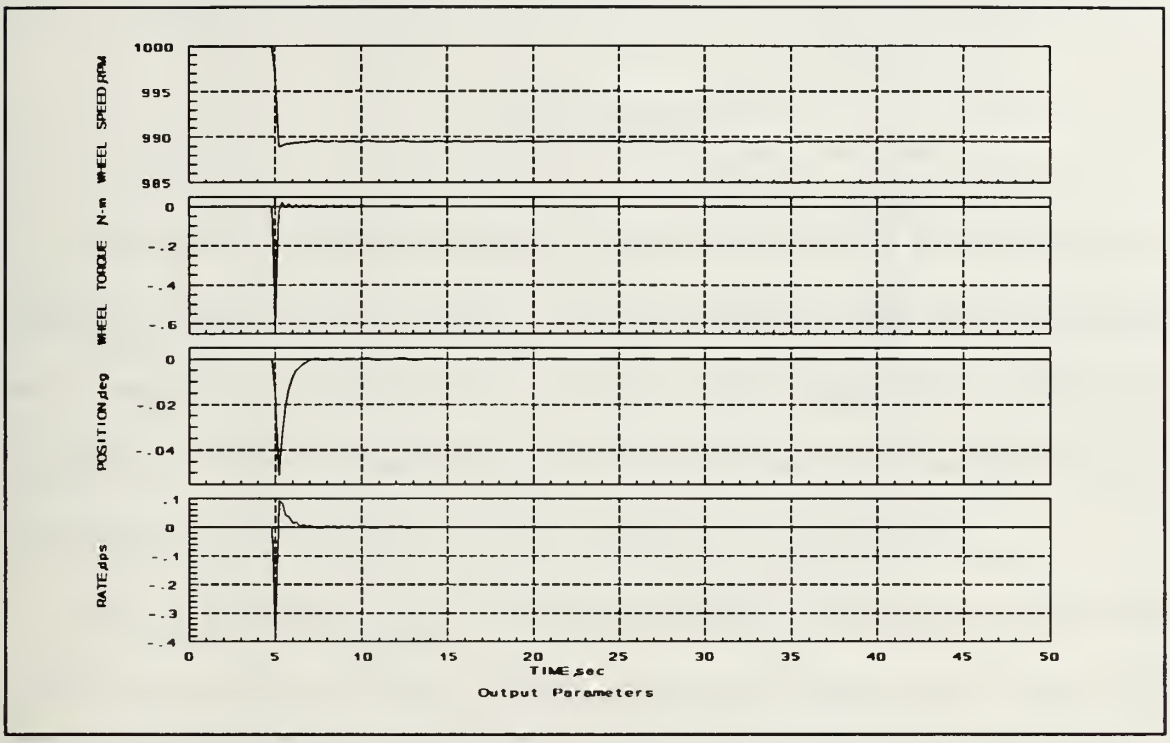

Figure 40 On-Orbit Mode, PD Control

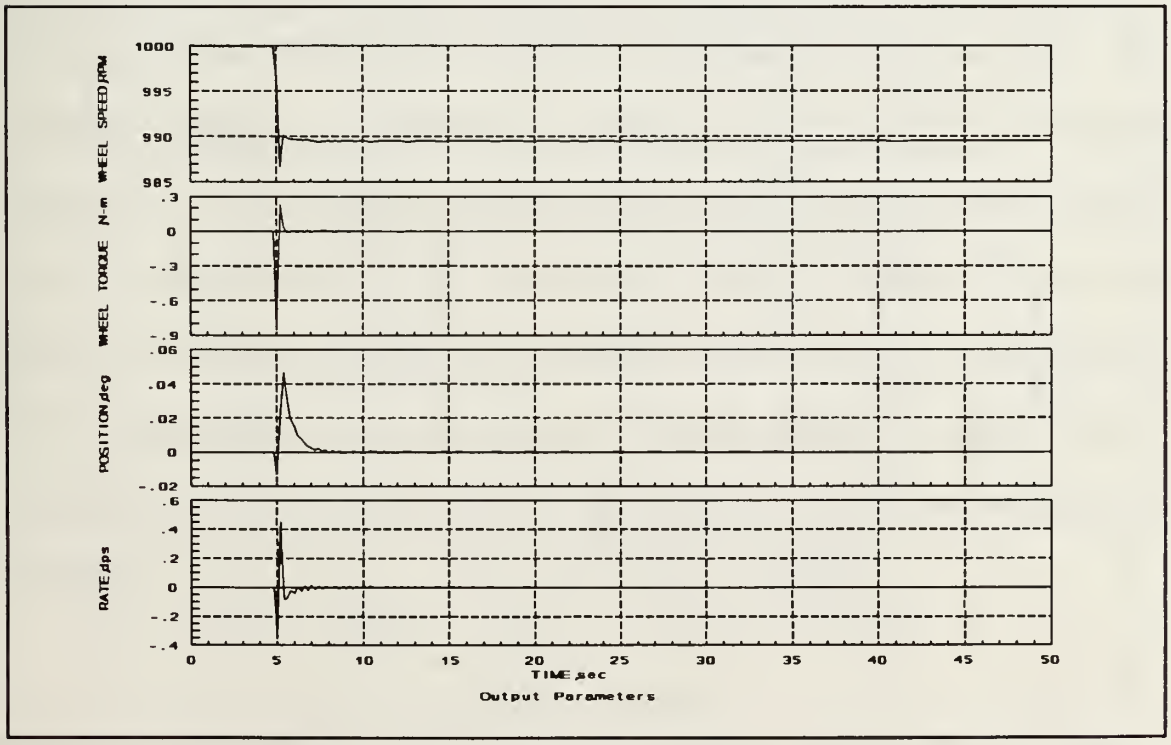

Figure 41 On-Orbit Mode, LQG Compensator

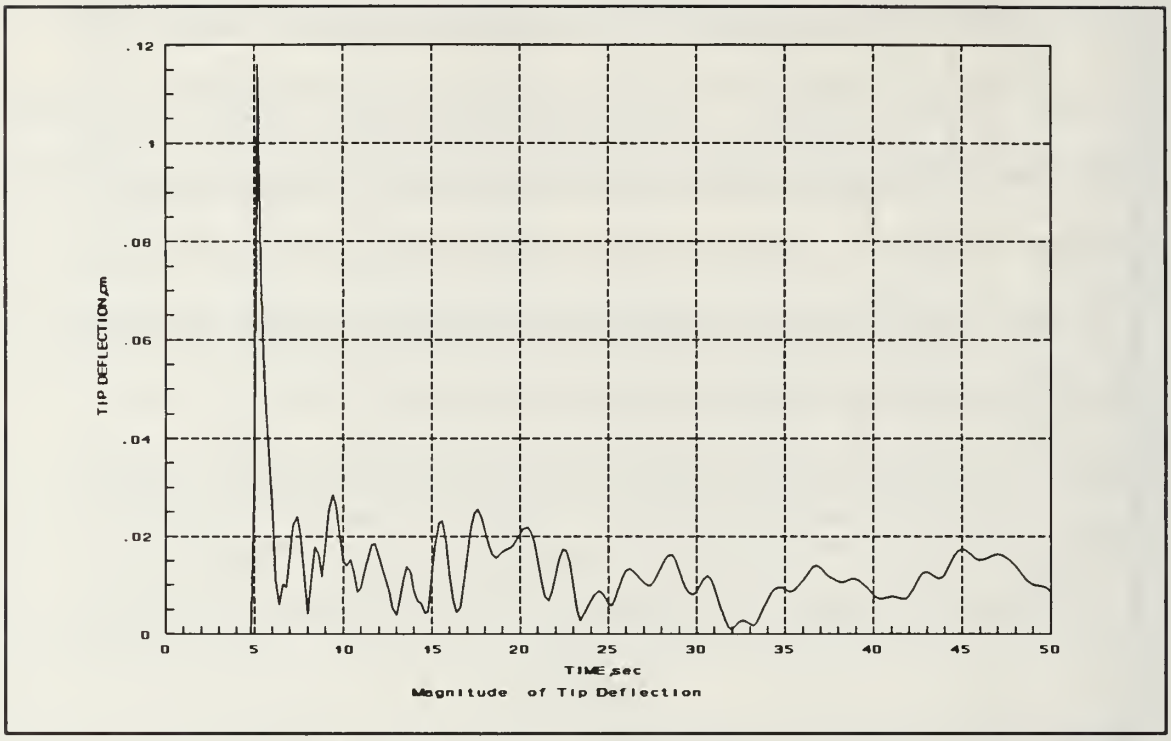

Figure 42 On-Orbit Mode, PD Control

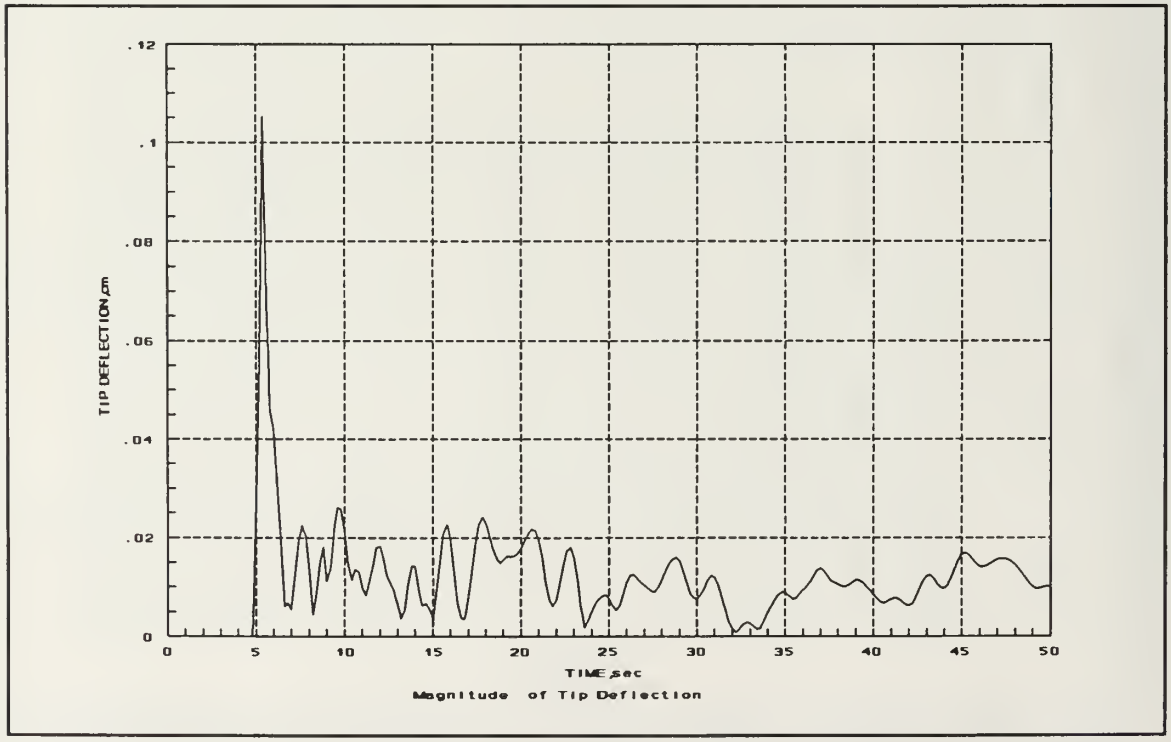

Figure 43 On-Orbit Mode, LQG Compensator

V. CONCLUSIONS

The Flexible Spacecraft Simulator, (FSS), is fully assembled and should become operational within the next few weeks. The initial operational configuration has sensors and an actuator on the central body. A picture of the present setup is provided in Appendix A. With this Phase I setup, actual experiments into the effect of flexible spacecraft structures on attitude dynamics and control can be carried out.

Both the PD control and the LQG compensator show that on-orbit control of the central body is readily achievable. Control of the antenna endpoint is not as good, with the maximum deflection reaching about one mm for a one N-m impulse disturbance. Slewing the central body at a fairly high rate of speed is possible, but at the expense of severe oscillations of the arm, and at some point, damage to the arm itself. The oscillations imposed by the rapid slew do not damp out quickly, but the torque imposed on the central body is small enough that the actuator can still maintain the position of the body. Results show that the LQG compensator is better for slewing the arm, but in order to use this type of control, two compensators will be required. One compensator will be set up for the on-orbit mode, and one for slewing the satellite model. Satisfactory control can be achieved, but the maximum slew rate will be about one deg/sec.

A. RECOMMENDATIONS FOR FURTHER STUDY

Experimental verification of the mode shapes and frequencies as well as the damping coefficient should be accomplished as soon as the instrumentation is available. Also, further work is required in optimizing the control design for the slew maneuver using only the single actuator. Control of the central body is readily achievable using both PD and LQG control, but at the expense of moderate to severe oscillations of the arm. Attempts to control the arm using the LQG compensator and weighting the time rate of change of the first two mode shapes result in minimizing the amplitude of the oscillations. However, control of the position of the central body is then lost. Weighting both the arm and the central body results in a slow maneuver of about one deg/sec and low amplitude oscillations of the arm. The magnitude of the time rate of change of the acceleration, otherwise known as "jerk", and more importantly, the length of time that the jerk is applied appear to have the most effect on the amplitude of the oscillations. By programming the body rate during the maneuver such that this effect is minimized, better control of the arm and a more rapid slew might be achieved.

The FSS can be easily expanded to using piezoelectric sensors and actuators on the flexible arm. In follow on phases, thrusters may be added to the central body, as well as liquid tanks. Endpoint sensing will be added and control of the arm's endpoint attempted. Deployment of space structures, such as antennas and solar arrays, can be tested. By adding a motor to the elbow and endpoint, space robotics experiments may be attempted. The FSS will be an extremely useful research and teaching tool in the challenging area of attitude dynamics and control. [Ref. 8]

The design of the experimental setup to simulate spacecraft structural/control interactions has been challenging. The current design simulates the classical control method where sensors and actuators are located on the central body. However, it can be easily extended to simulate control configurations where the sensors and actuators are distributed throughout the model. It is a versatile testbed for the investigation of techniques in dynamics and control of flexible spacecraft. More importantly, it allows experimental verification of analytical results prior to implementation on flight spacecraft.

APPENDIX A

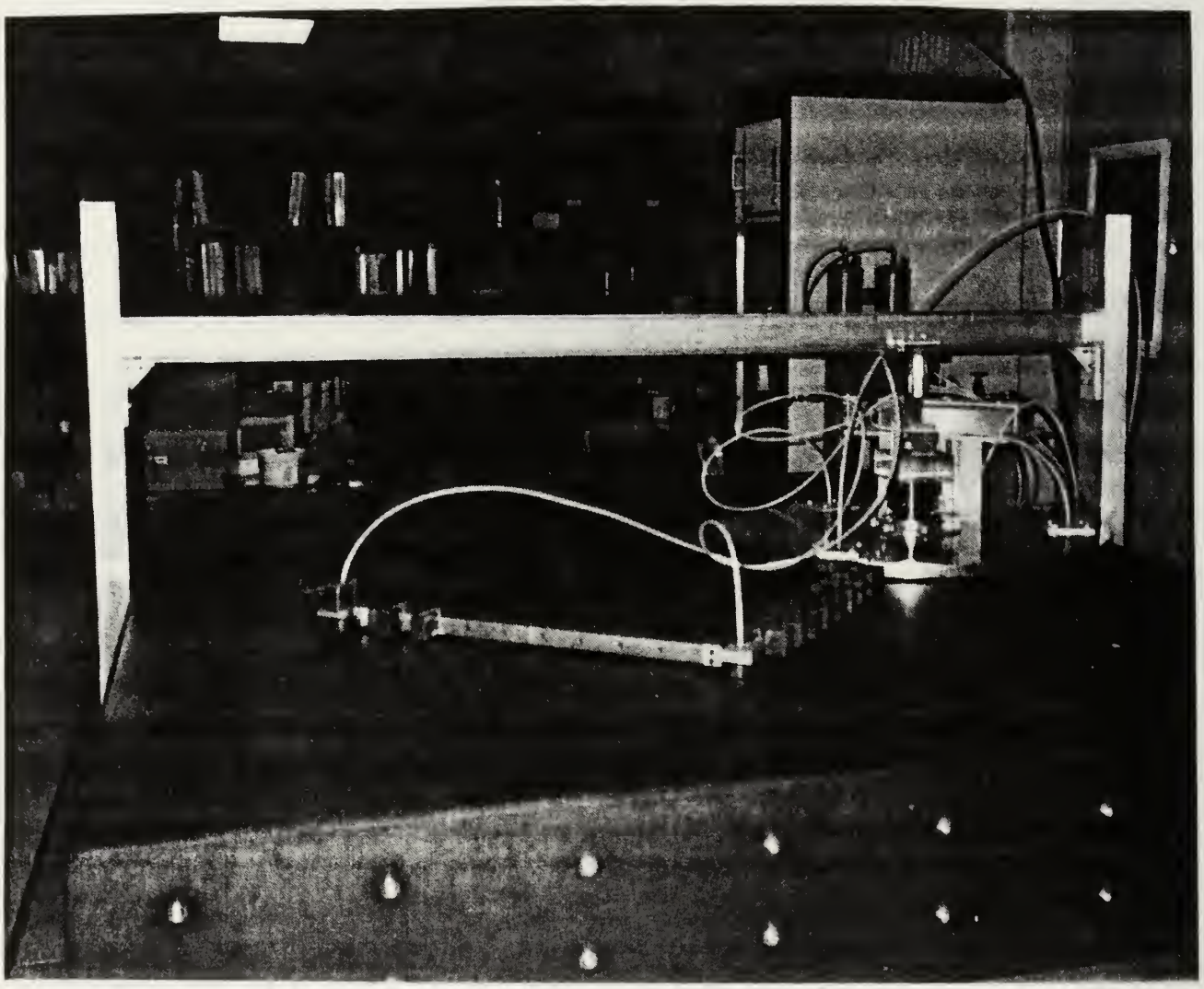

Figure 44 Flexible Spacecraft Simulator

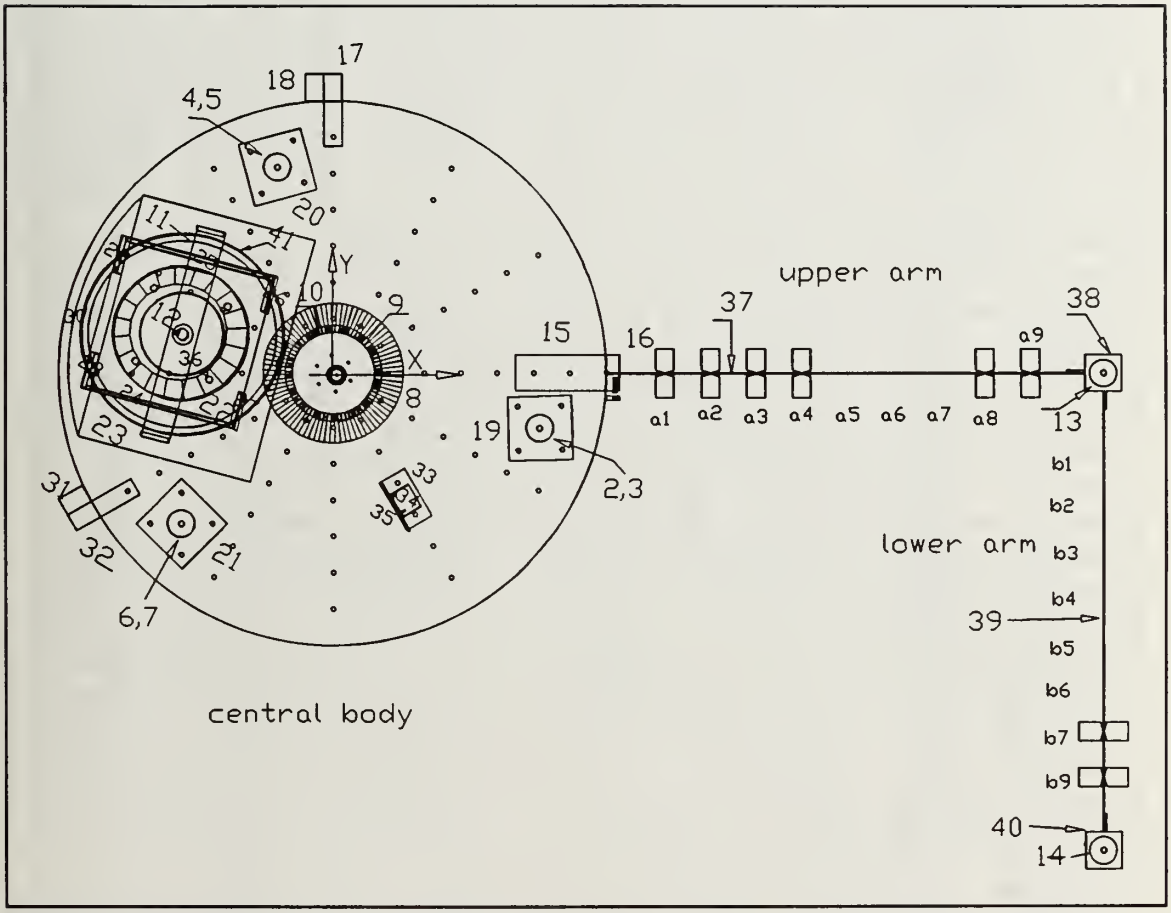

Figure 45 Key to Inertia Spreadsheet

Item #	type	material	dimensions			mass	center of mass coordinates			Orient.	Izz'	Izz	Ixx'	Ixx	Iyy'	Iyy
			a, in	b, in	c, in	lbm	r, in	theta, deg	z, in	phi, deg						
1	cylinder	aluminum	15.00		0.88	58.63	0.00	0.00	0.00	0.00	6,313	6,313	3,302	3,302	3,302	3,302
2	cylinder	aluminum	0.75		0.40	0.07	11.75	345.00	0.20	0.00	0.02	9.39	0.01	8.75	0.01	0.64
3	cylinder	air pad	0.75		0.66	0.12	11.75	345.00	-0.40	0.00	0.03	16.60	0.02	15.48	0.02	1.13
4	cylinder	aluminum	0.75		0.40	0.07	11.75	105.00	0.20	0.00	0.02	9.39	0.01	0.64	0.01	8.75
5	cylinder	air pad	0.75		0.66	0.12	11.75	105.00	-0.40	0.00	0.03	16.60	0.02	1.13	0.02	15.48
6	cylinder	aluminum	0.75		0.40	0.07	11.75	225.00	0.20	0.00	0.02	9.39	0.01	0.89	0.01	8.89
7	cylinder	air pad	0.75		0.66	0.12	11.75	225.00	-0.40	0.00	0.03	16.60	0.02	8.96	0.02	8.96
8	doughnut	aluminum	3.83	2.24	0.25	0.73	0.00	0.00	0.56	0.00	7.16	7.16	0.09	0.09	0.09	0.09
9	doughnut	aluminum	2.64	2.24	0.50	0.29	0.00	0.00	0.94	0.00	7.16	7.16	0.89	0.89	0.89	0.89
10	doughnut	aluminum	2.64	2.24	0.13	0.07	0.00	0.00	1.25	0.00	0.14	0.44	0.23	0.23	0.23	0.23
11	cylinder	steel	5.15		1.00	23.50	11.27	165.00	8.25	0.00	311.64	3,296	157.78	2,943	157.78	357.72
12	cylinder	motor	3.83		6.34	17.50	11.27	165.00	3.86	0.00	119.14	2,342	118.19	2,192	118.19	267.08
13	cylinder	air pad	0.75		0.66	0.10	42.25	0.00	-0.40	0.00	0.03	214.24	0.02	214.23	0.02	0.02
14	cylinder	air pad	0.75		0.66	0.12	49.74	328.10	-0.40	0.00	0.03	296.92	0.08	214.00	0.08	82.93
15	plate	aluminum	5.00	2.00	0.25	0.27	12.50	0.00	0.56	0.00	0.58	38.08	0.50	38.00	0.08	0.08
16	plate	aluminum	1.00	0.97	1.13	0.10	15.39	1.90	0.20	0.00	0.02	24.83	0.02	24.81	0.02	0.09
14	plate	aluminum	1.00	1.00	0.25	0.12	14.51	30.00	0.56	-90.90	0.14	20.35	0.13	20.22	0.08	0.13
18	plate	aluminum	2.00	1.50	0.75	0.22	15.75	91.90	0.00	-91.90	0.11	53.69	0.09	53.57	0.09	0.14
19	plate	aluminum	3.50	3.50	0.25	0.29	11.75	345.00	0.56	0.00	0.60	41.19	0.30	3.02	0.30	38.17
20	plate	aluminum	3.50	3.50	0.25	0.29	11.75	105.00	0.56	15.00	0.60	41.19	0.30	38.17	0.30	3.02
21	plate	aluminum	3.50	3.50	0.25	0.29	11.75	225.00	0.56	45.00	0.60	41.19	0.30	20.60	0.30	20.60
22	plate	aluminum	8.71	8.71	0.25	1.82	8.78	165.00	0.56	15.00	23.02	163.38	11.52	20.92	11.52	142.48
23	plate	aluminum	9.74	13.77	0.38	4.26	7.93	165.00	7.20	15.00	100.88	368.47	33.69	53.87	67.29	314.71
24	plate	aluminum	8.21	0.25	6.34	1.25	9.70	190.00	3.86	15.00	7.02	124.56	11.20	14.28	4.19	118.66
25	plate	aluminum	8.29	0.25	6.34	1.25	9.70	140.00	3.86	15.00	7.02	124.56	11.20	59.30	1.13	73.64
26	plate	aluminum	1.75	0.25	6.34	0.27	5.80	130.00	3.86	15.00	0.07	9.03	0.89	0.89	0.89	0.89
27	plate	aluminum	1.75	0.25	6.34	0.27	5.80	200.00	3.86	15.00	0.07	9.03	0.88	0.00	0.88	8.88
28	plate	aluminum	1.75	0.25	6.34	0.27	13.25	118.13	3.85	15.00	0.07	46.82	0.96	0.96	0.88	47.64
29	plate	aluminum	1.75	0.25	6.34	0.27	13.25	150.50	3.86	15.00	0.07	46.82	0.96	12.29	0.89	36.31
30	special	aluminum	3.00	13.77	0.38	1.49	14.63	165.00	7.20	15.00	24.61	342.92	1.13	23.95	23.52	319.00
31	plate	aluminum	2.00	1.50	0.75	0.22	15.75	208.10	0.00	61.90	0.11	53.69	0.08	11.94	0.05	41.77
32	plate	aluminum	4.00	1.00	0.25	0.10	14.51	210.00	0.56	60.00	0.14	20.35	0.13	5.09	0.01	15.26
33	plate	aluminum	3.00	1.50	0.25	0.11	8.00	300.00	0.56	60.00	0.10	7.01	0.08	5.22	0.02	1.79

Figure 46 Inertia of System

Ixy	Ixz	Iyz	cmcalc x	cmcalc y	cmcalc z	xdist	ydist	zdist	type	Item #
0.00	0.00	0.00	0.00	0.00	0.00	0.00	0.00	0.00	cylinder	1
-2.34	0.15	-0.04	0.01	0.00	0.00	11.35	-3.04	0.20	cylinder	2
-4.14	-0.54	0.15	0.01	0.00	0.00	11.35	-3.04	-0.40	cylinder	3
-2.34	-0.04	0.15	0.00	0.01	0.00	-3.04	11.35	0.20	cylinder	4
-4.14	0.15	-0.54	0.00	0.03	0.00	-3.04	11.35	-0.40	cylinder	6
4.68	-0.31	-0.31	0.00	0.00	0.00	-8.31	-8.31	0.20	cylinder	6
8.28	0.00	0.00	-0.01	-0.01	0.00	-8.31	-8.31	-0.40	cylinder	7
0.00	0.00	0.00	0.00	0.00	0.00	0.00	0.00	0.56	doughnut	8
0.00	0.00	0.00	0.00	0.00	0.00	0.00	0.00	0.00	doughnut	9
0.00	0.00	0.00	0.00	0.00	0.00	0.00	0.00	1.26	doughnut	10
-746.20	-2,111	565.51	-2.00	0.54	1.51	-10.89	2.92	8.25	cylinder	11
-555.68	-735.35	197.04	-1.49	0.00	0.53	-10.89	2.92	3.86	cylinder	12
0.00	-2.03	0.00	0.00	0.00	0.00	42.25	0.00	-0.40	cylinder	16
-133.19	-2.03	1.26	0.00	-0.02	0.00	42.23	-26.28	-0.40	cylinder	16
0.00	1.68	0.00	0.00	0.00	0.00	12.50	0.00	0.56	plate	16
0.82	0.00	0.00	0.00	0.00	0.00	15.38	0.51	0.00	plate	16
0.00	0.00	0.78	0.00	0.01	0.00	0.00	14.51	0.56	plate	16
-1.78	0.00	0.00	0.00	0.03	0.00	-0.52	15.74	0.00	plate	16
-10.15	1.87	-0.60	0.00	-0.01	0.00	11.35	-3.04	0.56	plate	16
-10.15	-0.54	1.87	-0.01	0.03	0.00	-3.04	11.35	0.56	plate	20
20.30	-1.37	-1.37	-0.02	-0.02	0.00	-8.31	-8.31	0.56	plate	24
-35.09	-8.68	2.32	-0.12	0.01	0.01	-8.48	2.27	0.56	plate	24
-58.50	-234.68	62.88	-0.25	0.07	0.01	-7.66	2.05	7.20	plate	24
18.35	-46.06	-8.12	-0.09	-0.02	0.01	-9.55	-1.68	0.95	plate	24
-59.63	-35.83	30.07	-0.07	0.00	0.01	-7.43	8.28	0.95	plate	24
-4.43	-3.83	4.57	-0.01	0.01	0.01	-3.73	4.44	3.86	plate	26
2.86	-0.60	-2.03	-0.01	0.00	0.01	-5.45	-1.98	3.86	plate	27
-0.51	-13.62	0.14	-0.09	0.00	0.01	-13.25	0.14	0.95	plate	28
-20.05	-11.85	6.71	-0.02	0.00	0.01	-11.53	6.52	3.86	plate	29
-73.98	-151.31	40.54	-0.16	0.00	0.00	-14.13	3.79	1.26	special	30
22.25	0.00	0.00	-0.02	-0.01	0.00	-13.89	-7.42	0.00	plate	31
0.00	-0.68	-0.34	-0.01	-0.01	0.00	-12.57	-7.26	0.56	plate	32
-3.02	0.24	-0.42	0.00	-0.01	0.00	4.00	-6.93	0.56	plate	33

Figure 47 Inertia of System, cont.

a1	plate	sensor	1.20	1.40	2.25	0.25	8.00	299.10	5.24	60.00	0.07	16.07	0.14	12.36	0.15	3.92
35	plate	aluminum	3.00	0.13	4.25	0.16	8.05	293.80	2.56	-30.00	0.11	10.03	0.35	8.62	0.23	1.87
35	plate	aluminum	1.55	12.00	0.13	0.22	11.27	165.00	9.49	105.00	2.72	31.07	0.04	4.40	2.68	26.67
a2	plate	aluminum	26.25	0.06	1.00	0.16	28.12	0.20	0.00	0.00	9.04	133.58	0.28	9.06	0.28	124.55
35	plate	steel	2.00	2.40	0.50	0.68	42.25	0.00	0.30	0.00	0.45	1,205.37	0.24	0.24	0.28	1,205.16
a2	plate	aluminum	24.25	0.06	1.50	0.15	44.21	342.70	0.00	0.00	7.13	291.51	7.14	32.29	0.28	259.25
a2	plate	steel	2.00	2.00	0.50	0.61	49.74	328.10	0.00	0.00	0.41	1,503.40	0.28	419.92	0.28	1,083.50
a1	doughnut	aluminum	5.50	5.30	2.00	1.30	11.27	165.00	0.00	0.00	3.96	169.44	2.06	13.14	2.06	156.45
a2	cylinder	aluminum	5.63		0.06	0.60	11.27	165.00	0.00	0.00	9.04	85.19	4.72	75.40	4.72	9.79
a1	pt. mass	steel	1.00	2.40	1.50	1.03	18.25	0.00	0.00	0.00	0.58	343.63	0.28	0.28	0.69	343.34
a2	pt. mass	steel	1.00	2.40	1.50	1.03	20.75	0.20	0.00	0.00	0.58	444.06	0.28	0.28	0.69	444.17
a1	pt. mass	steel	1.00	2.40	1.50	1.03	23.25	0.20	0.00	0.00	0.58	557.36	0.28	0.28	0.28	557.47
a1	pt. mass	steel	1.00	2.40	1.50	1.03	25.75	0.20	0.00	0.00	0.58	683.53	0.28	0.28	0.69	683.64
a2							28.25	0.20	0.00							
35							30.75	0.69	0.00							
a1							33.25	0.00	0.00							
a2	pt. mass	steel	1.00	2.40	1.50	1.03	35.75	0.20	0.00	0.00	0.58	1,316.98	0.28	0.28	0.28	1,317.09
a2	pt. mass	steel	1.00	2.40	1.50	1.03	38.75	0.20	0.00	0.00	0.58	1,507.53	0.28	0.28	0.28	1,507.64
a10	pt. mass	steel	1.00	2.00	1.50	1.03	42.25	0.20	0.00	0.00	0.58	1,839.19	0.28	0.28	0.28	1,839.30
b4							42.48	353.60	0.00							
a2							42.84	350.30	0.00							
a2							43.33	347.00	0.00							
b4							44.02	343.80	0.00							
a2							44.72	342.70	0.00							
b6							45.61	337.80	0.00							
b7	pt. mass	steel	1.00	2.40	1.50	1.03	46.61	334.90	0.00	-90.00	0.58	2,238.25	0.28	403.34	0.69	1,835.29
b8	pt. mass	steel	1.00	2.40	1.50	1.03	47.72	332.20	0.00	-90.00	0.58	2,346.09	0.28	510.88	0.69	1,835.61
b9	pt. mass	steel	2.00	4.80	1.50	2.06	49.74	328.10	0.00	-90.00	4.64	5,101.22	1.07	1,427.55	4.34	3,674.45

Figure 48 Inertia of System, cont.

-6.79	5.10	-9.16	0.01	-0.01	0.01	3.89	-6.99	5.24	plate	34
-3.61	1.27	-2.88	0.05	-0.01	0.00	3.25	-7.37	2.56	plate	42
-7.75	-23.06	6.18	-0.02	0.01	0.00	-10.89	2.92	0.00	plate	42
0.00	0.00	0.00	0.05	0.00	0.00	28.12	0.00	0.00	plate	34
0.00	0.00	0.00	0.22	0.00	0.00	42.25	0.00	0.00	plate	34
-80.74	0.00	0.00	0.05	-0.01	0.00	42.21	-13.15	0.00	plate	42
-674.29	7.70	-4.79	0.24	-0.12	0.00	42.23	-26.28	0.00	plate	42
41.37	-127.65	-34.20	-0.11	-0.03	0.00	-10.89	-2.92	0.00	doughnut	42
18.94	-58.43	-15.66	-0.05	-0.01	0.00	-10.89	-2.92	0.00	cylinder	42
0.00	0.00	0.00	0.15	0.00	0.00	18.25	0.00	0.00	pt. mass	a4
0.00	0.00	0.00	0.17	0.00	0.00	20.75	0.00	0.00	pt. mass	42
0.00	0.00	0.00	0.15	0.00	0.00	23.25	0.00	0.00	pt. mass	a9
0.00	0.00	0.00	0.21	0.00	0.00	25.75	0.00	0.00	pt. mass	a4
						28.25	0.00	0.00		a5
						30.75	0.00	0.00		a5
						33.25	0.00	0.00		42
0.00	0.00	0.00	0.00	0.00	0.00	35.75	0.00	0.00	pt. mass	a4
0.00	0.00	0.00	0.31	0.00	0.00	38.25	0.00	0.00	pt. mass	a9
0.00	0.00	0.00	0.31	0.00	0.00	42.25	0.00	0.00	pt. mass	a10
						42.22	-4.74	0.00		42
						42.23	-7.22	0.00		42
						42.22	-9.75	0.00		c9
						42.21	-12.28	0.00		c9
						42.21	-14.78	0.00		b5
						42.23	-17.23	0.00		a5
-860	0.00	0.00	0.34	-0.16	0.00	42.21	-19.77	0.00	pt. mass	b7
-968	0.00	0.00	0.34	-0.18	0.00	42.21	-22.26	0.00	pt. mass	b8
-2286	0.00	0.00	0.68	-0.42	0.00	42.23	-26.28	0.00	pt. mass	b9

Figure 49 Inertia of System, cont

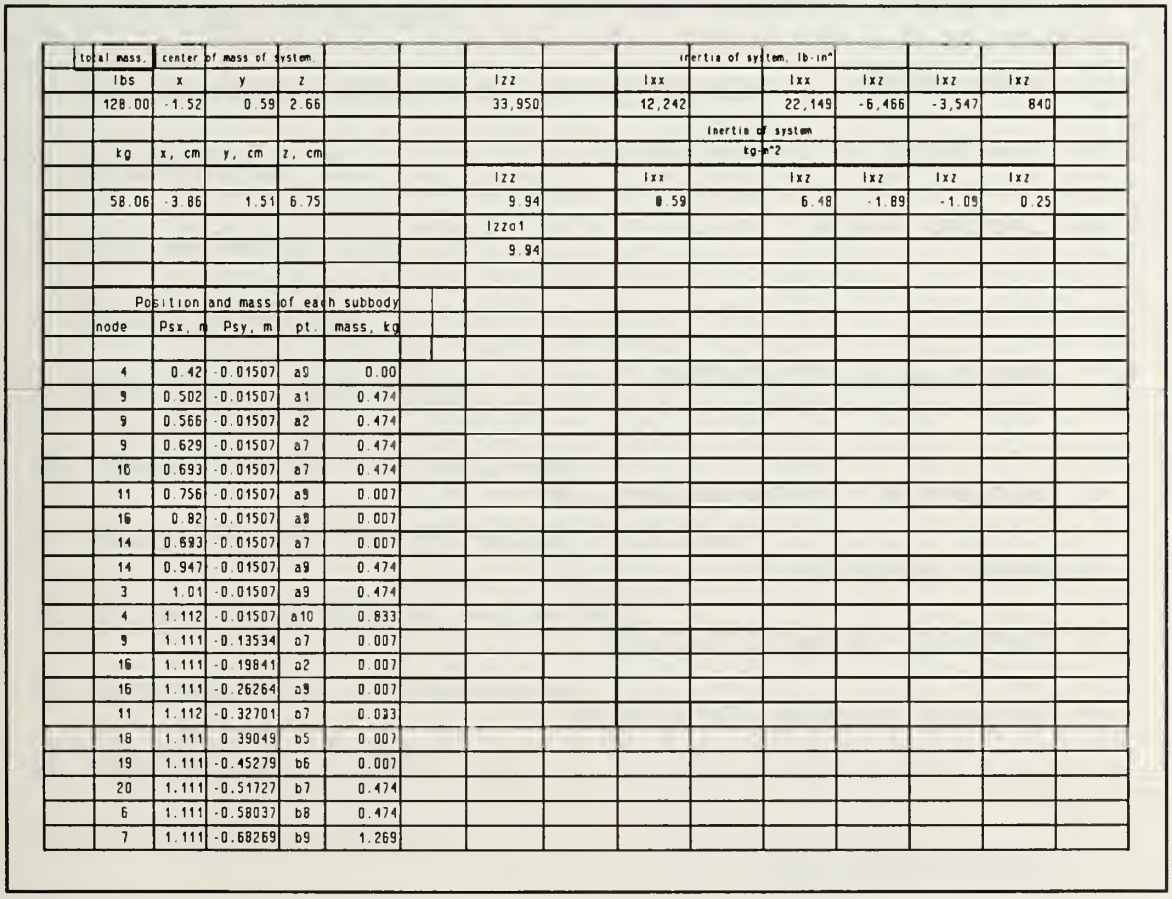

total mass,	center of mass of system							inertia of system, lb-in^2					
lbs	x	y	z			Izz		Ixx		Ixx	Ixz	Ixz	Ixz
128.00	-1.52	0.59	2.66			33,950		12,242		22,149	-6,466	-3,547	840
									inertia of system				
kg	x, cm	y, cm	z, cm						kg-m^2				
						Izz		Ixx		Ixz	Ixz	Ixz	Ixz
58.06	-3.86	1.51	6.75			9.94		0.59		6.48	-1.89	-1.09	0.25
						Izzo1							
						9.94							

Position and mass of each subbody				
node	Psx, m	Psy, m	pt.	mass, kg
4	0.42	-0.01507	a0	0.00
9	0.502	-0.01507	a1	0.474
9	0.566	-0.01507	a2	0.474
9	0.629	-0.01507	a7	0.474
10	0.693	-0.01507	a7	0.474
11	0.756	-0.01507	a9	0.007
16	0.82	-0.01507	a8	0.007
14	0.693	-0.01507	a7	0.007
14	0.947	-0.01507	a9	0.474
3	1.01	-0.01507	a9	0.474
4	1.112	-0.01507	a10	0.833
9	1.111	-0.13534	a7	0.007
16	1.111	-0.19841	a2	0.007
16	1.111	-0.26264	a9	0.007
11	1.112	-0.32701	a7	0.033
18	1.111	0.39049	b5	0.007
19	1.111	-0.45279	b6	0.007
20	1.111	-0.51727	b7	0.474
6	1.111	-0.58037	b8	0.474
7	1.111	-0.68269	b9	1.269

Figure 50 Inertia of System, cont

APPENDIX B

A. ROTARY VARIABLE DIFFERENTIAL TRANSFORMER

1. Manufacturer - Schaevitz Engineering
2. Model - R30D
3. Scale Factor - 0.126 VDC/degree
4. Linearity - 0.16%

B. ANGULAR RATE SENSOR

1. Manufacturer - Watson Industries, Inc
2. Model - ARS-C121-1A
3. Sensitivity - 30 deg/sec full scale
4. Frequency Response - DC to 50 Hz

C. ACCELEROMETER

1. Manufacturer - PCB Piezotronics, Inc
2. Model - 302A02
3. Resolution - 0.01 g
4. Frequency Range ($\pm$ 5%) - 0.05 to 5000 Hz

D. DC SERVO MOTOR

1. Manufacturer - PMI Motion Technologies
2. Model - JR16M4CH/F9T
3. Horsepower - 1.4 HP
4. Peak Torque - 5307.2 oz-in
5. Peak Acceleration without Load - 63.2 KRAD/SEC^2
6. Cogging Torque - 0
7. Terminal Voltage - 128.7 VDC
8. Current - 9.55 amp
9. Power Output - 1049.5 Watts
10. Torque Constant - 52.77 oz-in/amp
11. Mechanical Time Constant, no load - 3.15 msec
12. Electrical Time Constant - < 0.14 msec
13. Speed Regulation - 0.36 RPM/oz-in
14. Motor Diameter - 7.38 in
15. Motor Length - 4.50 in
16. Motor Weight - 17.50 lb

APPENDIX C

A. GIFTS OUTPUT

JOB:arm5 9-MAY-91 15:39:18 PAGE 1

FREQUENCIES

MODE	FREQ	EIGV
1	1.21602E-01	5.83767D-01
2	3.46436E-01	4.73812D+00
3	2.65877E+00	2.79075D+02
4	3.55180E+00	4.98031D+02
5	6.12919E+00	1.48308D+03
6	1.66874E+01	1.09935D+04

JOB:arm5 9-MAY-91 MODE 1 -- 1.216E-01 CPS 15:39:19 PAGE 1

DISPLACEMENT INFORMATION

POINT	U	V	W	RX	RY	RZ
1	0.000E+00	0.000E+00	0.000E+00	0.000E+00	0.000E+00	0.000E+00
2	1.390E-08	1.917E-03	1.114E-36	0.000E+00	0.000E+00	7.501E-02
3	1.529E-07	2.028E-01	1.499E-35	0.000E+00	0.000E+00	6.693E-01
4	1.824E-07	2.801E-01	2.078E-35	0.000E+00	0.000E+00	7.612E-01
5	9.730E-02	2.801E-01	2.726E-35	0.000E+00	0.000E+00	8.486E-01
6	5.192E-01	2.801E-01	3.567E-35	0.000E+00	0.000E+00	1.008E+00
7	6.219E-01	2.801E-01	3.804E-35	0.000E+00	0.000E+00	1.012E+00
8	3.127E-08	9.552E-03	2.934E-36	0.000E+00	0.000E+00	1.647E-01
9	4.865E-08	2.274E-02	4.733E-36	0.000E+00	0.000E+00	2.499E-01
10	6.602E-08	4.120E-02	6.498E-36	0.000E+00	0.000E+00	3.307E-01
11	8.339E-08	6.465E-02	8.218E-36	0.000E+00	0.000E+00	4.071E-01
12	1.008E-07	9.281E-02	9.936E-36	0.000E+00	0.000E+00	4.791E-01
13	1.181E-07	1.254E-01	1.165E-35	0.000E+00	0.000E+00	5.468E-01
14	1.355E-07	1.622E-01	1.337E-35	0.000E+00	0.000E+00	6.101E-01
15	1.524E-01	2.801E-01	2.851E-35	0.000E+00	0.000E+00	8.869E-01
16	2.098E-01	2.801E-01	2.975E-35	0.000E+00	0.000E+00	9.201E-01
17	2.692E-01	2.801E-01	3.099E-35	0.000E+00	0.000E+00	9.479E-01
18	3.301E-01	2.801E-01	3.223E-35	0.000E+00	0.000E+00	9.706E-01
19	3.923E-01	2.801E-01	3.346E-35	0.000E+00	0.000E+00	9.880E-01
20	4.555E-01	2.801E-01	3.469E-35	0.000E+00	0.000E+00	1.000E+00

JOB:arm5 9-MAY-91 MODE 2 -- 3.464E-01 CPS 15:39:19 PAGE 1

DISPLACEMENT INFORMATION

POINT	U	V	W	RX	RY	RZ
1	0.000E+00	0.000E+00	0.000E+00	0.000E+00	0.000E+00	0.000E+00
2	6.883E-08	-6.424E-03	-3.061E-28	0.000E+00	0.000E+00	-2.464E-01
3	7.571E-07	-3.852E-01	-4.119E-27	0.000E+00	0.000E+00	-6.276E-01
4	9.034E-07	-4.343E-01	-5.711E-27	0.000E+00	0.000E+00	-2.597E-01
5	-3.969E-03	-4.343E-01	-7.490E-27	0.000E+00	0.000E+00	1.782E-01
6	3.009E-01	-4.343E-01	-9.801E-27	0.000E+00	0.000E+00	9.829E-01
7	4.022E-01	-4.343E-01	-1.045E-26	0.000E+00	0.000E+00	1.005E+00
8	1.549E-07	-3.043E-02	-8.062E-28	0.000E+00	0.000E+00	-4.996E-01
9	2.409E-07	-6.859E-02	-1.301E-27	0.000E+00	0.000E+00	-6.922E-01
10	3.269E-07	-1.171E-01	-1.786E-27	0.000E+00	0.000E+00	-8.251E-01
11	4.130E-07	-1.721E-01	-2.258E-27	0.000E+00	0.000E+00	-8.996E-01
12	4.990E-07	-2.301E-01	-2.730E-27	0.000E+00	0.000E+00	-9.168E-01
13	5.851E-07	-2.874E-01	-3.202E-27	0.000E+00	0.000E+00	-8.767E-01
14	6.711E-07	-3.402E-01	-3.674E-27	0.000E+00	0.000E+00	-7.794E-01

15	1.360E-02	-4.343E-01	-7.833E-27	0.000E+00	0.000E+00	3.709E-01
16	4.258E-02	-4.343E-01	-8.174E-27	0.000E+00	0.000E+00	5.376E-01
17	8.132E-02	-4.343E-01	-8.515E-27	0.000E+00	0.000E+00	6.782E-01
18	1.282E-01	-4.343E-01	-8.854E-27	0.000E+00	0.000E+00	7.928E-01
19	1.815E-01	-4.343E-01	-9.193E-27	0.000E+00	0.000E+00	8.815E-01
20	2.396E-01	-4.343E-01	-9.531E-27	0.000E+00	0.000E+00	9.442E-01

JOB:arm5 9-MAY-91 MODE 3 -- 2.659E+00 CPS 15:39:19 PAGE 1

DISPLACEMENT INFORMATION

POINT	U	V	W	RX	RY	RZ
1	0.000E+00	0.000E+00	0.000E+00	0.000E+00	0.000E+00	0.000E+00
2	-4.969E-07	5.494E-02	-4.018E-18	0.000E+00	0.000E+00	2.014E+00
3	-5.466E-06	3.727E-01	-5.372E-17	0.000E+00	0.000E+00	-4.275E+00
4	-6.521E-06	-1.385E-01	-7.411E-17	0.000E+00	0.000E+00	-4.782E+00
5	-5.142E-01	-1.385E-01	-9.646E-17	0.000E+00	0.000E+00	-3.628E+00
6	-3.166E-01	-1.385E-01	-1.255E-16	0.000E+00	0.000E+00	5.428E+00
7	3.009E-01	-1.385E-01	-1.336E-16	0.000E+00	0.000E+00	6.403E+00
8	-1.118E-06	2.309E-01	-1.058E-17	0.000E+00	0.000E+00	3.306E+00
9	-1.739E-06	4.487E-01	-1.705E-17	0.000E+00	0.000E+00	3.367E+00
10	-2.360E-06	6.392E-01	-2.339E-17	0.000E+00	0.000E+00	2.517E+00
11	-2.981E-06	7.599E-01	-2.954E-17	0.000E+00	0.000E+00	1.267E+00
12	-3.602E-06	7.982E-01	-3.568E-17	0.000E+00	0.000E+00	-7.512E-02
13	-4.223E-06	7.486E-01	-4.183E-17	0.000E+00	0.000E+00	-1.500E+00
14	-4.845E-06	6.062E-01	-4.796E-17	0.000E+00	0.000E+00	-2.997E+00
15	-7.177E-01	-1.385E-01	-1.008E-16	0.000E+00	0.000E+00	-2.753E+00
16	-8.601E-01	-1.385E-01	-1.050E-16	0.000E+00	0.000E+00	-1.705E+00
17	-9.308E-01	-1.385E-01	-1.093E-16	0.000E+00	0.000E+00	-4.958E-01
18	-9.199E-01	-1.385E-01	-1.136E-16	0.000E+00	0.000E+00	8.632E-01
19	-8.183E-01	-1.385E-01	-1.178E-16	0.000E+00	0.000E+00	2.359E+00
20	-6.177E-01	-1.385E-01	-1.221E-16	0.000E+00	0.000E+00	3.979E+00

JOB:arm5 9-MAY-91 MODE 4 -- 3.552E+00 CPS 15:39:20 PAGE 1

DISPLACEMENT INFORMATION

POINT	U	V	W	RX	RY	RZ
1	0.000E+00	0.000E+00	0.000E+00	0.000E+00	0.000E+00	0.000E+00
2	-1.978E-06	-6.461E-02	-7.421E-13	0.000E+00	0.000E+00	-2.330E+00
3	-2.176E-05	-9.639E-02	-9.922E-12	0.000E+00	0.000E+00	2.818E+00
4	-2.596E-05	9.628E-02	-1.369E-11	0.000E+00	0.000E+00	2.391E-01
5	-1.943E-01	9.628E-02	-1.782E-11	0.000E+00	0.000E+00	-3.010E+00
6	-4.788E-01	9.630E-02	-2.318E-11	0.000E+00	0.000E+00	6.757E+00
7	3.414E-01	9.630E-02	-2.468E-11	0.000E+00	0.000E+00	8.730E+00
8	-4.450E-06	-2.597E-01	-1.954E-12	0.000E+00	0.000E+00	-3.498E+00
9	-6.922E-06	-4.736E-01	-3.150E-12	0.000E+00	0.000E+00	-2.995E+00
10	-9.395E-06	-6.177E-01	-4.320E-12	0.000E+00	0.000E+00	-1.436E+00
11	-1.187E-05	-6.529E-01	-5.456E-12	0.000E+00	0.000E+00	2.636E-01
12	-1.434E-05	-5.924E-01	-6.591E-12	0.000E+00	0.000E+00	1.576E+00
13	-1.681E-05	-4.612E-01	-7.725E-12	0.000E+00	0.000E+00	2.487E+00
14	-1.928E-05	-2.853E-01	-8.859E-12	0.000E+00	0.000E+00	2.983E+00
15	-4.093E-01	9.629E-02	-1.862E-11	0.000E+00	0.000E+00	-3.639E+00
16	-6.409E-01	9.629E-02	-1.941E-11	0.000E+00	0.000E+00	-3.532E+00
17	-8.426E-01	9.629E-02	-2.020E-11	0.000E+00	0.000E+00	-2.702E+00
18	-9.691E-01	9.629E-02	-2.099E-11	0.000E+00	0.000E+00	-1.167E+00
19	-9.764E-01	9.630E-02	-2.177E-11	0.000E+00	0.000E+00	1.050E+00
20	-8.219E-01	9.630E-02	-2.256E-11	0.000E+00	0.000E+00	3.925E+00

JOB:arm5 9-MAY-91 MODE 5 -- 6.129E+00 CPS 15:39:20 PAGE 1

DISPLACEMENT INFORMATION

POINT	U	V	W	RX	RY	RZ
1	0.000E+00	0.000E+00	0.000E+00	0.000E+00	0.000E+00	0.000E+00
2	-1.587E-06	1.130E-01	3.628E-16	0.000E+00	0.000E+00	3.885E+00

```
     3 -1.746E-05 -6.445E-01  4.931E-15  0.000E+00  0.000E+00  5.642E+00
     4 -2.083E-05  1.459E-01  6.886E-15  0.000E+00  0.000E+00  6.691E+00
     5  4.542E-01  1.459E-01  9.133E-15  0.000E+00  0.000E+00  1.199E+00
     6 -1.567E-01  1.460E-01  1.205E-14  0.000E+00  0.000E+00  1.417E+00
     7  7.650E-02  1.460E-01  1.288E-14  0.000E+00  0.000E+00  2.733E+00
     8 -3.571E-06  3.975E-01  9.561E-16  0.000E+00  0.000E+00  4.293E+00
     9 -5.555E-06  5.800E-01  1.544E-15  0.000E+00  0.000E+00  1.004E+00
    10 -7.539E-06  4.984E-01  2.123E-15  0.000E+00  0.000E+00 -3.540E+00
    11 -9.523E-06  1.609E-01  2.690E-15  0.000E+00  0.000E+00 -6.641E+00
    12 -1.151E-05 -2.880E-01  3.257E-15  0.000E+00  0.000E+00 -7.049E+00
    13 -1.349E-05 -6.774E-01  3.824E-15  0.000E+00  0.000E+00 -4.767E+00
    14 -1.547E-05 -8.373E-01  4.390E-15  0.000E+00  0.000E+00  1.696E-01
    15  4.635E-01  1.459E-01  9.565E-15  0.000E+00  0.000E+00 -7.967E-01
    16  3.670E-01  1.460E-01  9.996E-15  0.000E+00  0.000E+00 -2.128E+00
    17  2.080E-01  1.460E-01  1.043E-14  0.000E+00  0.000E+00 -2.764E+00
    18  3.123E-02  1.460E-01  1.086E-14  0.000E+00  0.000E+00 -2.683E+00
    19 -1.174E-01  1.460E-01  1.128E-14  0.000E+00  0.000E+00 -1.877E+00
    20 -1.919E-01  1.460E-01  1.171E-14  0.000E+00  0.000E+00 -3.489E-01

JOB:arm5        9-MAY-91    MODE  6 -- 1.669E+01 CPS  15:39:20    PAGE  1
                        DISPLACEMENT INFORMATION
POINT      U           V           W           RX          RY          RZ
    1  0.000E+00   0.000E+00   0.000E+00  0.000E+00  0.000E+00  0.000E+00
    2 -2.502E-06   4.201E-01  -1.665E-10  0.000E+00  0.000E+00  1.237E+01
    3 -2.750E-05   3.589E-01  -2.232E-09  0.000E+00  0.000E+00  2.310E+00
    4 -3.280E-05  -2.598E-02  -3.084E-09  0.000E+00  0.000E+00 -6.379E+00
    5 -6.684E-01  -2.601E-02  -4.025E-09  0.000E+00  0.000E+00 -4.134E+00
    6  1.220E-01  -2.611E-02  -5.246E-09  0.000E+00  0.000E+00  6.290E-01
    7 -2.433E-02  -2.613E-02  -5.587E-09  0.000E+00  0.000E+00 -2.474E+00
    8 -5.630E-06   9.551E-01  -4.385E-10  0.000E+00  0.000E+00  5.754E-01
    9 -8.757E-06   3.730E-01  -7.071E-10  0.000E+00  0.000E+00 -1.690E+01
   10 -1.188E-05  -7.914E-01  -9.703E-10  0.000E+00  0.000E+00 -1.545E+01
   11 -1.501E-05  -1.353E+00  -1.226E-09  0.000E+00  0.000E+00 -2.824E+00
   12 -1.813E-05  -1.231E+00  -1.481E-09  0.000E+00  0.000E+00  5.951E+00
   13 -2.126E-05  -6.937E-01  -1.737E-09  0.000E+00  0.000E+00  1.017E+01
   14 -2.438E-05  -4.728E-02  -1.992E-09  0.000E+00  0.000E+00  9.311E+00
   15 -8.606E-01  -2.603E-02  -4.206E-09  0.000E+00  0.000E+00 -1.850E+00
   16 -8.995E-01  -2.604E-02  -4.387E-09  0.000E+00  0.000E+00  6.154E-01
   17 -7.887E-01  -2.606E-02  -4.566E-09  0.000E+00  0.000E+00  2.786E+00
   18 -5.617E-01  -2.607E-02  -4.746E-09  0.000E+00  0.000E+00  4.202E+00
   19 -2.786E-01  -2.609E-02  -4.925E-09  0.000E+00  0.000E+00  4.500E+00
   20 -1.872E-02  -2.610E-02  -5.103E-09  0.000E+00  0.000E+00  3.449E+00
```

B. FORTRAN PROGRAM FORM

```
      PROGRAM FORM
C
C     AUTHOR:  R. J. WATKINS
C
C     DATE:  MAY 18, 1991
C
C     THIS PROGRAM READS IN DATA GIVEN BY GIFTS OUTPUT AND
```

```
C    PUTS IT INTO A FORMAT FOR STATE-SPACE MODELING
C
     DOUBLE PRECISION A(16,16), B(16), AI, BI
     REAL OMEGA(6),U(6,20),V(6,20),PSX(20),PSY(20),MS(20),IZZO1
    1,DS(6), ES(6), FS(6), GS(6), IW, IZZO2,HS(6),JS(6)
     OPEN (UNIT=10, FILE='RESXDAT.LPT', STATUS='OLD')
     OPEN (UNIT=11, FILE='PS.DAT',STATUS='OLD')
     OPEN (UNIT=12, FILE='MS.DAT',STATUS='OLD')
     OPEN (UNIT=13, FILE='CHECK.DAT',status='new')
     OPEN (UNIT=14, FILE='ADMP',status='new',CARRIAGECONTROL='LIST')
     OPEN (UNIT=15, FILE='BDMP',status='new',CARRIAGECONTROL='LIST')
C
C    READ IN OUTPUT FROM PR_OUT BATCH FILE
C
C
     READ(10,5)
  5  FORMAT (///)
     DO 6 I=1,6
        READ(10,7) OMEGA(I)
  6  CONTINUE
  7  FORMAT (10X,E11.5)
     DO 12 I=1,6
         READ(10,5)
         DO 15 J=1,20
            READ(10,13) U(I,J), V(I,J)
 15       CONTINUE
 12  CONTINUE
 13  FORMAT(7X,E10.3,1X,E10.3)
C
C    READ IN MS AND PS DATA FILES
C    PS IS POSITION OF EACH NODE (SUBBODY) IN METERS
C    AND MS IS THE MASS OF EACH SUBBODY IN KG.  NOTE 1: FIRST
C    ENTRY IN MS.DAT IS THE INERTIA TERM FOR THE SYSTEM (IZZO1)
C    NOTE 2: MASS AND POSITION OF EACH NODE MUST BE IN SAME
C    SEQUENCE AS OUTPUT IN PR_OUT FILE!!
C
     DO 20 I=1,20
        READ (11,*) PSX(I), PSY(I)
 20  CONTINUE
     READ (12,*) IZZO1
     DO 30 I=1,20
        READ (12,*) MS(I)
 30  CONTINUE
```

```
C
C   FORM THE TERMS FOR THE A AND B MATRIX. ALSO CALCULATE
C   CHECK MATRIX ES:  ALL ENTRIES SHOULD BE APPROX 1 IF
C   DATA INPUT CORRECTLY. OUTPUT IS IN CHECK.DAT (ASCII)
C   INPUT DAMPING FOR ARM (ZETA) NOTE: COULD BE CHANGED
C   TO VECTOR IF NECESSARY
C
    ZETA=0.02
    IZZO2=IZZO1
    DO 35 I=1,6
        DS(I)=0.0
        ES(I)=0.0
        DO 32 J=1,20
            DS(I)=DS(I)+(V(I,J)*PSX(J)-U(I,J)*PSY(J))*MS(J)
            ES(I)=ES(I)+(U(I,J)**2+V(I,J)**2)*MS(J)
 32      CONTINUE
        WRITE(13,*) ES(I)
        IZZO2=IZZO2-DS(I)**2
 35 CONTINUE
    DO 38 I=1,6
        FS(I)=DS(I)*OMEGA(I)**2
        GS(I)=(OMEGA(I)**2)*IZZO2+DS(I)*FS(I)
        HS(I)=2.0*OMEGA(I)*ZETA*DS(I)
        JS(I)=2.0*ZETA*OMEGA(I)*IZZO2+DS(I)*HS(I)
 38 CONTINUE
C
C   FORM A AND B MATRIX
C
    DO 45 I=1,14
        DO 42 J=1,14
            A(I,J)=0.0
 42      CONTINUE
 45 CONTINUE
    DO 50 I=1,7
        A(I,I+7)=1.0
 50 CONTINUE
    DO 57 I=2,7
        A(8,I)=FS(I-1)/IZZO2
 57 CONTINUE
    DO 65 I=9,14
        DO 60 J=2,7
            A(I,J)=-DS(I-8)*FS(J-1)/IZZO2
 60      CONTINUE
```

```
      DO 63 J=9,14
         A(I,J)=-DS(I-8)*HS(J-8)/IZZO2
 63    CONTINUE
      A(I,I)=-JS(I-8)/IZZO2
      A(8,I)=HS(I-8)/IZZO2
      A(I,I-7)=-GS(I-8)/IZZO2
 65  CONTINUE
C
C   FORM CONTROL INPUT MATRIX B
C
    DO 70 I=1,7
       B(I)=0.0
 70  CONTINUE
    B(8)=1.0/IZZO2
    DO 75 I=9,14
       B(I)=-DS(I-8)/IZZO2
 75  CONTINUE
C
C   WRITE MATRIX TO FILES. USE MATRIXX SUBROUTINE MATSAV TO
C   CONVERT DATA INTO READABLE FORM FOR MATRIXX.  OUTPUT
C   IS IN ADMP AND BDMP.
C
C
    CALL MATSAV(14,'ASYS',16,14,14,0,A,AI,'(1P2E24.15)')
    CALL MATSAV(15,'BSYS',16,14,1,0,B,BI,'(1P2E24.15)')
C
C   END OF PROGRAM
C
    STOP
    END
```

APPENDIX D

The following table is reprinted for convenience:

TABLE IV Weighting Factors

	R_{xx}						R_{uu}
Designation	1	q1	q2	$\dot{\Psi}$	$\dot{q}1$	$\dot{q}2$	T
C4	1	0	0	0	0	0	.001
C2	1	10	10	0	0	0	0.1
C3	1	10^4	10^4	0	0	0	0.1
C4	1	0	0	0	●	●	0.1
C5	1	0	0	0	10^4	10^4	0.1
C6	1	0	0	1	0	0	0.1
C7	1	0	0	1	0.2	0.2	100
C8	1	0	0	1	0.7	0.5	1000

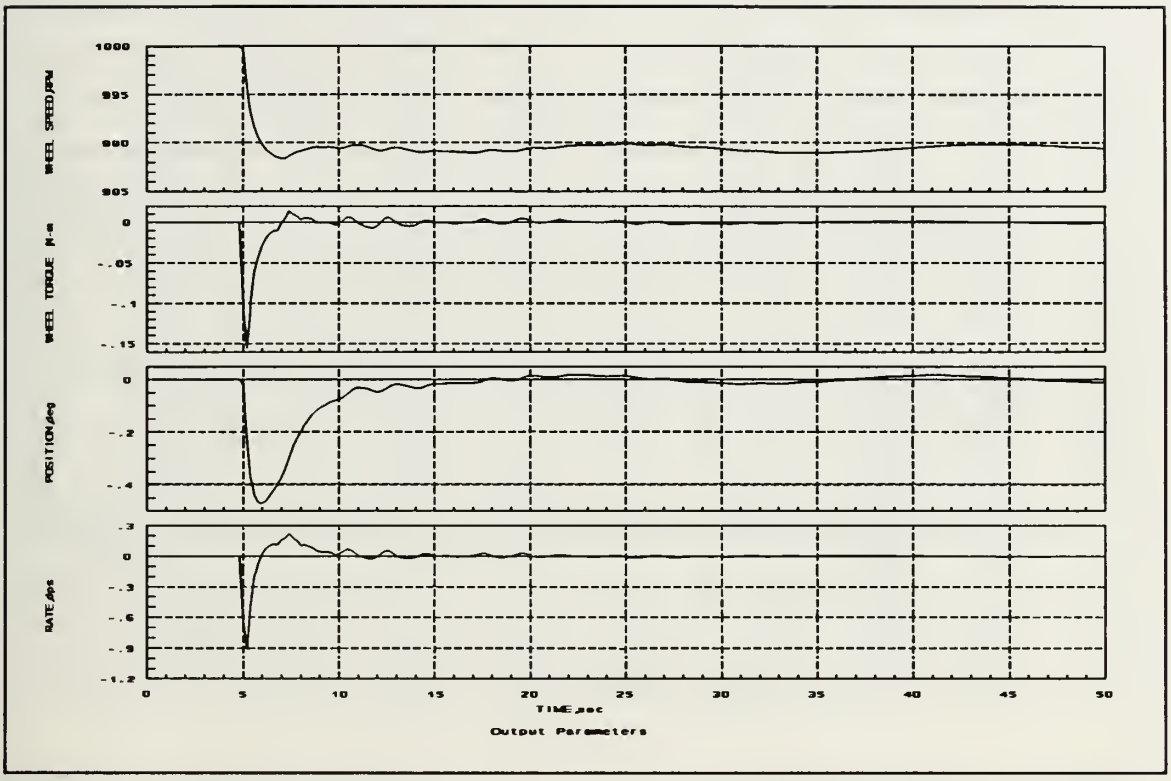

Figure 51 Impulse Response, PD2

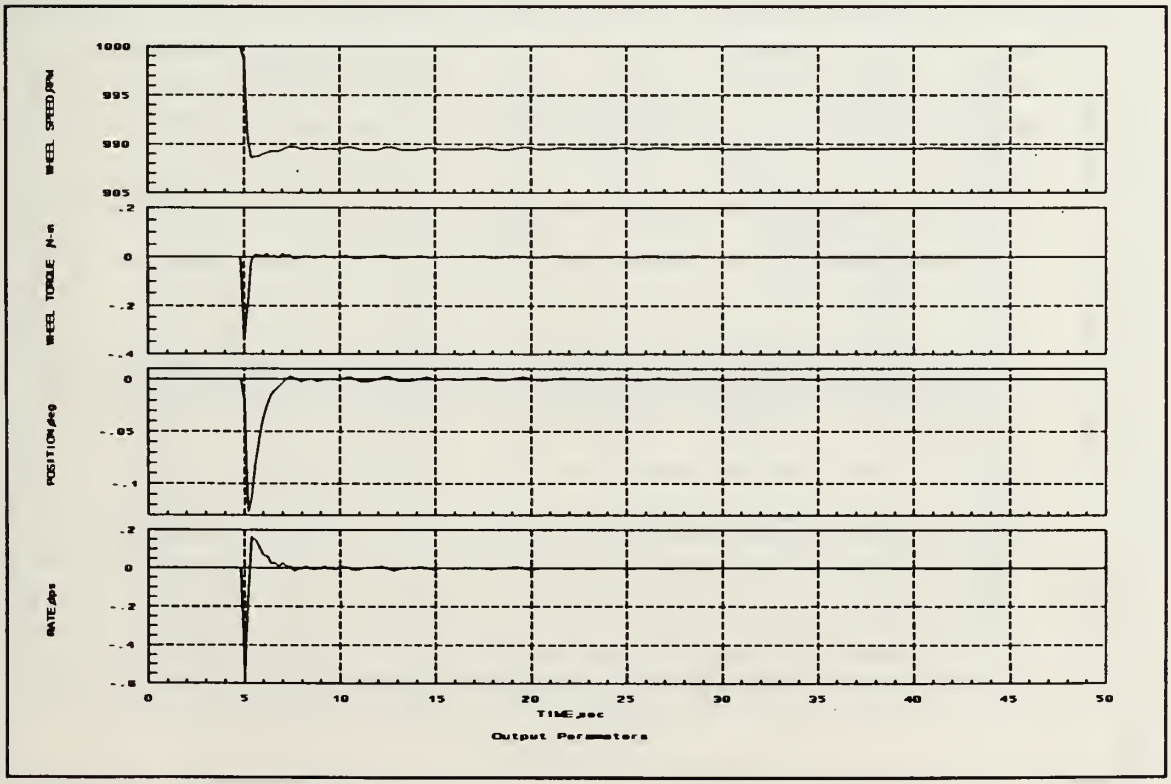

Figure 52 Impulse Response, PD3

Figure 53 Impulse Response, C1

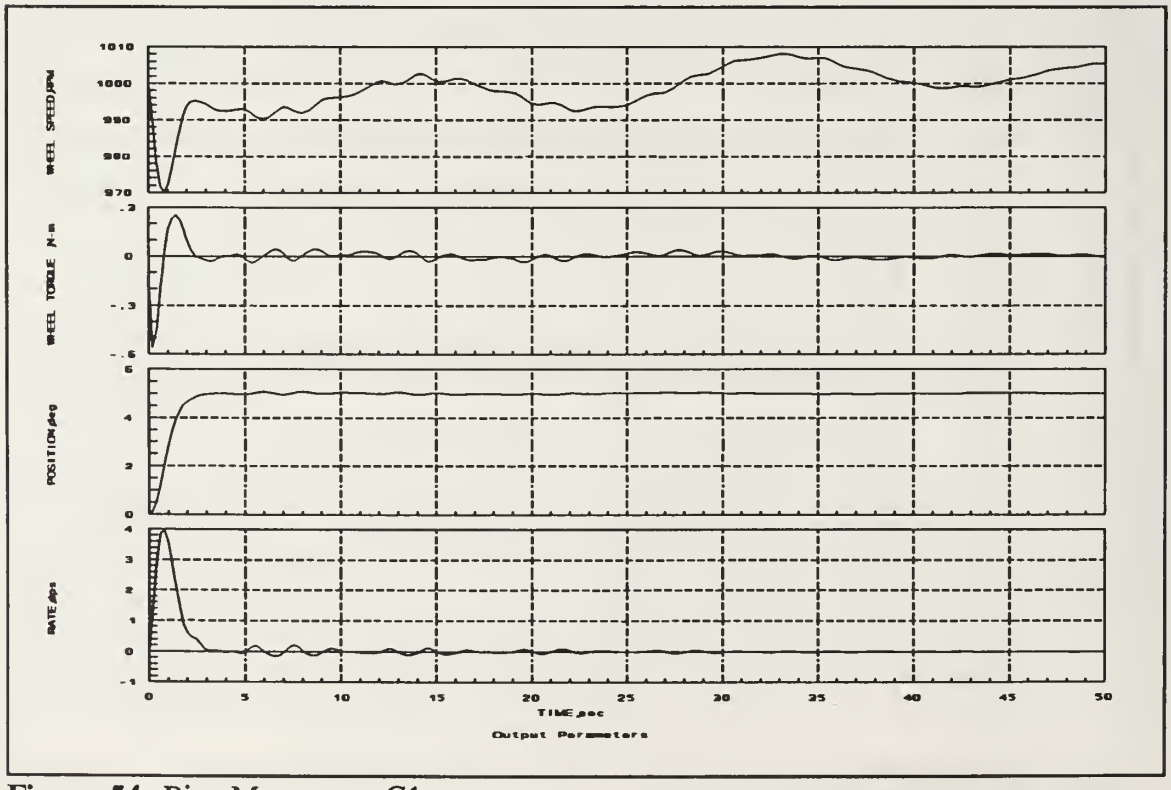

Figure 54 Bias Maneuver, C1

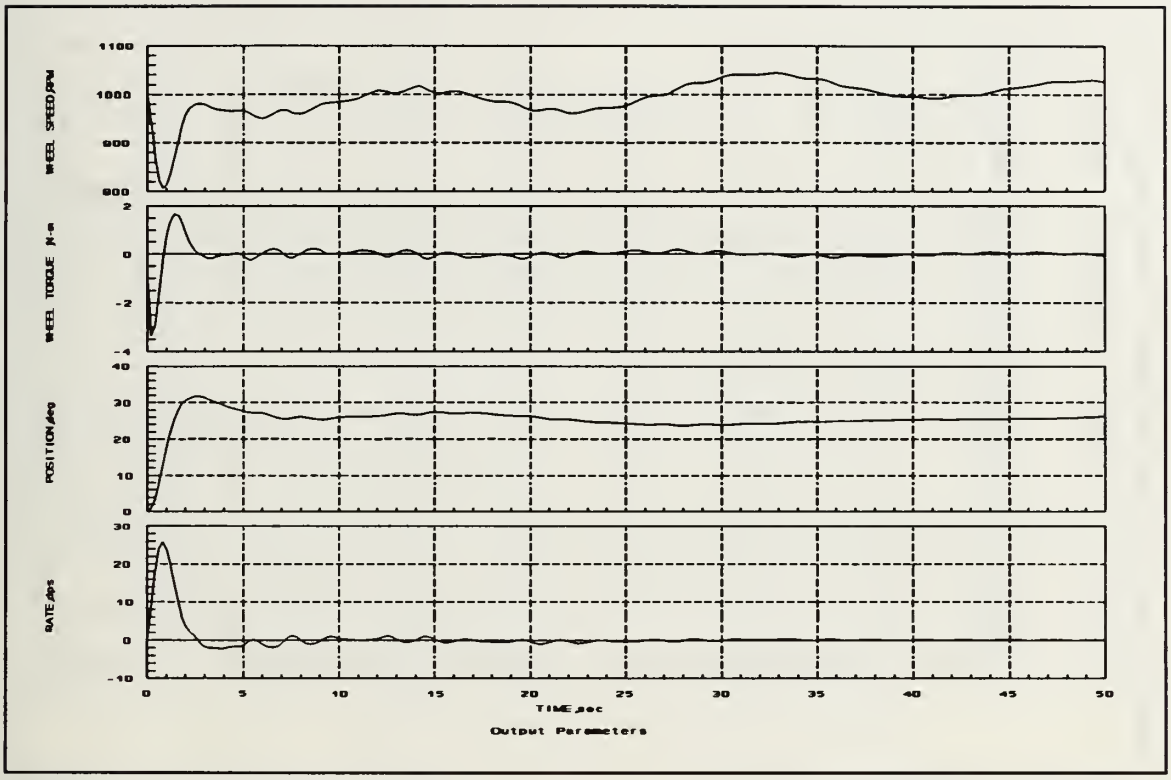

Figure 55 Slew Maneuver, C2

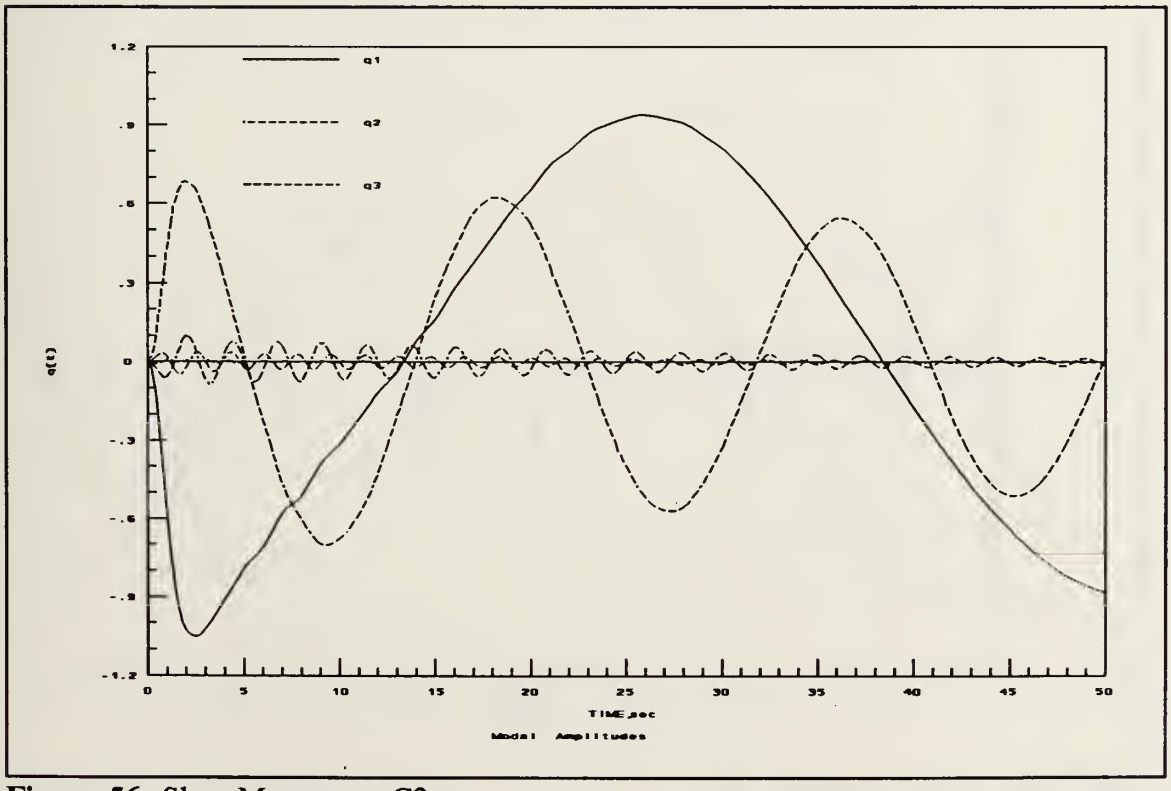

Figure 56 Slew Maneuver, C2

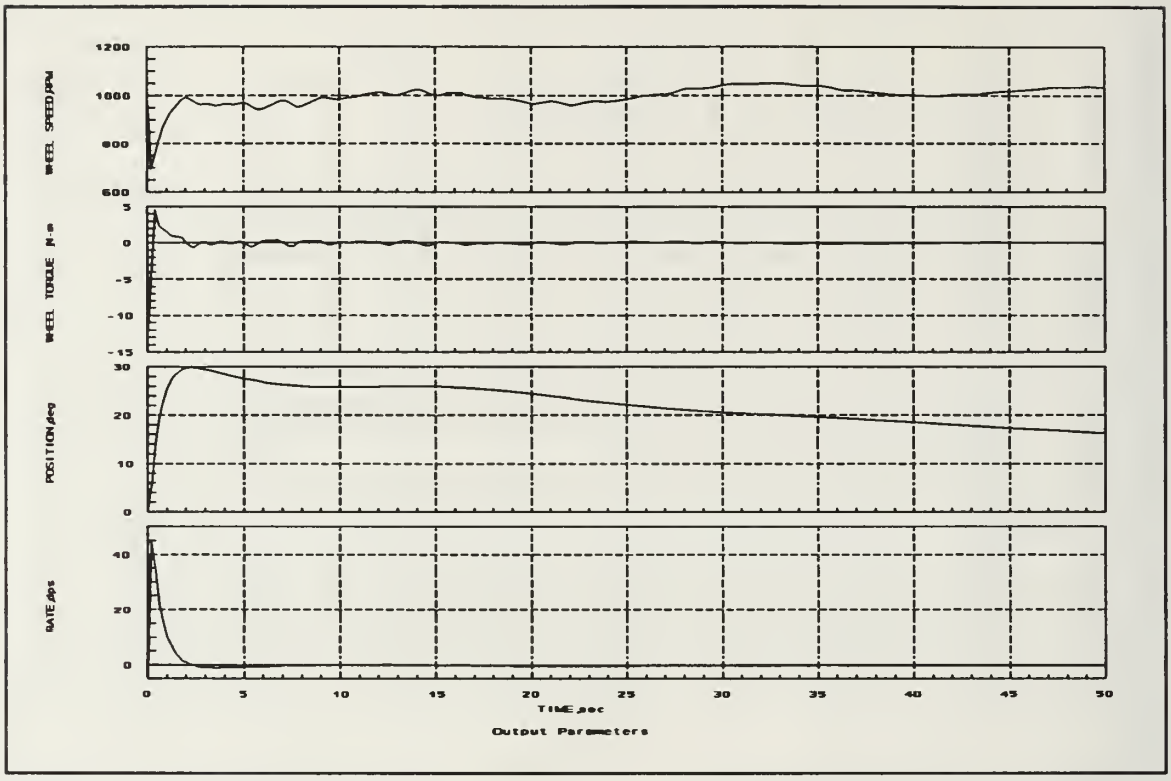

Figure 57 Slew Maneuver, C3

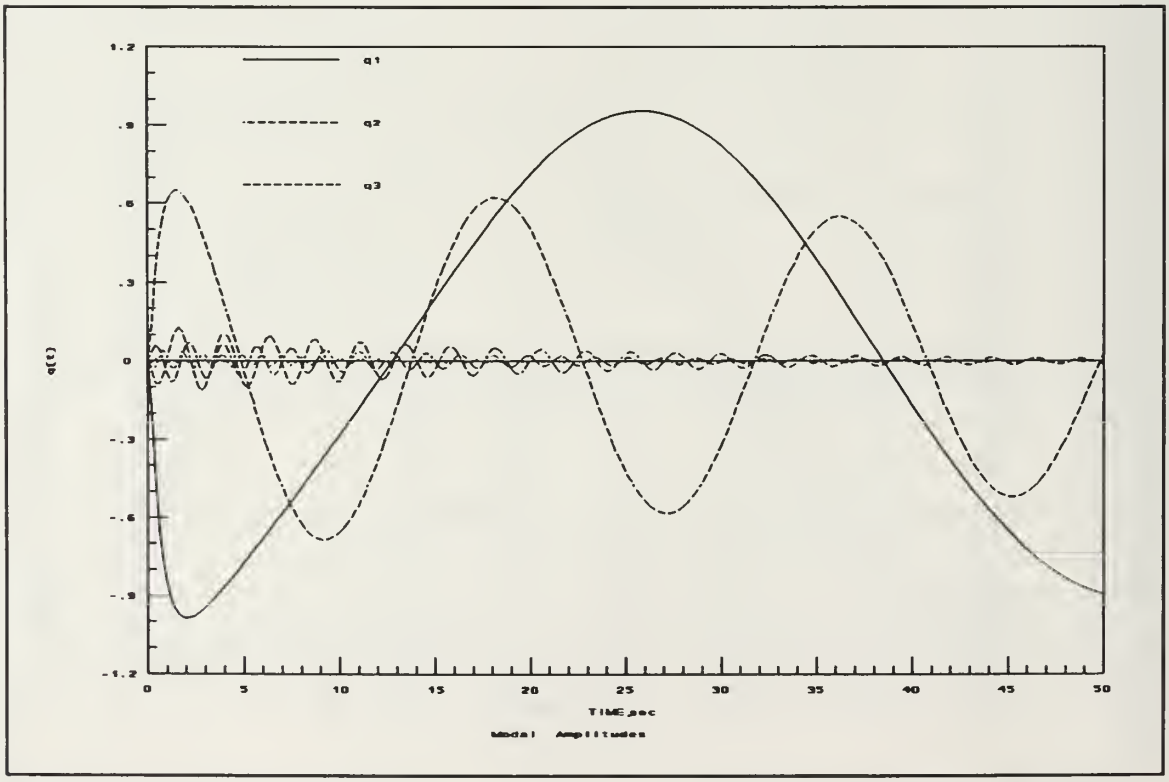

Figure 58 Slew Maneuver, C3

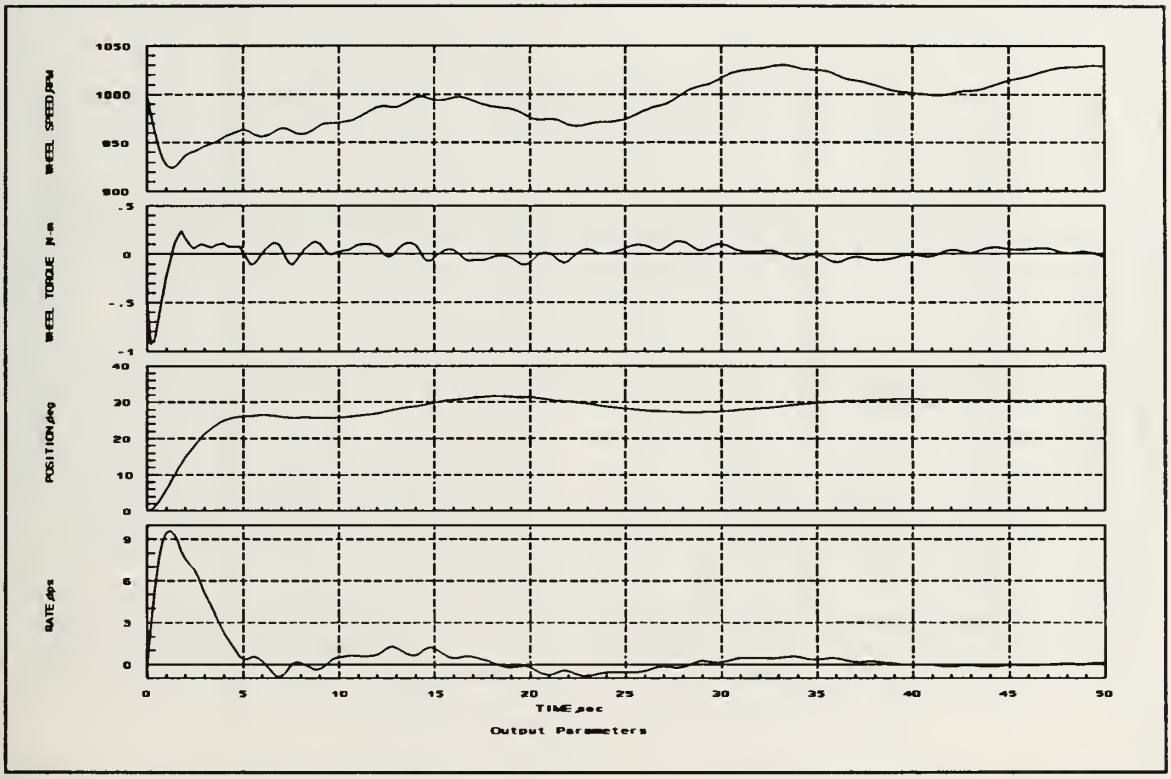

Figure 59 Slew Maneuver, C4

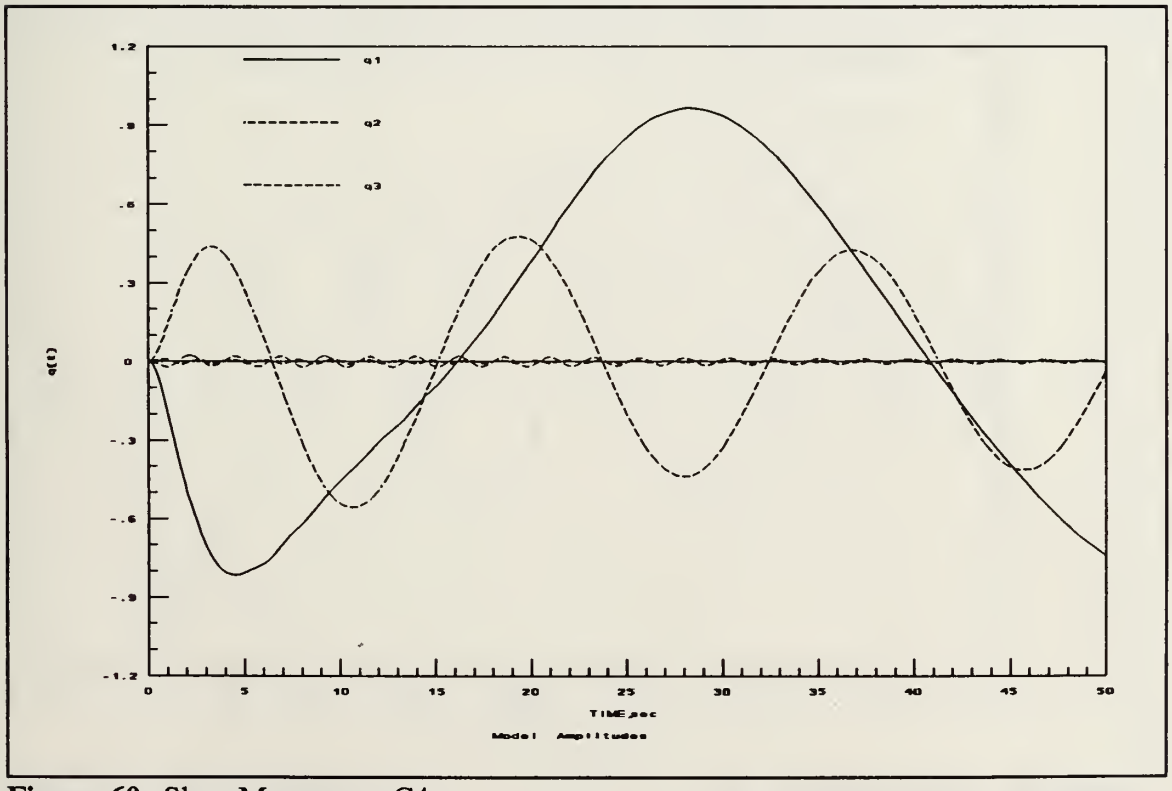

Figure 60 Slew Maneuver, C4

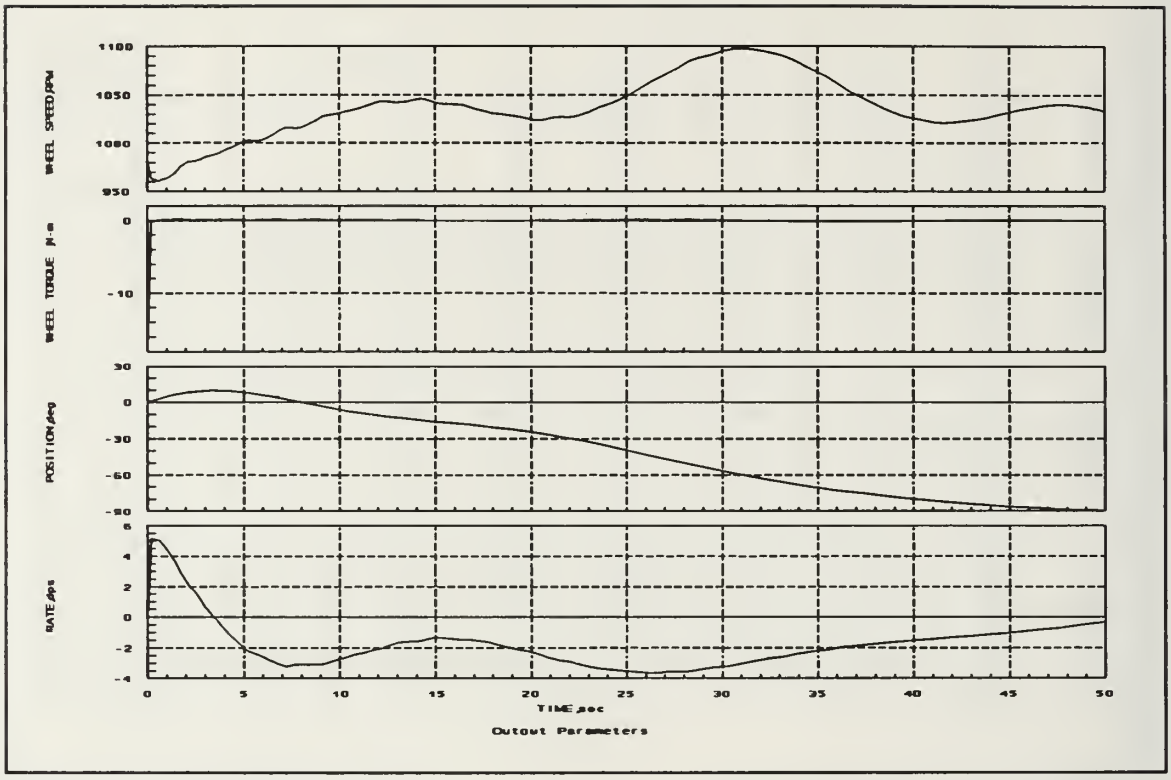

Figure 61 Slew Maneuver, C5

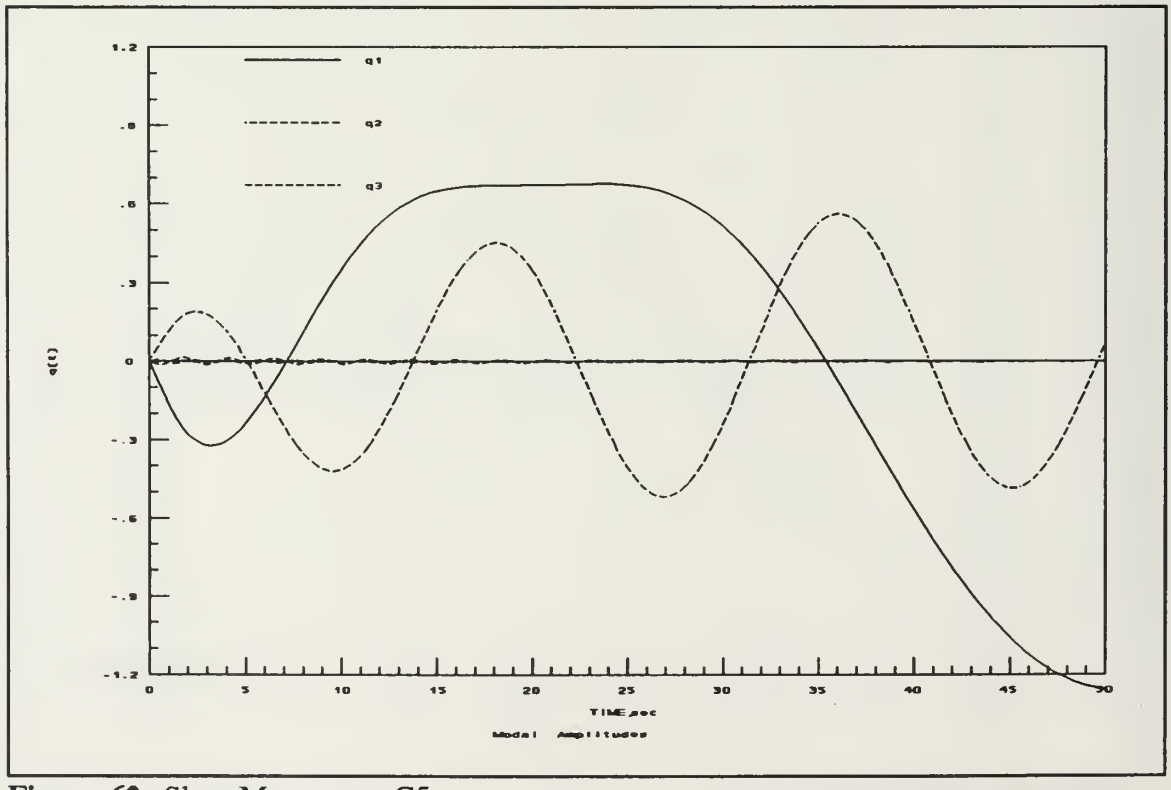

Figure 62 Slew Maneuver, C5

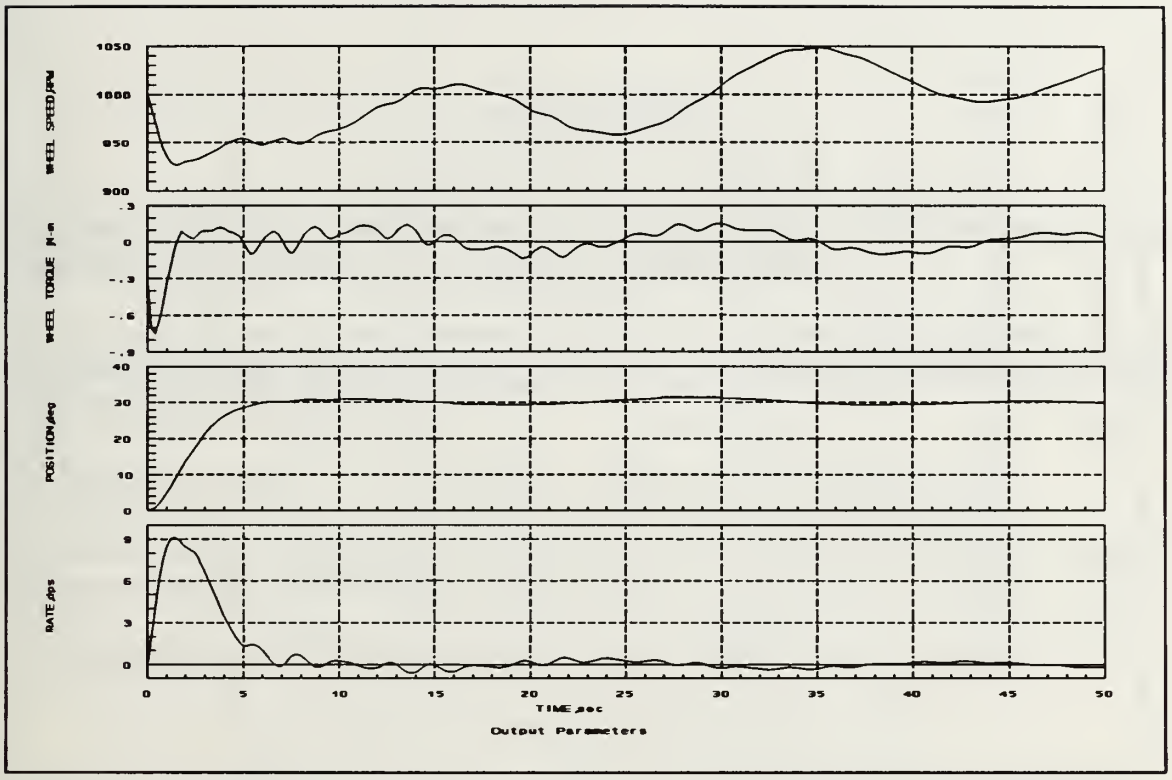

Figure 63 Slew Maneuver, C6

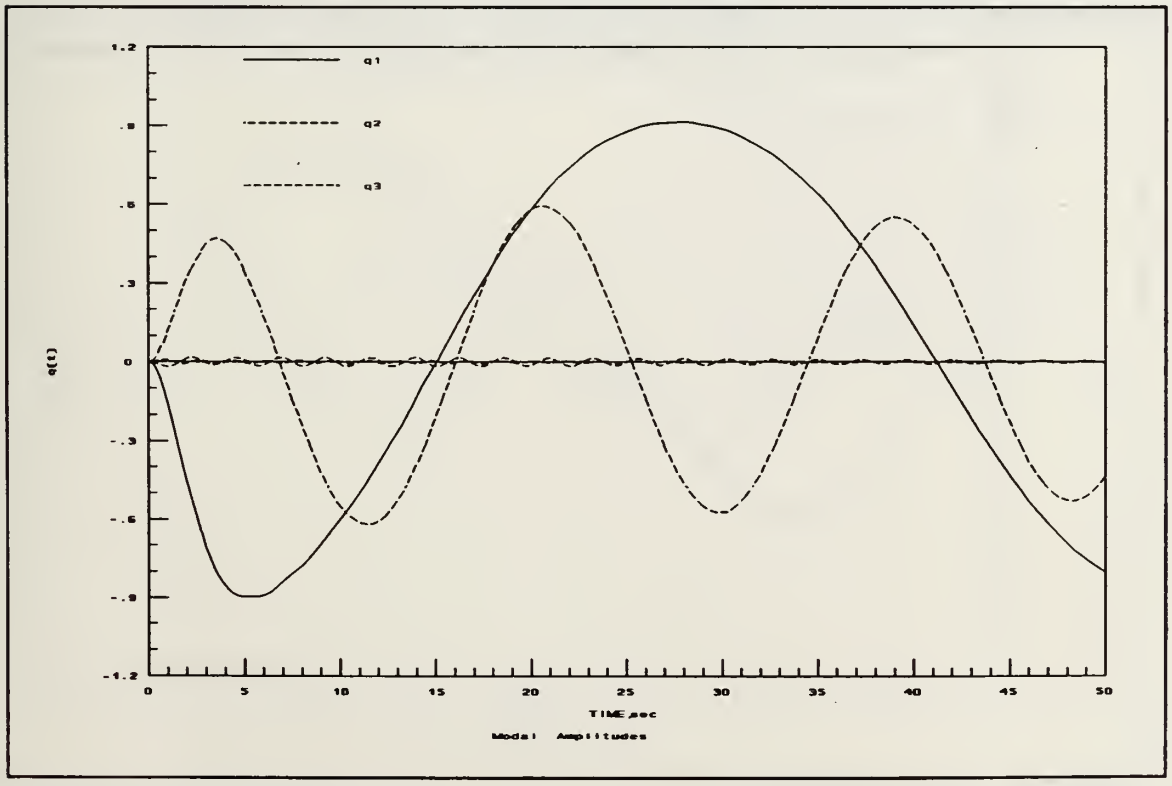

Figure 64 Slew Maneuver, C6

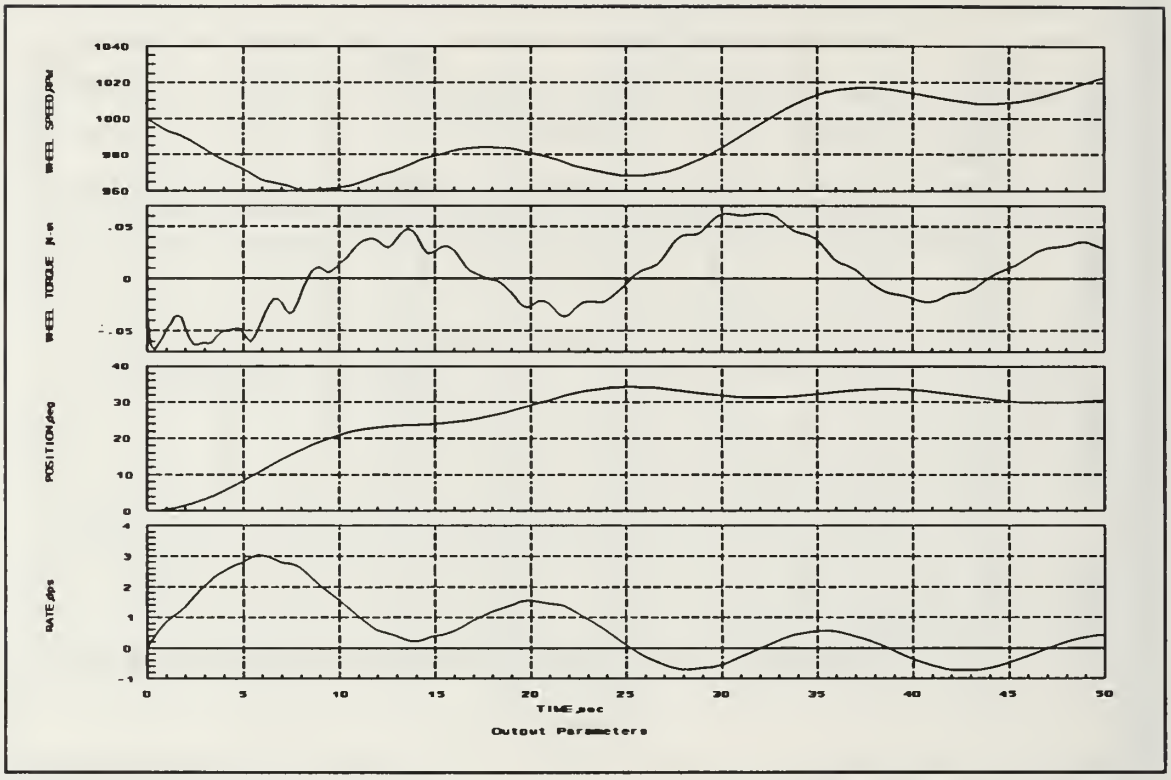

Figure 65 Slew Maneuver, C7

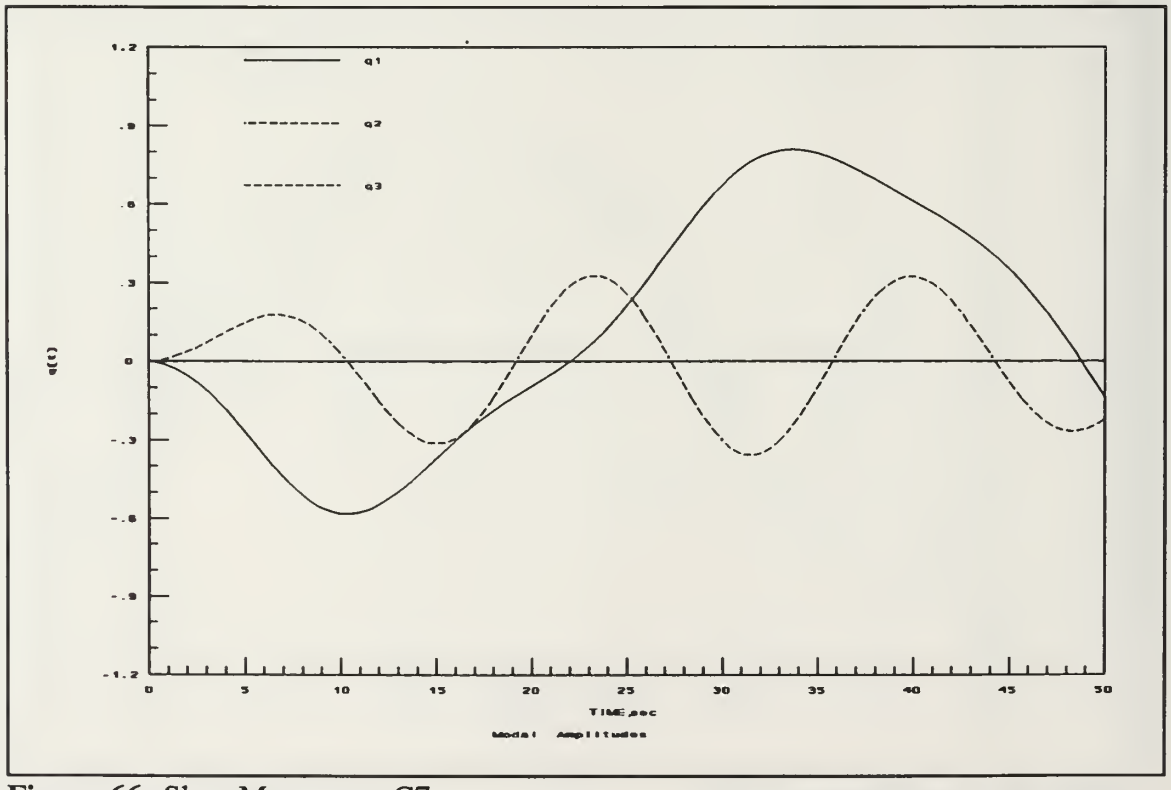

Figure 66 Slew Maneuver, C7

REFERENCES

1. Ward, Christina C., *Attitude Control of Flexible Structures*, Master's Thesis, Naval Postgraduate School, Monterey, California, September 1990.

2. Oakley, Celia M., and Cannon, Robert H. Jr. "Equations of Motion for an Experimental Planar Two-Link Flexible Manipulator", Proceedings of the ASME Winter Annual Meeting, December, 1989.

3. Integrated Systems Inc., *AC-100 Users Guide*, V2.4.05, February 1991.

4. NASA Technical Report 32-1329, *Dynamics and Control of Flexible Space Vehicles*, by Peter W. Likens, February 15, 1969.

5. Agrawal, Brij N., *Design of Geosynchronous Spacecraft*, Prentice-Hall, 1986.

6. Friedland, Bernard, *Control System Design*, McGraw-Hill, 1986.

7. Integrated Systems Inc., *MATRIX$_X$ Core*, 7th ed., January 1990.

8. Agrawal, Brij N., and Watkins, R. Joseph, "Experimental Simulation of Attitude Control of Flexible Spacecraft," Proceedings of Eighth VPI and SU Symposium on Dynamics and Control of Large Structures, May 1991.

INITIAL DISTRIBUTION LIST

1.	Defense Technical Information Center Cameron Station Alexandria, Virginia 22304-6145	2
2.	Library, Code 52 Naval Postgraduate School Monterey, California 93943-5002	2
3.	Chairman, Code AA Department of Aeronautics and Astronautics Naval Postgraduate School Monterey, California 93943	1
4.	Professor Brij N. Agrawal, Code AA/Ag Department of Aeronautics and Astronautics Naval Postgraduate School Monterey, California 93943	2
5.	CDR Carl Josefson, Code 9100-C Naval Research Laboratory 4555 Overlook Ave. S.W. Washington, DC 20375-5000	1
6.	Professor Jeffrey Burl, Code EC/Bl Department of Electrical and Computer Engineering Naval Postgraduate School Monterey, California 93943	1